TEMPERATURE EFFECTS IN THIN FILMS OF SILICON OXIDE

by

Alan Richard MORLEY

A thesis submitted for the Degree of Doctor of Philosophy in the University of London.

Electrical Engineering Department
Imperial College of Science and Technology.

June 1968

ABSTRACT

The use of thin film capacitors as a component in microminiaturized electrical circuits has made it necessary to obtain a more complete understanding of the conduction mechanisms occurring in these films. Silicon oxide was chosen as the dielectric material for study and the temperature behaviour of thin film capacitors was investigated in order that films with low temperature ageing and a high stability could be prepared.

D.C. and A.C. conduction processes in dielectric films have been examined with particular reference to the amorphous nature of the dielectric materials considered. The theoretical contributions to the temperature coefficient capacitance have been outlined.

Apparatus was designed and constructed so that complete metal-dielectric-metal sandwiches could be prepared and measurements performed on them without breaking the vacuum.

The effects of deposition conditions and post-deposition heat treatment was investigated and empirical equations were obtained for the reduction in loss and capacitance during the annealing treatment.

D.C. results were similar to those obtained by previous workers. A precise interpretation of these

results was not possible due to uncertainties in the spatial and energy band structure of the amorphous films. From observation of the decay of the absorption current a low frequency loss peak was predicted. The audio frequency results were influenced by this peak, particularly at high temperatures. Above the audio frequency region both the loss and permittivity were independent of frequency with a very low activation energy (< 0.1 eV) which was probably due to some form of electron hopping conduction.

The temperature coefficient of capacitance was found to depend on the loss, particularly for high loss materials. The intrinsic contribution to the temperature coefficient of capacitance was probably due to the temperature dependence of the ionic polarizability.

ACKNOWLEDGMENTS

I am very much indebted to Professor J. C. Anderson for his support and advice throughout the course of this work. I am also extremely grateful to Mr. D. S. Campbell for his help and guidance and also for suggesting the course of study.

In addition, I am obliged to Professor Anderson for the use of laboratory facilities in the Science of Materials Group at Imperial College and also to members of his section for many useful discussions.

I would like to thank members of the Allen Clark Research Centre, Caswell, for their helpful advice and discussions and, in particular, Dr. P. J. Harrop.

Financial support was provided by a Research Studentship from the Science Research Council, to whom I am grateful. I would like to acknowledge the use of the IBM 7090 computer of the Imperial College Computer Unit.

Finally, I would like to thank Miss Anne Gidlow who typed this thesis.

INDEX

USUAL DEFINITION OF SYMBOLS

γ_c	-	Temperature Coefficient of Capacitance
γ_p	-	Temperature Coefficient of Permittivity
A.C.	-	Alternating Current
D.C.	-	Direct Current
Tan δ	-	Loss Tangent
C	-	Capacitance
R	-	Resistance
δ	-	Loss Angle
j	-	Imaginary Number $\sqrt{-1}$
ω	-	Angular Frequency
f	-	Frequency
ε	-	Permittivity
ε_o	-	Permittivity of Free Space
Z	-	Complex Impedance
ε'	-	Real Part of Permittivity
ε''	-	Imaginary Part of Permittivity
d	-	Electrode Separation
t	-	Electrode Separation and Time
α_e	-	Linear Expansion Coefficient
γ_m	-	Work Function of Metal
γ_i	-	Work Function of Insulator
x	-	Electron Affinity of Insulator
E_b	-	Forbidden Energy Gap
S.E.	-	Schottky Emission

P.F. - Poole-Frenkel

J - Current Density

I - Current

V - Voltage

ϕ - Potential Barrier Height

β - Cole-Cole Distribution Function

k - Boltzman's Constant

h - Planks Constant

e - Electronic Charge

m - Electronic Mass

E - Potential Energy

q - Potential Energy

E_i - Ionisation Energy

l - Site Separation

μ - Mobility

N_t - Trap Density

P - Polarization

α_m - Polarizability

α_e - Electronic Polarizability

α_a - Atomic Polarizability

α_d - Dipole Polarizability

α_i - Interfacial Polarizability

$\alpha(t)$ - Decay Factor

τ - Relaxation Time

τ_z - Mean Relaxation Time

ε_s - Static Dielectric Constant

ε_∞	-	High Frequency Dielectric Constant
$G(\tau)$	-	Distribution of Relaxation Times
$G(q)$	-	Distribution of Energies
r	-	Distance Parameter
σ	-	Conductivity
G	-	Conductance
D	-	Diffusion Constant
L_D'	-	A Debye Length
λ	-	Mean Free Path

CHAPTER 1

INTRODUCTION

1.1 Introduction

Over the last ten years, the electronic component industry has been putting increasing emphasis on the miniaturisation of components. This was encouraged originally by the needs of the space programme, but it has now been recognised that miniaturisation techniques are often worth employing in their own right, due to the increase in reliability and decrease in cost that can result. Three main techniques have evolved during the ten years; they are silicon solid circuitry[1], thin films[2, 3] and thick films[4]. In the first of these a silicon slice is doped at various levels so that not only transistors and diodes, but resistors and capaciotrs are prepared in the same slice. In the second, thin layers of metal or dielectric are deposited directly on a support which is quite often of glass, to form resistors, connectors or capacitors. Active devices[5-7] have also been produced by thin film techniques but these are at present not commercially viable. Thick film techniques involve the preparation of inks such as organo-metallic glasses on a suitable support, which are then fired to give the required

component. Fairly satisfactory resistors can be manufactured in this way, but capacitors are more difficult to prepare. One of the chief advantages of this technique, however, is the relatively low cost of production involved compared with the other two methods, although the components prepared are generally not of precision quality.

Of these three techniques, by far the heaviest industrial involvement is on silicon solid circuits. However, although many different types of sophisticated circuits can be prepared in one chip, it has not yet been found possible to prepare high quality components. Such components should have tolerances of better than 0.1%, a very low temperature coefficient and low ageing, and where these are necessary, thin film techniques are now being employed to provide them. This is commercially feasible as interconnection patterns for the solid state circuits are often prepared by thin film techniques in any case.

Given this background, it can be seen that investigations into thin film components tend to concentrate on the high quality aspects of them.

The temperature behaviour, as has been mentioned above, is of importance for thin film components.

In general the heat will be supplied from two sources, i.e. from the particular environment and from the dissipation of electrical energy. Although miniaturisation of size is always accompanied by reduction in the operating power level, this is not always sufficient to overcome the temperature increases resulting from the high packing densities involved.

An illustration of the use of thin film components used in filter networks has been given by Blackburn et al[8]. The R-C networks define the pass-band of the filter making it important that the thin film components have a good temperature stability. Thin film resistors are produced with a temperature coefficient of resistance of less than 20 p.p.m./^{o}C[9, 10]. However, thin film capacitors often have a temperature coefficient of capacitance which is an order greater than this.

For the reasons just outlined, the work will be concerned with the preparation and properties of highly stable films. Before considering the specific aims of this thesis an introduction will be given to the important parameters concerned with dielectric films.

1.2 Important Parameters Concerned With Dielectric Films

1.2.1 Loss and Permittivity Concepts

With all dielectrics there will be associated both direct current (D.C.) and alternating current (A.C.) conductivities depending on the nature of the applied voltage. The D.C. conductivity can simply be studied by measuring the current flow across the dielectric when a D.C. voltage is applied. Study of the relevant mechanisms of conduction can generally be split into two regions involving either low or high field effects.

The A.C. conductivity is usually discussed in terms of the loss tangent, tan δ, defined by

$$\text{Tan } \delta = \frac{1}{\omega RC} \qquad (1)$$

where 'R' and 'C' are the parallel components of A.C. resistance and capacitance as shown in Figure (2). The angle 'δ' is defined in Figure (1). The complex impedance 'Z' of the parallel circuit in Figure (2) is given by

$$Z = \frac{1}{1 + j\omega CR} \qquad (2)$$

Another method of introducing the concept of dielectric loss is to consider the dielectric to have a complex permittivity. The term permittivity can be

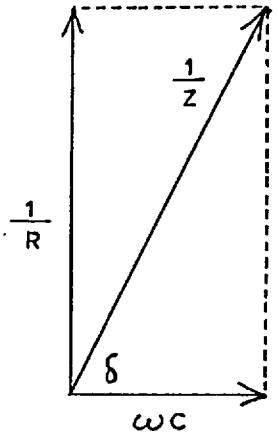

FIG. 1 ADMITTANCE VECTOR DIAGRAM SHOWING PARALLEL COMPONENTS OF CAPACITANCE AND RESISTANCE

LOSS TANGENT $\tan \delta = \frac{1}{\omega RC}$

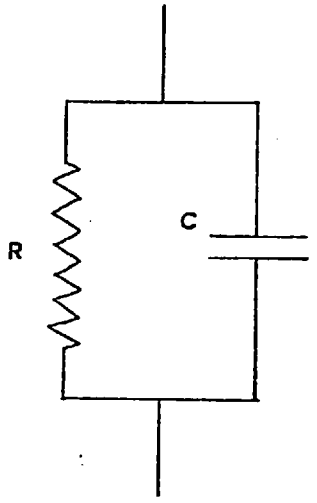

FIG. 2 EQUIVALENT PARALLEL RESISTANCE AND CAPACITANCE

COMPLEX IMPEDANCE $Z = \frac{R}{1 + j\omega CR}$

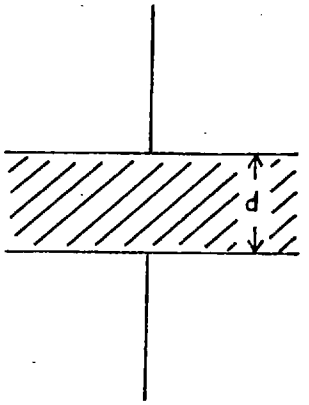

AREA OF EACH ELECTRODE A

FIG. 3 PARALLEL PLATE CAPACITOR

CAPACITANCE $C = \frac{\varepsilon A}{d} = \varepsilon C_o = \varepsilon_r \varepsilon_o C_o$

COMPLEX IMPEDANCE $Z = \frac{1}{j\omega C_o \varepsilon_o (\varepsilon' - j\varepsilon'')}$

defined as the ratio of the capacitance of a parallel plate condensor, 'C', with the dielectric present to the capacitance of the equivalent vacuum filled capacitor 'C_o'. The equation for the capacitance of a parallel plate capacitor is given by

$$C = \frac{\varepsilon A}{d} = C_o \qquad (3)$$

The parameters are defined in Figure (3).

In this text, the term permittivity will henceforth refer to the dielectric constant, sometimes called the relative permittivity 'ε_r', given by

$$\varepsilon = \varepsilon_r \varepsilon_o$$

where ε_o is the permittivity of free space.

For a capacitor having loss, 'ε_r' will be the complex permittivity and can therefore be split into its real and imaginary components

$$\varepsilon_r = \varepsilon' - j\varepsilon''$$

The impedance of the parallel plate capacitor is

$$Z = \frac{1}{j\omega C} = \frac{1}{j\omega C_o \varepsilon_o (\varepsilon' - j\varepsilon'')} \qquad (4)$$

Comparing equations (2) and (4) and equating real and imaginary parts,

$$C = C_o \varepsilon_o \varepsilon'$$

and

$$\frac{1}{R} = \omega \varepsilon_o C_o \varepsilon''$$

Combining these gives

$$\frac{1}{\omega RC} = \frac{\varepsilon''}{\varepsilon'}$$

which has previously been defined as tan δ, the loss tangent.

The conductivity of the dielectric is defined by[11]

$$\sigma = \omega \varepsilon_o \varepsilon''$$

A capacitor is introduced into a circuit as a component to store charge and the associated loss can introduce complications. It is therefore desirable to keep the loss to a minimum. This is particularly important in capacitors involved in filter networks in which it is necessary that losses are kept below $0.1^{o}/o$ (i.e. tan δ = .001). However, high permittivity capacitors, used in such applications as de-coupling capacitors, can tolerate loss as high as $3^{o}/o$.

1.2.1.1 Extrinsic Conduction

In general there are two types of loss, intrinsic and extrinsic. The latter is generally due

to such inhomogeneities as 'pin-holes' and gives no information about the bulk properties of the dielectric. However, these play an important role in thin film capacitors and consist of micro-fissures or flaws. Their origin is uncertain and a number of explanations have been put forward. These include shadowing by lumps of evaporant from the source, and the presence of dust on the substrate. However, it seems likely that the flaws originate during the coalescent stage of film growth when islands merge to form an almost continuous surface. Electron micrography[12] has shown that the flaws do not form continuous straight paths through the film but probably exist as random worm-like paths. This is supported by the fact that when films are etched, the etch usually manages to find its way right through the film so as to etch the metal base electrode, and this can be observed in the electron microscope.

The most usual method of removing the pin-holes is to discharge a capacitor at about 100 volts[142] across the electrodes. The majority of the current passes through the 'pin-hole' causing local heating and the top metal electrode is usually vaporised[45]. This effect of 'burning out' a 'pin-hole' is something of a misnomer since the 'pin-hole' still exists but no longer has an electrical contact to it.

Great care is required in interpreting results when 'pin-holes' are present as the 'pin-hole' conduction will probably dominate.

1.2.1.2 Intrinsic Conduction

Once all extrinsic effects have been removed, the conduction will be determined by intrinsic factors; either by the bulk properties as in A.C. conductivity and some forms of D.C. conductivity, or by electrode limitation as observed in certain types of D.C. conductivity. Both D.C. and A.C. conduction will be discussed in later sections.

There are essentially three types of dielectric film which can be deposited, which are single crystal, polycrystalline or amorphous films. In general the former are difficult to prepare and do not make good insulators. Therefore, films deposited as capacitor dielectrics will have an amorphous structure (see Section (2.1)) and direct electrical paths through the material are unlikely.

1.2.2 Mechanical Stability

The mechanical stability of films is measured in terms of stress. The majority of dielectric films are in a state of tensile stress after deposition

which usually makes them mechanically unsuitable for use as capacitor dielectrics. The tensile stress causes the films to crack, developing electrical shorts[13, 14]. A small compressive stress appears to produce the more acceptable films electrically. However, high values of compressive stress will cause the films to buckle, and again they will be electrically useless.

Silicon oxide[46] and zinc sulphide[15, 16] are two materials which can be deposited in a state of compressive stress, but the stress depends very much on the evaporation conditions. The stress in zinc sulphide is increased by increasing the rate of evaporation but decreased by increasing both the thickness and the temperature.

Priest and Caswell[46] showed that at low pressures, $< 5.10^{-6}$ Torr, the residual mechanical stress in silicon oxide was a function of the evaporation source temperature only, which implied that the composition of silicon oxide film was a function of evaporation source temperature.

In 1962 Priest et al[47] studied the effect of residual gases on the stress in silicon oxide. Above 1500°C they found that residual gases had little effect but at lower temperatures, water vapour had the most pronounced effect. They suggested that the water vapour

roduced stress by promoting oxidation, since water vapour was found to be the principal residual gas in an unbaked system, being an order of magnitude more prevalent than oxygen. By increasing the pressure from 10^{-7} to 210^{-6} Torr, the refractive index was reduced from 2.0 to 1.6 indicating the formation of a higher oxide, by either water vapour or oxygen oxidation. However, at low pressures and fast rates of deposition, the films were incompletely oxidised and hence unstable as they ruptured when exposed to air.

Carpenter[17] has recently been investigating the electrical properties of silicon oxide films as a function of their stress. Figure (4) shows the loss tangent as a function of stress from which it is clear why films in compressive stress are prepared as capacitor dielectrics. He also found that the aluminium electrodes and source size affected the stress.

Stress in dielectric films is far from understood and it is essential to define the deposition parameters and subsequent heat treatment when referring to the state of stress.

1.2.3 Breakdown Field

As in the case of loss in dielectric films, breakdown can be either extrinsic or intrinsic[45].

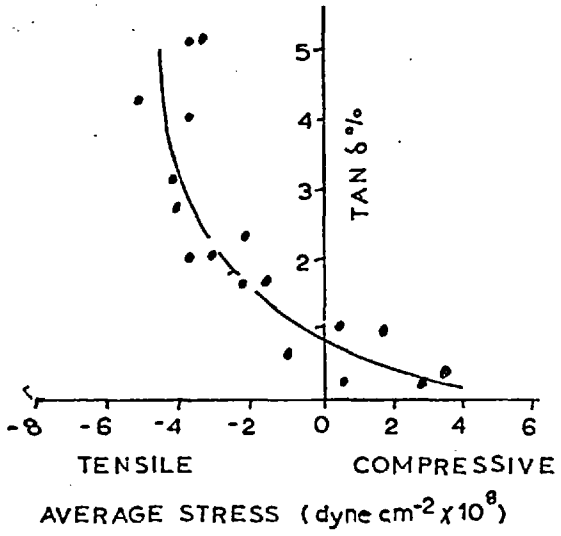

FIG. 4 : LOSS AS A FUNCTION OF STRESS FOR ALUMINIUM-SILICON MONOXIDE FILMS.

Extrinsic breakdown is probably due to pin-holes, whereas intrinsic breakdown is due to rapid local heating giving rise to thermally-excited ions or electrons initiating 'avalanches' of current carriers. In practical applications, the field at which breakdown occurs is required to be as high as possible which can be achieved by increasing the film thickness. However, this results in a reduction of capacitance per unit area and so it is often necessary to use an intermediate thickness as a compromise.

1.2.4 Low Ageing and High Temperature Stability

Both the permittivity and loss of a freshly produced capacitor tend to exhibit ageing effects. This phenomenon can usually be removed by a high temperature anneal (up to 400°C). The effect of temperature on the permittivity is measured in terms of the temperature coefficient of capacitance (T.C.C.) defined by

$$\gamma_c = \frac{1}{C}\left(\frac{\partial C}{\partial T}\right)_P$$

This is related to the permittivity through the equation for a parallel plate capacitor

$$C = \frac{\varepsilon_o \varepsilon' A}{d}$$

Differentiating with respect to temperature at constant pressure gives

$$\frac{1}{C}\left(\frac{\partial C}{\partial T}\right)_P = \frac{1}{\varepsilon'}\left(\frac{\partial \varepsilon'}{\partial T}\right)_P + \alpha_l$$

where α_l is the linear expansion coefficient, assuming that the dielectric has isotropic expansion.

Defining $\frac{1}{\varepsilon'}\left(\frac{\partial \varepsilon'}{\partial T}\right)_P = \gamma_P$ (the temperature coefficient of permittivity) then $\gamma_C = \gamma_P + \alpha_l$

1.3 Aim of Project

From the previous pages it is clear that the good temperature stability is a necessary and important feature of thin film dielectrics. The effect of temperature on the capacitance is not yet fully understood and in order to examine this, it is important to consider annealing behaviour and both D.C. and A.C. loss mechanisms.

The main aim of this project is to study the temperature coefficient of capacitance and permittivity, (γ_C and γ_P) with a view to determining the factors involved.

Evaporated SiO has been selected for the study as such films are widely used in thin film circuits.

CHAPTER 2

BASIC CONCEPTS AND THEORY

2.1 Energy Band Structure

The majority of thin dielectric films, deposited as capacitor dielectrics, have an amorphous or poly-crystalline structure. Energy band considerations are usually associated with the periodicity of the crystal lattice, applied to metals and semi-conductors. Lamb[18] discusses its applicability to amorphous materials in which there is a complete absence of long range order. There is, however, short range order which is evidenced by radial distribution function measurements on electron diffraction patterns[19]. The broadening of discrete energy levels into bands occurs for two atoms as they approach one another. Therefore, if the separation of atoms varies only slightly, because of the short range order, this broadening will occur irrespective of the long range order. The disorder of an amorphous material introduces variation of the broadening into energy bands between atoms, which gives rise to diffuse edges to the energy bands as shown by Gubanov[20].

Although the form of the energy band diagram as applied to amorphous insulators is rather uncertain, it is necessary to give a qualitative picture in order to

identify parameters used in electrical conductivity equations. Semi-conductor terminology will be used and the difficulties of applying the concepts to dielectric materials will be shown.

Figure (5) shows the energy band diagrams of a metal and an insulator before contact is made. The effect of surface states may be considered to be negligible implying that there will be no extrinsic band bending in the insulator before contact.

The work functions of possible metal electrodes ψ_m varies from 1.8 eV for caesium to 5.3 eV for platinum, with the work function of aluminium of 4.2 eV, probably the most common electrode material. The work function of the insulator is made up of the elctron affinity χ, which appears to be an unknown quantity, but probably of the order of 1 eV, and the energy separation of the insulator fermi level and the bottom of the conduction band, E_b. In the undisturbed insulator, E_b will be equal to half the forbidden energy band gap, E_g, which will be greater than 8 eV for most of the common dielectric insulators, and equal to 11 eV for silica [21]. For most metal-insulator combinations, therefore, the work function of the insulator will be greater than the work function of the metal.

When contact is made between a metal and insulator

FIG. 5

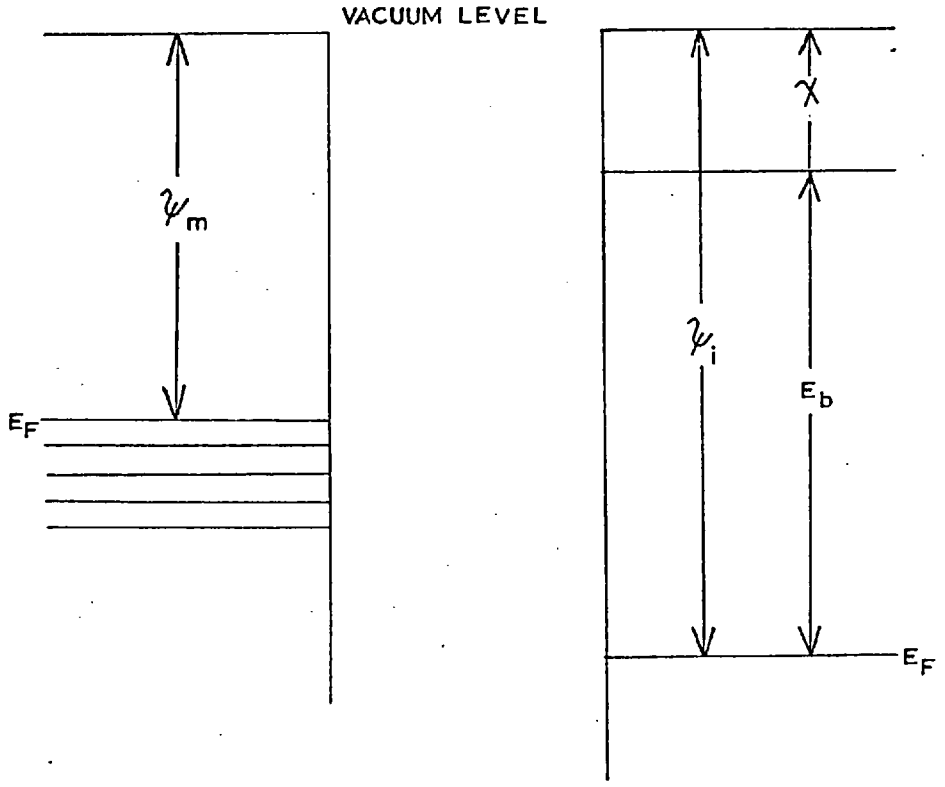

ENERGY BAND DIAGRAMS OF METAL AND SEMI-INSULATOR BEFORE CONTACT

thermodynamic equilibrium will have to be re-established and certain conditions have to be fulfilled. The fermi levels of the two materials will align and the vacuum level will be continuous across the interface[22, 23]. In the case of the semi-conductor with $\psi_{s.c.} > \psi_{m}$, electrons will flow from the metal into the semi-conductor, building up a space charge layer at the interface. An electrostatic field will be set up which will eventually limit further flow of electrons. The potential drop across the space charge region is given by the difference in work functions called the **contact** potential. This situation is shown in Figure (6) where the band bending is confined to a narrow region at the interfaces.

In the case of insulators, however, there will not generally be sufficient charge transport to allow complete band bending in the interface region. Simmons[24] suggested that for most insulators, the flat band condition is never reached, as the band bending extends to depths greater than the thickness of most dielectric films. Thermodynamic equilibrium was then attained by shifting the fermi level of the insulator towards the conduction band. This situation is illustrated in Figure (7).

In general, however, in order to describe the D.C. conduction parameters used in Section (2.2) we will use

FIG. 6

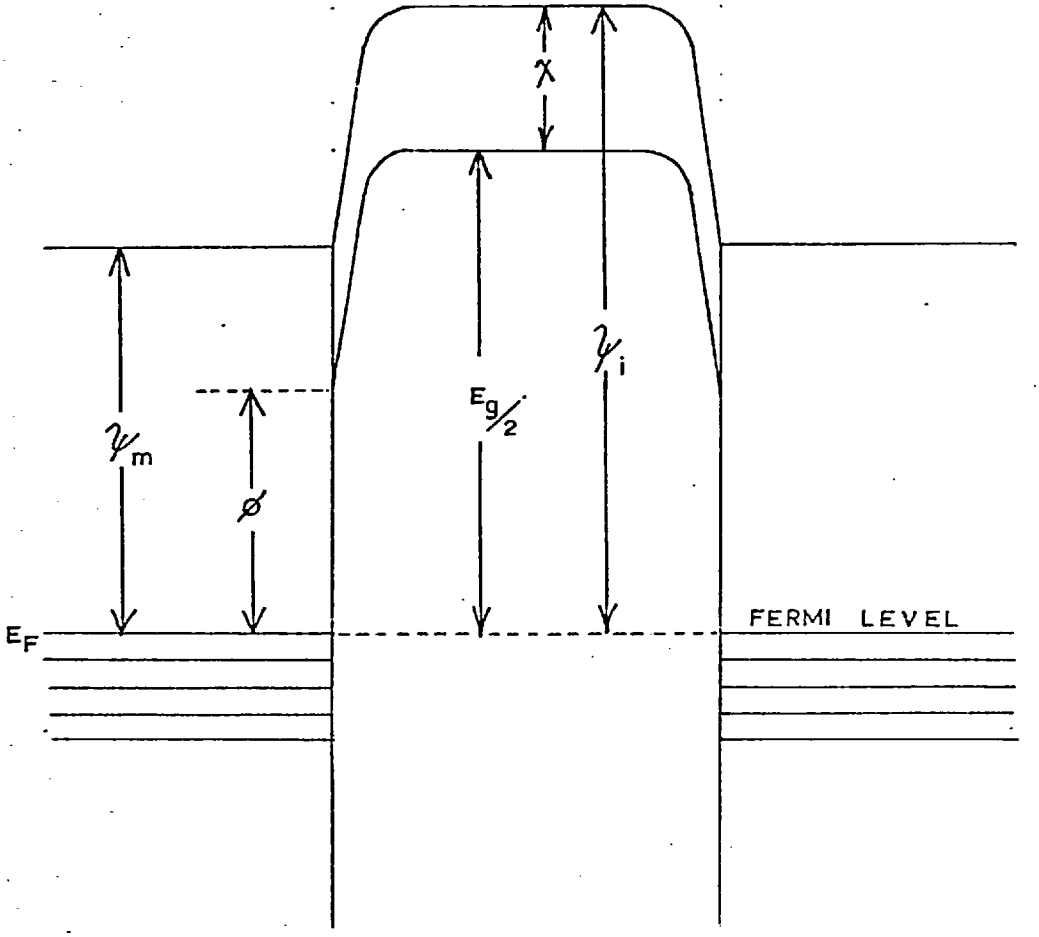

ILLUSTRATION OF ENERGY BAND DIAGRAM FOR METAL – SEMI-INSULATOR – METAL SANDWICH AT ZERO BIAS ($\psi_i > \psi_m$)

FIG. 7

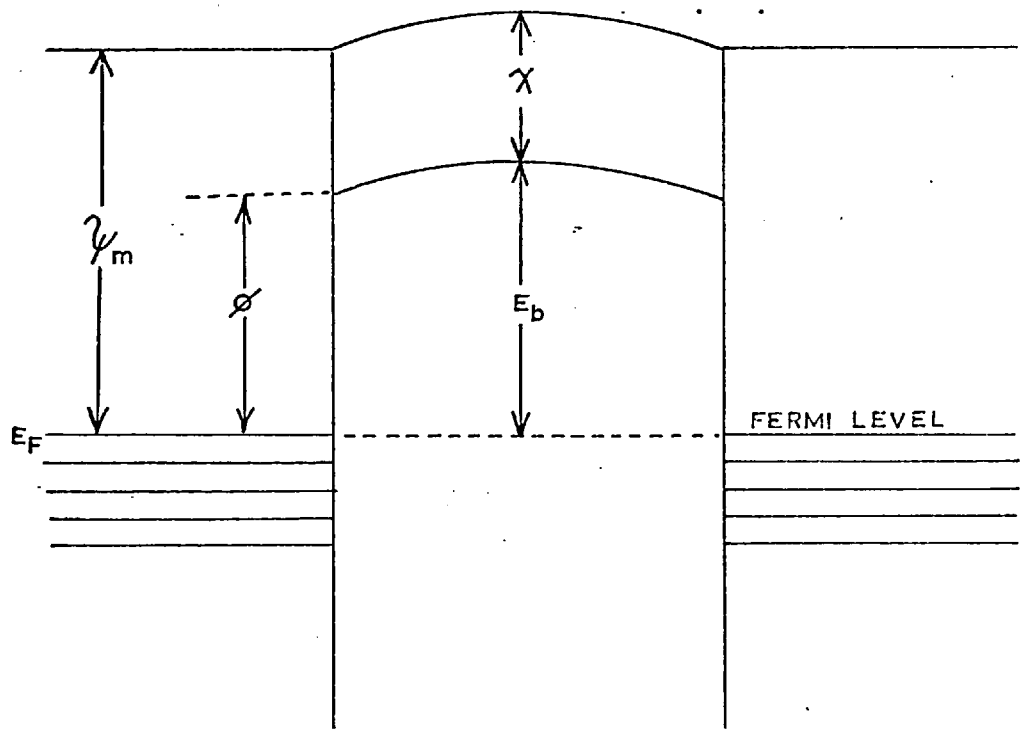

ENERY BAND DIAGRAM OF METAL-INSULATOR-METAL SANDWICH AT ZERO BIAS WHERE FLAT BAND CONDITION IS NOT REACHED

a band picture, for simplicity, in which the flat band condition is reached.

A consequence of any general amorphous structure is the creation of localised energy levels due to time dependent fluctuations of local atomic arrangements. These fluctuations will be numerous[18] and will have a life-time long enough to capture electrons. In liquids, the life-time will be of the order of 10^{-12} seconds, but in amorphous dielectrics these 'states' can be considered as effectively frozen in. Such states will be spatially localised and will generally have energies within the forbidden energy gap. Jonscher[25] points out that impurity densities of at least 10^{19} cm^{-3} are required to make an impression on the intrinsic conductivity of many amorphous dielectric films. Such a density of donors or acceptors in a crystalline material would change the conductivity considerably. However, in the semiconductor, the donor or acceptor atoms are gnerally ionized, contributing free carriers to the bulk material. In the dielectric, with the localised states having energies well within the band-gap, the carriers are mainly trapped. Thus, to account for the conductivities actually observed in the dielectric, it is necessary to postulate densities of localised states of 10^{19} cm^{-3} or more.

2.1.1 Electrical Contacts

We will now consider the behaviour of electrical contacts with particular reference to the proposed band picture of the dielectric.

Considering first the case of zero or low fields, the situation shown in Figure (6) will apply. For usual values of $\emptyset$, such as for silicon oxide, the contact will be blocking to electrons for conduction band processes. Therefore, for films thick enough to have a negligible tunnelling contribution, i.e. > 50Å thick, the only electronic current will be by impurity hopping conduction (see Section (2.2.4)). In the case of amorphous insulators, the impurity states will probably be the localised states discussed in the previous section. If the energy levels of these sites are sufficiently close to the fermi level, then electrons will be able to enter these levels from the metal. The electrical contact can therefore be considered blocking to conduction band processes but ohmic with respect to impurity type conduction.

At high fields, electrons may enter the conduction band of the insulator (see Section (2.2.2). In such a case the contact can be termed ohmic as defined by Hill[26] as a contact at which there is an inexhaustible supply of free carriers.

It is likely that, due to the distribution of localised states throughout the forbidden band, an ohmic contact will exist at low fields with almost any electrode material, as observed experimentally.

2.2 D.C. Conduction Mechanisms in Dielectric Thin Films

2.2.1 Introduction

There are three modes of conduction in a dielectric under an applied D.C. field, each of which can be space charge limited. Figure (8) illustrates the possible conduction mechanisms and shows the situation with a field applied. In the first type of conduction, the current is carried by electrons in the conduction band of the insulator. There are several possibilities as to the source of the electrons. If the barrier ϕ is small, say less than 'kT', then electrons will be supplied directly from the metal at sufficiently high temperatures. However, in most practical cases, ϕ is a few electron volts and thermal excitation has to be sufficient to surmount the interface barrier which is lowered by the applied field. This process is referred to as Schottky Emission (S.E.). The electrons may also be thermally excited into the conduction band from "trapping" levels in the forbidden band of the insulator

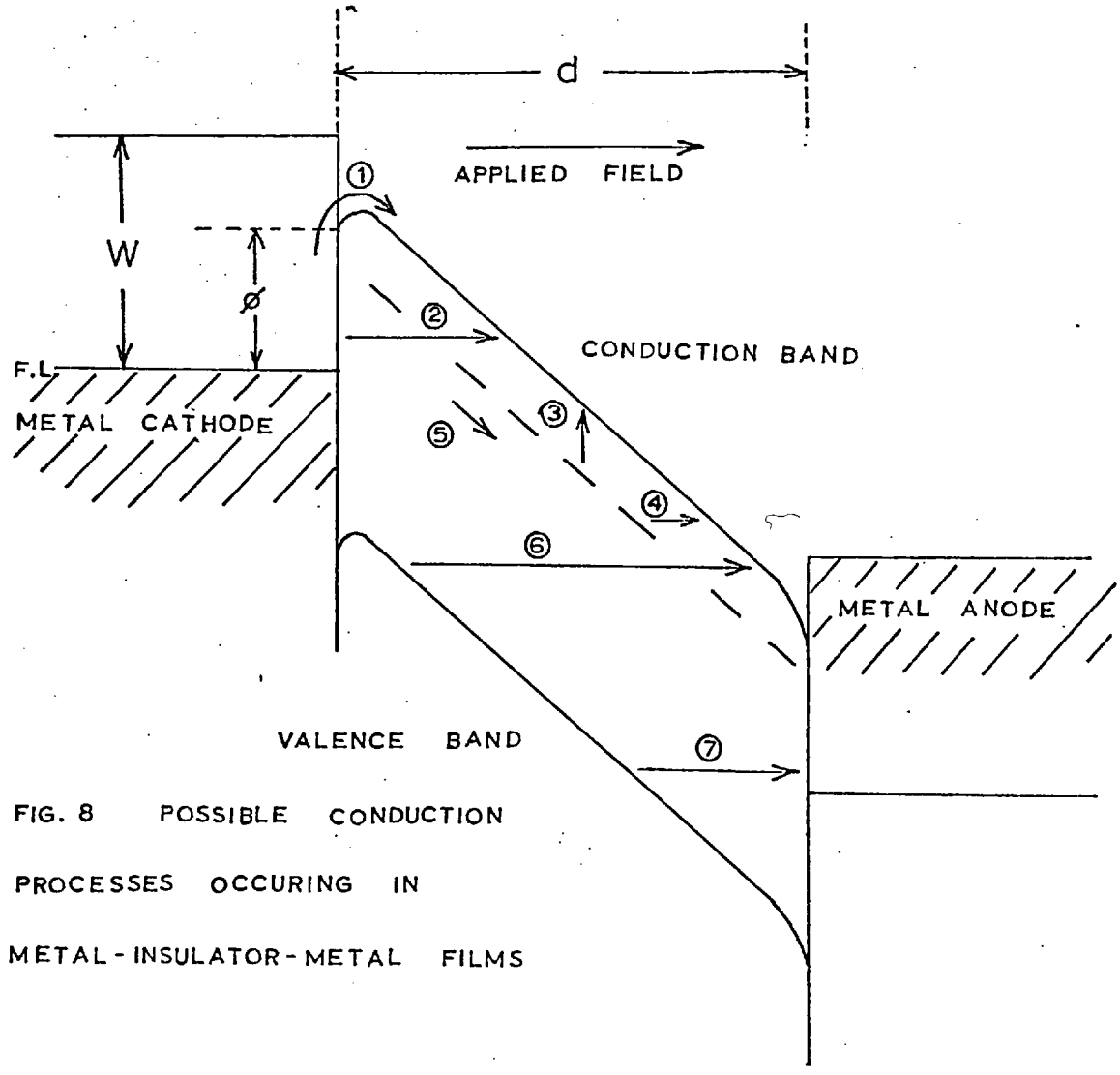

FIG. 8 POSSIBLE CONDUCTION PROCESSES OCCURING IN METAL-INSULATOR-METAL FILMS

① THERMAL OR SCHOTTKY EMISSION.

② TUNNELING FROM CATHODE TO CONDUCTION BAND FIELD EMISSION IN VACUUM CASE.

③ THERMAL EXCITATION FROM TRAPS INTO CONDUCTION BAND.

④ FIELD IONIZATION FROM LOCALIZED IMPURITY LEVELS INTO THE CONDUCTION BAND.

⑤ IMPURITY CONDUCTION.

⑥ TUNNELING FROM VALENCE TO CONDUCTION BAND.

⑦ TUNNELING FROM VALENCE BAND TO ANODE.

⑧ TUNNELING DIRECT FROM CATHODE TO ANODE - REQUIRES LOW VOLTAGES AND SMALL 'd' — NOT ILLUSTRATED.

and this is referred to as the Poole-Frenkel effect.

The second type of conduction involves the tunnelling of electrons. They may tunnel into the conduction band of the insulator directly from the metal cathode, from the trapping levels in the insulator or from the valence band of the insulator. The latter may also be the source of electrons tunnelling directly into the metal anode. Tunnelling may also take place between the two metal electrodes, if the dielectric is thin enough. In general tunnelling can only take place where the electronic wave functions overlap the region of allowed energy states.

The last type of conduction involves defects, which may be impurities in the dielectric, causing either impurity or ionic conduction. Impurity conduction involves electron flow from one stationary donor to the next, whereas ionic conduction is the actual movement of the impurity or defect contributing to the current.

In many of these cases, such as that of charge injection into the conduction band, tunnelling or impurity conduction, the rate limiting process is space charge build up in the dielectric. Most of the applied voltage is then dropped across the space charge region causing a non-uniform field distribution across the dielectric.

These various conduction mechanisms will be studied in a little more detail and where possible the resulting current-voltage characteristic given.

2.2.2 Electron Conduction in the Conduction Band of the Insulator

For the case of Schottky Emission into the conduction band and neglecting trapping and space charge effects, the current density in the dielectric is given by[18]

$$J = A(1 - r)T^2 \exp (\beta V^{\frac{1}{2}} - \phi)/kT \qquad (1)$$

where $\beta = \frac{1}{2} \left(\frac{e^3}{\pi + \varepsilon' \varepsilon_o}\right)^{\frac{1}{2}}$ and $A = \frac{4\pi emk}{h^3}$

V is the applied voltage and ϕ is the height of the surface potential as shown in Figure (6). A is the Dushman-Richardson constant and has the numerical value of 120 amps/cm^2/degree, r is the reflection coefficient of electrons at the barrier.

In the case of the Poole-Frenkel effect, the current density is given by[18]

$$J = B \exp (2\beta V^{\frac{1}{2}} - \phi)/kT$$

where B is a constant and β has the same definition

as for Schottky Emission. The energy ϕ in this case is associated with a trap depth below the conduction band of the insulator. In this case, however, it is the trap barrier which is lowered by twice the amount for Schottky Emission lowering.

It will be seen that the current-voltage relationship is the same form for the above two cases. They may be distinguished by their different temperature behaviour and their different coefficients of $V^{\frac{1}{2}}$.

Jonscher[25] has examined the assumptions explicit in the derivation of the Poole-Frenkel equation. He modified the model of the Poole-Frenkel effect by allowing for the fact that the probability of escape will be a function of the direction of escape compared to the direction of the applied field. The Poole-Frenkel lowering of the trap barrier will only apply in the direction of the applied field and an electron will find it more difficult to escape in other directions. The resulting barrier lowering will be $\beta(V \cos \theta)^{\frac{1}{2}}$ where θ is the angle between the applied field direction and the direction of escape. After release there are two possibilities as to the fate of the electron.

Firstly, the electron may be re-trapped in the first centre that it comes across in its path. For a high field the current can then be approximated by

$$I = I_o \left(\frac{kT}{\beta V^{\frac{1}{2}}}\right) \exp\left(\frac{\beta V^{\frac{1}{2}}}{kT}\right)$$

where I_o is a constant.

The second possibility is that the electron will have a constant life-time before being retrapped.

The results of Servini[27] suggested that the first possibility was the more likely.

Jonscher also points out that it is unlikely that the potential barrier of a trap will be Coulombic. Even at a field of 10^5 V/cm the maximum in the potential barrier will be at 50Å from the centre of the trap. He suggests that the inside of the potential well will be much steeper than Coulombic. This would result in an artificially high dielectric constant for the Poole-Frenkel effect.

2.2.3 Conduction Involving Tunnelling

The various modes of tunnelling discussed in the introduction will not be discussed individually. A general analysis of the situation has been given by Price and Radcliffe[28]. Fowler and Nordheim[29] discuss transmission probabilities in an early paper and other workers in the field such as Harrison[30], Schnupps[31, 32] and Hill[26] have discussed the subject in some detail.

The formation of the current-voltage relationships

is difficult due to the complex nature of the parameters involved. Basically, this involves the calculation of electron tunnelling probabilities through a potential barrier. The main difficulty arises in formulating the barrier shape and electron supply functions and performing the resulting integrations. Simmons[33] has performed numerical calculations for specific situations. The shape of the potential barrier will depend on space charge[34-37], image forces[38] and the position and density of traps in the insulators[39].

The resulting current-voltage characteristics are dependent to a large extent on the applied voltage but are generally of the form

$$J = AV^n \exp(-\frac{B}{V})$$

A and B are constants and $1 \leqslant n \leqslant 3$.

The tunnelling processes mentioned above, generally occur at high fields but for films less than 50Å thick[22], direct tunnelling between the electrodes can occur at low fields.

2.2.4 Electronic Conduction Via Impurities

This type of conduction is often difficult to observe since the low mobility of electrons in the impurity level is generally masked by electrons in the

conduction band. However, by definition an insulator will have a very low density of thermally generated free carriers in the conduction band. In the case of semi-conductors both donors and acceptors must be present, the latter removing electrons from the donors so that conduction can take place between occupied and unoccupied donors.

There are two possible modes of transition of an electron between donors. The electrons can either tunnel through the potential barrier separating the sites[40, 41] or it may gain sufficient energy to surmount the barrier[42, 43]. Present evidence favours tunnelling as is suggested by Johansen[44].

Hill[26] determines the current-voltage relationship by considering the effect of the field on the potential barrier of an impurity. If E_i is the energy required to ionise an impurity for no applied field 'E' then the current density is given by

$$J = BV^{\frac{1}{2}} \exp\left(-\frac{E_i}{kT}\right) \sin h \frac{2\beta V^{\frac{1}{2}}}{kT}$$

where $$B = -2n_i e\left(\frac{x_o e}{2m^*}\right)^{\frac{1}{2}}$$

and $$\beta = \left(\frac{e^3}{4\pi\varepsilon_o \varepsilon' t}\right)^{\frac{1}{2}}$$

n_i is the density of impurity states and x_o represents the separation of sites.

Clearly, at low fields the relationship becomes ohmic. At high fields the sink term is replaced by an exponential term and results in a modified Poole-Frenkel relationship. Impurity conduction, often referred to as hopping, is tentatively suggested by Mead[48] to occur in Ta_2O_5 at low voltages and high fields. Hickmott[49] used impurity conduction to explain a negative resistance region.

For high concentrations of impurity it is possible for the site separation to be reduced to such an extent that metallic-like conduction will occur. This transition is discussed by Mott[50] in a recent review.

It should be emphasised that when discussing impurity conduction in amorphous insulators, the impurity sites refer to localised sites as discussed in the previous section. Since not all the localised sites will be occupied by electrons, it is not necessary to have the compensating acceptors, required by donor sites.

2.2.5 Conduction by Impurity or Defect Movement

Conduction involving the actual migration of impurities or defects is termed ionic conduction. The form of the current-voltage characteristics will

depend on the applied field E.

If the applied field is less than 10^5 V/cm, i.e. Eel << kT, then a calculation is employed similar to that in determining the jump frequency of diffusing ions. An ohmic characteristic results, of the form

$$J = C V e^{-\frac{\phi}{kT}}$$

where C is a constant, ϕ is the potential barrier height between two nearest neighbour defect sites separated by a distance 'l'.

For Eel $\simeq$ kT the barrier becomes appreciably distorted by the field and the current-voltage relationship becomes

$$J = A \exp - [(\phi - \frac{elV}{2t})/kT]$$

For very high fields such that Eel >> kT, the analysis becomes complicated by the occurrence of multiple hops. This region has been investigated by Bean[51], Young[52] and Vermilyea[53].

However a difficulty arises in distinguishing between ionic charge carriers and electronic carriers as discussed in the previous section, since an ohmic characteristic can result from both types of carrier. Generally, an activation energy ϕ of less than 0.1 eV, combined with a high mobility, will be electronic and

an activation energy greater than 0.6 eV with a low mobility will be ionic. There are three methods of distinguishing between ionic and electronic charge carriers when intermediate values of activation energy are involved. If the carrier is ionic, it means that after a sufficient time of application of a D.C. voltage, it will be possible physically to detect the transported material at the cathode. Secondly, the large transit time involved in the transport of ions could be detected by applying rectangular voltage pulses and observing the decay in current response.

The third method is to observe the current decay to a steady D.C. level, after applying a D.C. voltage. This decay is due to polarization effects and there are two theories to explain them. These involve different interpretations of the experimental results. The first was proposed by Joffe[54] and occurs when the electrodes are blocking, i.e. the carrier charges are not neutralised at the electrodes. This will cause a space charge to build up, across which most of the applied voltage will be dropped. The equation for current flow then refers to the initial current. The second theory suggests that there is a time dependent change in the dielectric constant which would be a property of the bulk dielectric, rather than an electrode

effect. The equation of current flow will then apply after a certain time when the the transient effect has died away.

2.2.6 Space Charge Limitations

The processes already mentioned may not necessarily be the rate limiting ones and it is very likely that space charge build-up in the dielectric may be the major impedance. We are not concerned in this summary with two carrier space charge limitations as they will apply to semi-conductors only. The two cases which apply to dielectrics will concern one carrier with or without traps, which can be either deep or shallow.

The case of no traps[35, 55, 56] is analogous to the case of the vacuum diode except that scattering of electrons in transit will occur. The Mott and Gurney equation[35] for the current density gives

$$J = \frac{9}{8} \varepsilon_s \mu \frac{V^2}{t^3}$$

This equation only applies to low fields and is not valid near the injecting contact where the field is nearly zero, and the current becomes a diffusion current.

The effect of localised shallow traps is to reduce

the current by a factor θ , the ratio of free to trapped charge, which can be as low as 10^{-7}:

$$J = \frac{9}{8} \theta \varepsilon_s \mu \frac{V^2}{t^3}$$

The effect of deep trapping levels which are not localised is to charge the characteristcs considerably in a manner determined by the energy distribution of traps. In this case, the current density is given by

$$J = \frac{9}{8} \varepsilon_s \mu \frac{V}{t^2} \left(\frac{n_o e}{C}\right) e^{nV}$$

where n_o is the free carrier concentration, C is the capacitance of the film and $n = \dfrac{C}{N_t e t kT}$ is the trap density.

A plot of log J versus log V should indicate the type of conduction which is applicable but this is not always straightforward.

2.2.7 Other Processes

Experimental results show that charge transport in a dielectric is often not clearly defined by a particular conduction process, with a straightforward form for the current-voltage characteristics. Such an example was described by O'Dwyer[57], who machine-calculated the current-voltage characteristics

for his model over several decades of current. The model required a single deep trapping level with numerous shallow traps. He took into account Fowler-Nordheim emission[29], into the dielectric and subsequent space charge build-up in the body of the dielectric and he found that log I α $V^{\frac{1}{2}}$ over several decades of current, which was not the case when electron injection into the dielectric was by Schottky Emission.

In order to explain the anomalous Poole-Frenkel effect observed in silicon oxide, Simmons[58] postulated a model which took into account field-assisted thermionic emission from a deep donor centre into a shallow neutral trapping level. The resulting bulk conductivity was field dependent and had the same form as Schottky Emission, although the Poole-Frenkel effect was the operating mechanism.

2.2.8 Summary on D.C. Conduction Processes

It now becomes possible to generalise D.C. conduction processes to dielectric films that are suitable for capacitor applications by taking into account the general band picture which was established in Section (2.1). Since the materials of interest will have band gaps greater than 8 eV, then the interface barrier $\emptyset$ will be more than 1 eV. Therefore, at low

fields Schottky Emission can be eliminated (see Hill[26]). Film thickness will need to be greater than 1000Å due to breakdown considerations and therefore the tunnelling processes illustrated in Figure (8) can be neglected. There remains only electronic impurity conduction and ionic conduction as low field conduction mechanisms, both of which result in ohmic characteristics. It is possible to postulate electronic "impurity" conduction because the localised states in an amorphous material will be distributed throughout the forbidden band[25]. An electron will therefore be able to enter the dielectric probably with a thermally assisted jump into a localised level.

In the case of high fields it is not possible to generalise to the same extent as for low field conduction. However, the low field conduction processes will probably be overshadowed by electrons entering the conduction band of the insulator. The extent to which high field conduction processes can be investigated will be limited, ultimately, by the breakdown strength of the material. The most likely process to occur will be Schottky Emission and the Poole-Frenkel effect or some modified form of these mechansims. It is possible also that space charge accumulation might be the controlling factor (see Frank and Simmons[23]).

2.3 A.C. Conduction

2.3.1 Introduction

The basic concepts of permittivity and loss associated with a dielectric were briefly outlined in the introduction. The D.C. contributions discussed in the previous section will always be present but will only be significant at very low frequencies. It is usual to apply only low field A.C. voltages. The loss resulting from D.C. contributions will be given by $\text{Tan } \delta = 1/\omega RC$ where R is the D.C. resistance and will therefore decrease proportionally with frequency. However, at frequencies in the audio range and even at frequencies as low as .01 c/s, the D.C. conduction can be masked by relaxation losses. An increase in temperature generally causes relaxation peaks to shift to higher frequencies and since D.C. conductivity increases exponentially with temperature, the D.C. contribution will tend to dominate at low frequencies.

2.3.2 Basic Mechanisms of Dielectric Polarization

The polarization 'P' of a dipole is determined by the local field E_i, acting upon it and is given by

$$P = \frac{\alpha_n}{V} E_i \qquad (1)$$

where α_m is the polarizability of a macroscopically small volume of dipoles V. For the case of infinitely small, mutually interacting dipoles, the local field 'E_i' is given by the Lorentz[11] equation

$$E_i = \frac{(\varepsilon' + 2)}{3} E \qquad (2)$$

where E is the applied field.

Combining equations (1) and (2) gives the well-known Clausius-Mosotti equation

$$\frac{(\varepsilon' - 1)}{(\varepsilon' + 2)} = \frac{\alpha_m}{3\varepsilon_o V}$$

In general the polarizability can be split into its four contributions

$$\alpha_m = \alpha_e + \alpha_a + \alpha_d + \alpha_i$$

where 'α_e' and 'α_a' are the electronic and atomic contributions and are intrinsic properties of the material, and 'α_d' and 'α_i' are the dipole and interfacial contributions and will usually be extrinsic properties. Each contribution will now be considered in more detail.

2.3.2.1 Electronic Polarizability α_1

This mechanism, sometimes referred to as the optical polarizability, is the displacement of the electron cloud of an atom with respect to its positive nucleus, under the influence of an applied field. For materials with small constituent ions, such as polymers, this mechanism will often dominate. The permittivity is given by the refractive index squared and is significant at ultra-violet and lower frequencies. For the frequencies dealt with in this thesis, this polarization can be considered to take place instantaneously and will therefore not contribute to the loss[59].

2.3.2.2 Atomic Polarizability α_a

The atomic polarizability can be considered as arising from two sources[11]. Firstly, a dipole is formed by the separation of two molecules of opposite sign. Although the movement is not so rapid as in the case of electronic polarization, it can be considered instantaneous in this context, and will therefore not contribute to loss.

For relatively simple compounds such as the alkali halides, the permittivity is given by the Born equation[60]

$$\varepsilon_i = \frac{e^2}{2 \xi_o \omega_o^2 a^2} \left(\frac{1}{M} + \frac{1}{m}\right)$$

where 'M' and 'm' are the masses of the constituent ions, 'a' is the lattice constant and ω_o the infrared absorption frequency.

The second type of atomic polarizability involves the deformation of the electron cloud as a consequence of the movement of ions. This is particularly important for such compounds as oxides where the oxygen ion is large and very deformable[61]. Again, the contribution to loss can be neglected.

For both types of ionic polarizability the polarization will only be operative for frequencies at and beyond the infrared.

2.3.2.3 Orientational Polarizability α_d

This could be described as a third type of atomic polarizability in which the atoms are able to rotate about an axis of symmetry[11]. The atom could be either a constituent atom of the material giving intrinsic polarization or an impurity atom giving extrinsic polarization. There is generally a single relaxation time involved and the frequency behaviour of both the loss and permittivity are related by the Debye equations. The temperature dependence will usually be determined by the Langevin relationship[11].

2.3.2.4 Interfacial Polarizability α_i

Interfacial or space charge polarization represents rather a different situation from the previous mechanisms. In this case, transport of charge carriers occurs, causing a pile up of charge, either at the dielectric-metal interface or against inhomogeneities. This will have the effect of large scale distortions on the elctric field. The image charge, induced by the accumulation of charge at a barrier, produces an effective dipole. This mechanism will probably dominate at frequencies less than 1 c/s. Although the process is usually described mathematically as a single relaxation time process, in practice a distribution of relaxation times occurs.

Because of the low frequency nature of interfacial effects, they will sometimes appear as anomalous absorption currents superimposed on a steady D.C. conduction process.

2.3.3 Single Relaxation Time Processes

The frequency behaviour of the permittivity and loss tangent, 'Tan δ' near a dispersion can be described by the Debye equations. Because the dielectric flux density 'D' will generally lag behind the applied field 'E', the permittivity 'ε_r' will be a complex

function, described by the integral equation[11]

$$\varepsilon_r = \varepsilon_\infty + \int_0^\infty \alpha(t)\, e^{-j\omega t}\, dt \qquad (1)$$

where 'ε_∞' is the permittivity at an infinite frequency and '$\alpha(t)$' is the decay factor which takes into account the polarization lag.

The Debye equations are a result of putting the decay factor in the form

$$\alpha(t) = \alpha(0)\, e^{-\frac{t}{\tau}} \qquad (2)$$

which introduces the relaxation time 'τ' of the mechanism. '$\alpha(0)$' is merely a constant.

Splitting up the complex permittivity into its real and imaginary parts,

$$\varepsilon_r = \varepsilon' - j\varepsilon''$$

the following equations result:-

$$\frac{(\varepsilon' - \varepsilon_\infty)}{(\varepsilon_s - \varepsilon_\infty)} = \frac{1}{1 + \omega^2 \tau^2}$$

$$\frac{\varepsilon''}{(\varepsilon_s - \varepsilon_\infty)} = \frac{\omega \tau}{1 + \omega^2 \tau^2}$$

$$\text{Tan } \delta = \frac{\varepsilon''}{\varepsilon'} = \frac{(\varepsilon_s - \varepsilon_\infty)\, \omega \tau}{(\varepsilon_s + \varepsilon_\infty \omega^2 \tau^2)}$$

ε_s is the static or D.C. permittivity.

The energy dissipated / sec / vol is proportional to the power factor, 'sin δ', where δ represents the phase lag. However, for small values of $\delta < 0.1$, 'sin δ' is approximated by tan δ which is called the dielectric loss. These equations apply to nearly all types of relaxation mechanisms with a single relaxation time.

A convenient way of plotting results in order to determine the constants involved was derived by Cole and Cole[62]. Eliminating the frequency, ω, from the equations for 'ε'' and 'ε''' gives the following equation which is in the form of a semi-circular plot as shown in Figure (9)

$$[\varepsilon' - \frac{(\varepsilon_s + \varepsilon_\infty)}{2}]^2 + \varepsilon''^2 = \frac{(\varepsilon_s - \varepsilon_\infty)^2}{2}$$

Another similar method of plotting results was proposed by Scaife[63] in which the polarizabilities are plotted. This method has the advantages of giving more weight to high frequency measurements and since $0 \leqslant \alpha \leqslant 1$, it enables comparisons of materials whose permittivit es differ widely.

Using $$\alpha = \frac{\varepsilon_r - 1}{\varepsilon_r + 2} = \alpha' - j\alpha''$$

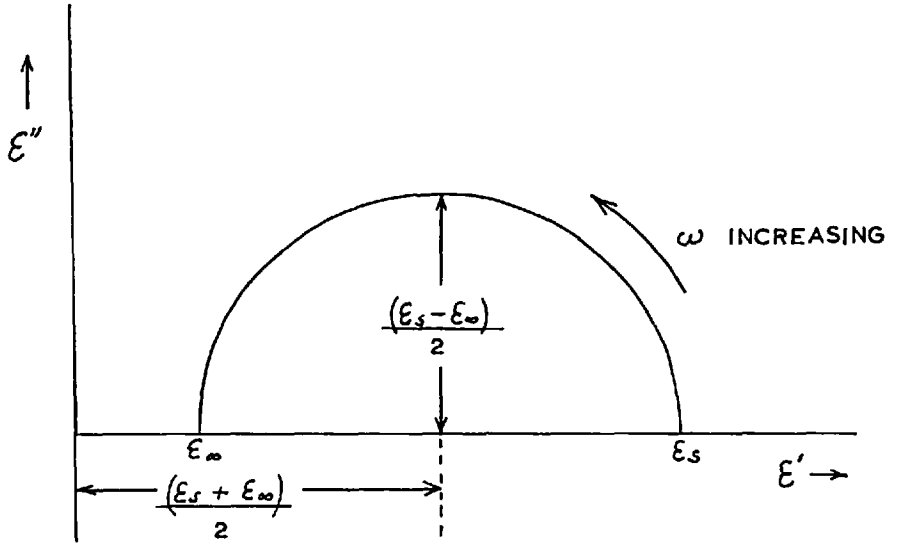

$$(\varepsilon')^2 - \varepsilon'(\varepsilon_s + \varepsilon_\infty) + \varepsilon_s \varepsilon_\infty + (\varepsilon'')^2 = 0$$

FIG. 9 COLE-COLE DIAGRAM FOR SINGLE RELAXATION TIME.

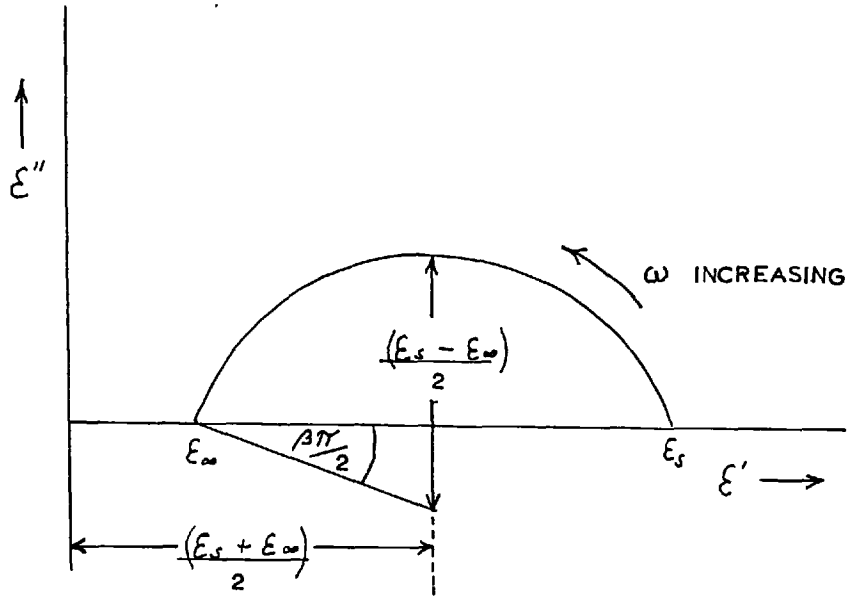

$$(\varepsilon')^2 - \varepsilon'(\varepsilon_s + \varepsilon_\infty) + \varepsilon_s \varepsilon_\infty + \varepsilon'' \mathrm{TAN}(\beta\pi/2)(\varepsilon_o - \varepsilon_\infty) + (\varepsilon'')^2 = 0$$

FIG. 10 COLE-COLE DIAGRAM FOR A DISTRIBUTION OF RELAXATION TIMES.

$$\alpha' = \frac{(\varepsilon' - 1)(\varepsilon' + 2) + \varepsilon''^2}{(\varepsilon' + 2)^2 + \varepsilon''^2}$$

$$\alpha'' = \frac{3\varepsilon''}{(\varepsilon' + 2)^2 + \varepsilon''^2}$$

A dispersion with a single relaxation time is characterised by a decrease in capacitance over about two decades of frequency (see curves for $\beta = 0$ in Figures (11) and (12).

2.3.4 Multiple Relaxation Time Processes

Very often in practice when the Cole-Cole diagram is plotted, a truncated semi-circle results. This is due to a distribution of relaxation times. If the angle $\frac{\beta\pi}{2}$ is defined as shown in Figure (10) then it can be shown that the complex permittivity is of the form

$$\varepsilon_r = \varepsilon' - j\varepsilon'' = \varepsilon_\infty + \frac{(\varepsilon_s - \varepsilon_\infty)}{1 + (j\omega\tau_o)^{1-\beta}}$$

where τ_o is the mean relaxation time and $0 < \beta < 1$. (The value of $\beta = 0$ is the case of the single relaxation time).

Defining $x = \log_e \omega\tau_o$

$$\frac{(\varepsilon' - \varepsilon_\infty)}{(\varepsilon_s - \varepsilon_\infty)} = \frac{1}{2}\left[1 - \frac{\sin h(1-\beta)x}{\cos h(1-\beta)x + \sin\frac{\beta\pi}{2}}\right]$$

$$\frac{\varepsilon''}{(\varepsilon_s - \varepsilon_\infty)} = \frac{1}{2} \frac{\cos \frac{\beta\pi}{2}}{\cos h(1 - \beta)x + \sin \frac{\beta\pi}{2}}$$

These curves have been calculated during the present work using a computer and are plotted in Figures (11) and (12). It becomes clear that for $\beta > 0$ the effect of a distribution of relaxation times is significant over several decades of frequency. For frequencies well removed from the relaxation frequency given by $\omega_o = \frac{1}{\tau_o}$ certain approximations can be made for the conductivity.

2.3.4.1 Limiting Approximations

For frequencies much less than $\frac{1}{\tau_o}$ i.e. $x \ll 0$, ε'' is given by

$$\varepsilon'' = \frac{1}{2} \frac{(\varepsilon_s - \varepsilon_\infty) \cos \frac{\beta\pi}{2}}{\cos h(1 - \beta)x + \sin \frac{\beta\pi}{2}}$$

but $\cos h(1 - \beta)x \gg 1$

$$\therefore \quad \varepsilon'' = \frac{1}{2} \frac{(\varepsilon_s - \varepsilon_\infty) \cos \frac{\beta\pi}{2}}{\cos h(1 - \beta)x}$$

$$2 \cos h(1 - \beta)x = e^{(1 - \beta)x} + e^{-(1 - \beta)x}$$

but $e^{-(1 - \beta)x} \gg e^{(1 - \beta)x}$

Using $x = \log_e \omega \tau_o$

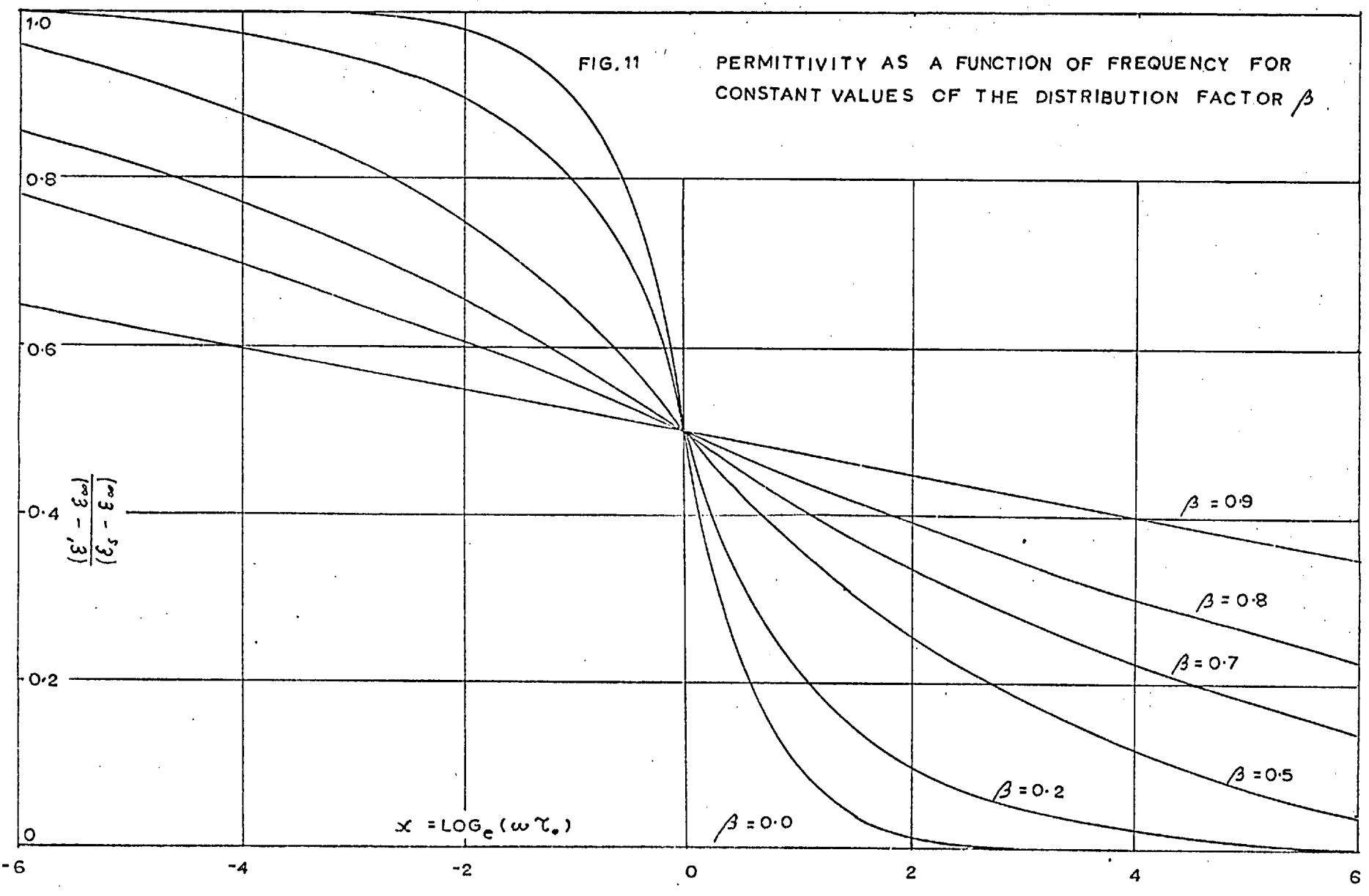

FIG. 11 PERMITTIVITY AS A FUNCTION OF FREQUENCY FOR CONSTANT VALUES OF THE DISTRIBUTION FACTOR β.

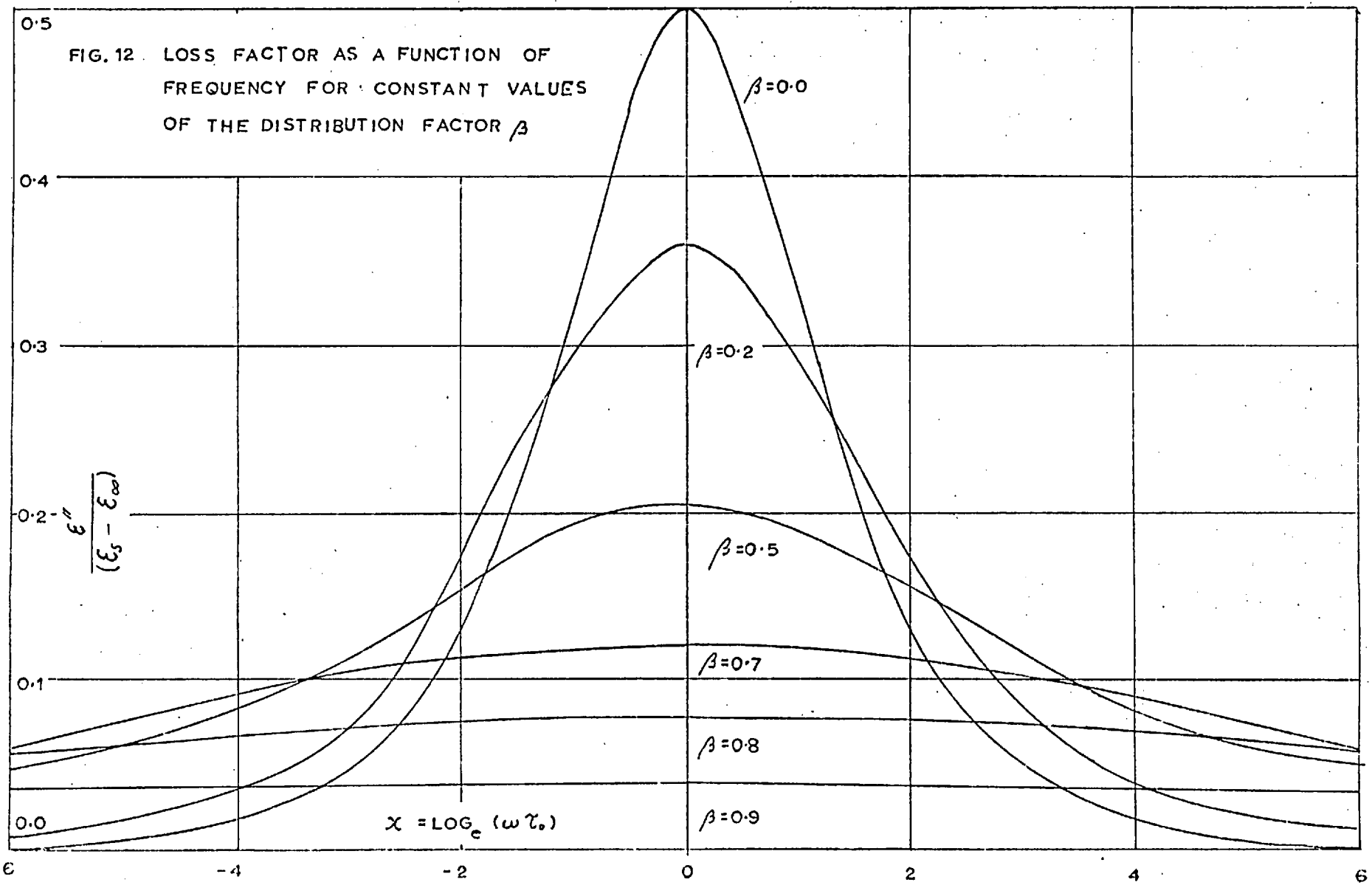
FIG. 12 LOSS FACTOR AS A FUNCTION OF FREQUENCY FOR CONSTANT VALUES OF THE DISTRIBUTION FACTOR β
β=0·0
β=0·2
β=0·5
β=0·7
β=0·8
β=0·9
0·5
0·4
0·3
0·2
0·1
0·0
ε″/(ε_s − ε_∞)
x = log_e (ω τ_0)
-6
-4
-2
0
2
4
6

$$\varepsilon'' = \frac{1}{2} (\varepsilon_s - \varepsilon_\infty) \cos \frac{\beta\pi}{2} (\omega \tau_o)^{1-\beta}$$

The conductivity is given by

$$\sigma = \omega \varepsilon_o \varepsilon''$$

$$\therefore \quad \sigma = \frac{1}{2} (\varepsilon_s - \varepsilon_\infty) \varepsilon_o \cos \frac{\beta\pi}{2} \tau_o^{(1-\beta)} \omega^{2-\beta}$$

$$\sigma \propto \omega^{2-\beta}$$

For frequencies much greater than $\frac{1}{\tau_o}$, i.e. $x \gg 0$, similar arguments give

$$\sigma = \frac{1}{2} \frac{(\varepsilon_s - \varepsilon_\infty) \varepsilon_o \cos \frac{\beta\pi}{2} \omega^\beta}{\tau_o^{1-\beta}}$$

Therefore by plotting log conductivity versus log frequency the resulting slopes will be $(2 - \beta)$ or β, depending whether the frequency is much less than or much greater than $\frac{1}{\tau_o}$.

2.3.4.2 Other Distributions of Relaxation Times

The Cole-Cole analysis for a distribution of relaxation times is considered the most convenient to combine with experimental results. However, other distributions do exist and these will be just briefly mentioned.

A distribution of relaxation time is defined by the quantity $G(\tau)$ which is defined using the complex permittivity:-

$$\varepsilon_r = \varepsilon_\infty + \int_o^\infty \frac{G(\tau)(\varepsilon_s - \varepsilon_\infty)}{1 + j\omega\tau} \, d\tau$$

where $\int_o G(\tau) \, d\tau = 1.$

For a single relaxation time process, 'τ' is a constant and it can be shown that the Debye equation results

$$\varepsilon_r = \varepsilon_\infty + \frac{(\varepsilon_s - \varepsilon_\infty)}{1 + j\omega\tau}$$

The distribution function for the above Cole-Cole analysis is[62]:-

$$G(s) = \frac{1}{2\pi} \frac{\sin \beta\pi}{\cos h(1 - \beta)s - \cos \beta\pi}$$

where $s = \log \left(\frac{\tau}{\tau_o}\right).$

A different distribution was given earlier by Wagner[64] who assumed a modified Gaussian distribution of relaxation times

$$G(\tau) \, d\tau = \frac{b}{\sqrt{\pi}} e^{-b^2 s^2} \, ds$$

where $s = \log \frac{\tau}{\tau_o}$ and b is a constant, representing the distribution.

Fuoss and Kirkwood[65] produced a different distribution function to fit their experimental data:

$$G(s) = \frac{\alpha}{\pi} \frac{\cos \frac{\alpha\pi}{2} \cos h\, \alpha s}{[\cos^2 \frac{\alpha\pi}{2} + \sin h^2\, \alpha s]}$$

where $s = \log(\frac{\tau}{\tau_o})$ but $\alpha \neq \beta$.

Another empirical equation is that of Taylor[66]

$$G(\tau)\, d\tau = \frac{1}{2\pi} \frac{1}{\cos h \frac{s}{2}}\, ds$$

where $s = \log \frac{\tau}{\tau_o}$.

The above-mentioned distributions are all symmetrical about the relaxation frequency. However, this is not always the case experimentally.

Davidson and Cole[67] showed that skewed functions would be generated by a simple modification of the Debye equation:-

$$\varepsilon_r = \varepsilon_\infty + \frac{(\varepsilon_s - \varepsilon_\infty)}{(1 + j\omega\tau)^\beta} \qquad 0 < \beta < 1.$$

The distribution of relaxation times to describe this will be logarithmic below a maximum cut-off value.

Owen[140] produced an equation for the complex permittivity:-

$$\varepsilon_r = B \frac{2}{1 + (1 + j\omega\theta)^{\frac{1}{2}}}$$

where θ represents the relaxation time.

He found that his equation fitted his results, which showed asymmetry, reasonably well.

2.3.4.3 Significance of the Distribution Factor β

The significance of the Cole-Cole distribution factor β is similar to that of the constants α and b mentioned above, in that they represent the width of the distribution of relaxation times.

This can be seen mathematically by determining the bandwidth of the loss peaks (in terms of ε'') at the points $\frac{d^2\varepsilon''}{dx^2} = 0$.

The resulting quadratic equation in $\cos h(1 - \beta)x$ means four roots for x.

$$\cos h^2(1 - \beta)x - \sin \frac{\beta\pi}{2} \cos h(1 - \beta)x - 2 = 0$$

Since only positive values of $\cos h(1 - \beta)x$ are allowed and the two real roots are symmetrical about the origin $x = 0$, then the resulting bandwidth is

$$B.W. = \frac{2}{1 - \beta} \cos h^{-1} R$$

where $$R = \sin \frac{\beta\pi}{2} + \sqrt{\sin \frac{\beta\pi}{2} + 2}$$

The limiting values of $\cos h^{-1} R$ for $\beta = 0$ and

$\beta = 1$ are 0.88 and 1.32 respectively so that the B.W. is determined mainly by $(1 - \beta)^{-1}$. Therefore, large values of the distribution factor β result in very broad loss peaks.

An increase in the B.W. will result in a decrease in the peak height, which is given by

$$\frac{\varepsilon''}{(\varepsilon_s - \varepsilon_\infty)} = \frac{1}{2} \frac{\cos \frac{\beta\pi}{2}}{1 + \sin \frac{\beta\pi}{2}} \qquad (\text{at } x = 0).$$

ε'', therefore, will vary from $\frac{(\varepsilon_s - \varepsilon_\infty)}{2}$ for $\beta = 0$ and will approach zero as 'β' approaches unity.

2.3.5 Interfacial Polarization

A number of authors[68-71] have found low frequency relaxation mechanisms occurring in thin dielectric films. These have all been interpreted in terms of interfacial polarization, i.e. relaxation of charge build-up at interfaces. This can be described phenomenologically by means of the Maxwell-Wagner model[11, 72]. The dielectric is considered as being composed of two layers of different conductivities and thicknesses.

This shows that the model results in a straightforward single relaxation time process described by the Debye equations, except that the loss contains an

experimental results[68, 69] indicate that a distribution of relaxation times is involved. It would be in order to describe a distribution by a mean activation energy and a value of β. However, the mechanism appears to restrict the values of these two parameters. Experimental activation energies are usually in the range 0.7 - 1.0 eV[68, 69] and values of β are about 0.5[68, 75].

2.3.5.1 Absorption Current

A simple method for the measurement of loss at very low frequencies has been derived by Hamon[76], who relates the loss of a capacitor at a particular frequency to the absorption current at a particular time.

The application of a low field D.C. voltage across a capacitor results in a current which decays with time to a steady D.C. level determined by the leakage resistance of the capacitor. If the applied voltage is V and the leakage resistance R, then the total current is given by:-

$$I = \frac{C\,V}{\tau}\, e^{-\frac{t}{\tau}} + \frac{V}{R}$$

where τ is the relaxation time of the polarizing process.

Section (2.3.3) showed that the complex permittivity could be written in the form:

$$\varepsilon_r = \varepsilon_\infty + \frac{(\varepsilon_s - \varepsilon_\infty)}{\tau} \int_0^\infty e^{-j\omega t} e^{-\frac{t}{\tau}} dt$$

If we let τ be the relaxation time for the current decay process, then it can be shown that the loss measured in terms of ε'' can be written:

$$\varepsilon'' = \frac{1}{C_a} \left[\frac{1}{\omega R} + \frac{1}{V} \int_0^\infty I(t) \sin \omega t \, dt\right]$$

where C_a is the air-filled capacitance. Hamon assumed the empirical relationship:

$$I(t) = B t^{-n}$$

where n and B were constants for a particular dielectric. Substitution and integration results in:

$$\varepsilon'' = \frac{1}{C_a} \left[\frac{1}{\omega R} + B \omega^{n-1} \Gamma(1 - n) \cos \frac{n\pi}{2}\right]$$

which is valid only for $0 < n < 2$. Hamon showed that if the last term of the above equation could be expressed in terms of the absorption current $I(t_1)$ at a time t_1, and if ω and t_1 are related by the equation

$$\omega t_1 = \left[\Gamma(1 - n) \cos \frac{n\pi}{2}\right]^{-\frac{1}{n}} \qquad (1)$$

then ε'' can be expressed:

$$\varepsilon'' = \frac{1}{\omega C_a}\left[\frac{1}{R} + I(t_1)\right]$$

The right hand side of equation (1) has a mean value of $0.63 \pm 3\%$ for values of n in the range $0.3 < n < 1.2$.

The absorption current $i(t)$ is then related to ε'' by the equation

$$\varepsilon'' \simeq \frac{i(t)}{C_a V 2 f}$$

where $$t = \frac{0.1}{f}$$

This equation is referred to as Hamon's equation and if the quoted values of 'n' are not exceeded, the equation will have a maximum error of $\pm 15\%$.

2.3.6 General Frequency Behaviour

Above the region where low loss peaks dominate there appears a frequency band from about 1 Kc/s to 1 Mc/s where both permittivity and loss are almost indpendent of frequency. This phenomenon was first noticed in bulk glasses (see Section (2.5)) and theoretical explanations were given by Govers[77, 78] and Garton[79].

The theory of Govers[77] will be briefly described as it adds a useful contribution to the theory of temperature coefficient of capacitance, considered later. They assumed that amorphous or polycrystalline materials, with their large numbers of inhomogeneities such as defects and disorder, will have an extremely broad distribution of relaxation times. The particles which give rise to loss, which could be dipoles, particles having a certain conductivity, or ions, are subjected to Van der Waal's forces and Coulomb forces due to their surroundings. Each particle will have a potential energy 'q' which will in general be different from that of its neighbour. Govers[77] related 'q' to an activation energy and Boltzman statistics give a relaxation time $\tau = \tau_o e^{\frac{q}{kT}}$. The main assumption is that the random structure will produce a broad distribution of 'q' , G(q) which is flat over a large energy range. The polarization of the particles is given by:

$$dP = N G(q) \alpha(q) dq$$

where N is the number of particles per unit volume and $\alpha(q)$ is the polarizability of a particle of energy q.

By using straightforward dielectric theory and

several relevant approximations, Gevers showed that the loss did not vary appreciably over several orders of magnitude of frequency. The simplified equation for loss was given by:

$$\tan \delta = B \frac{\exp [\beta T \log (\frac{1}{\omega} \dot{\tau}_o)]}{\log (\frac{1}{\omega} \dot{\tau}_o)}$$

where B and β are constants and τ_o is the mean relaxation time.

The permittivity was shown to decrease very slightly for an increase in frequency or loss, the relevant equation being:

$$\frac{1}{\varepsilon'} \frac{\partial \varepsilon'}{\partial \log \omega} = - \frac{2}{\pi} \tan \delta$$

A similar result is obtained by the analysis of Garton[79]. He suggested the presence of temporary thermal wells, together with deep wells. The dipole or particle giving rise to loss will oscillate between the two types of well. The resulting equation for ε'' is:

$$\varepsilon'' = (\pi - 1) \frac{B}{2kT} e^{\frac{E_o}{kT}}$$

where B is a constant and E_o is the depth of the

As ε' was again independent of frequency, the loss was independent of frequency. Garton pointed out that the only form of the distribution function $G(\tau)$ giving rise to loss indpendent of frequency over a reasonable range was the reciprocal relationship:

$$G(\tau) \propto \frac{1}{\tau}$$

The Cole-Cole[97] analysis may also be used to describe, mathematically, loss which is almost invariant with frequency, given by values of β approaching unity. The limiting value of $\beta = 1$ results in a conductivity proportional to frequency given by:

$$\sigma = \omega \varepsilon_o \varepsilon'' = \frac{\varepsilon_o(\varepsilon_s - \varepsilon_\infty)\,\omega}{\tau_o}$$

and therefore loss indpendent of frequency.

It was shown in the previous section that the only D.C. conduction processes relevant at low fields were "impurity" and ionic conduction. A.C. fileds are usually restricted to this ohmic region. Ionic conduction has been found to give near invariant loss at low temperatures[52, 80, (81)]. However, it is thought that impurity conduction is the more likely process at room temperature, considering the very low activation energies involved (generally < 0.1 eV).

It should be pointed out that Jonscher and his co-workers[25, 82] suggest that in the case of 2-centre hopping, the conductivity can be proportional to a higher power of the frequency than unity.

In order to obtain a qualitative picture of the frequency behaviour of impurity hopping, let us consider the analysis of Pollack and Geballe[83]. They found loss near-invariant with frequency ($\sigma \propto \omega^{0.8}$) in the audio-frequency range in doped semi-conductors at very low temperatures. Hopping between pairs only was considered. In amorphous materials, however, the hopping centres will probably be localised states (as discussed in Section (2.1)) although the presence of such states has not been fully established[84]. Therefore, since the nature of the states is probably dissimilar, it is not possible to make a direct mathematical comparison with the analysis of Pollack and Geballe[83]. The important point which arises from their theory and also that of Miller and Abrahams'[40] is the exponential dependence of a relaxation time 'τ' on the pair separation 'r'. This implies that at any one frequency, the contribution to loss will be from a small distribution of site separations only. Therefore the conductivity over the total frequency range is determined by super-

imposing the responses of a distribution of relaxation times $G(\tau)$, which is necessarily very broad. The conductivity is then

$$\sigma = \varepsilon_o(\varepsilon_s - \varepsilon_\infty) \int_o^\infty \frac{G(\tau)\ \omega^2\ \tau^2\ d\tau}{1 + \omega^2\ \tau^2}$$

As has already been noted, the only value of $G(\tau)$ giving a frequency-invariant loss will be:

$$G(\tau) = \frac{\text{const}}{\tau}$$

For an activation energy close to kT , Pollack and Geballe[118] found the following form of the conductivity

$$\sigma = \frac{B}{kT} \int_o^\infty \frac{r^2\ \tau^{-1}\ (\omega\tau)^2\ r^2\ dr}{(1 + \omega^2\ \tau^2)} \qquad (2)$$

where B is a constant involving the density of hopping sites.

A very crude estimation of the relationship between a relaxation time and the corresponding pair separation can be made by comparing equations (1) and (2). Comparing the integrals and then integrating, results in an equation of the form:

$$\tau = \tau_o \exp\ (A\ r^5/kT)$$

where A is a constant and τ_o is the relaxation time corresponding to a minimum separation 'r_o' which is small compared to 'r'. This crude analysis merely serves to demonstrate the exponential dependence between a particular relaxation time and the pair separation.

Pollack[85, 86] considers further the case of activation energies differing from kT and also the effect of multiple hopping. However, the analyses become extremely complex and these effects will not be discussed here.

Theory predicts that the activation energy associated with a hopping mechanism is temperature dependent. Experimentally, however, this is not always observed, probably because of the small temperature range of the measurements.

2.3.7 High Frequency Behaviour

The frequency invariant loss region will extend into the megcycle range. However, the distributed resistance of the capacitor plates[87] and the lead resistance begin to have a significant effect. Figure (13) shows the equivalent circuit where the capacitor plate and lead resistance are represented by a single series resistance R'. By equating complex impedances and comparing real and imaginary parts, the measured

FIG. 13

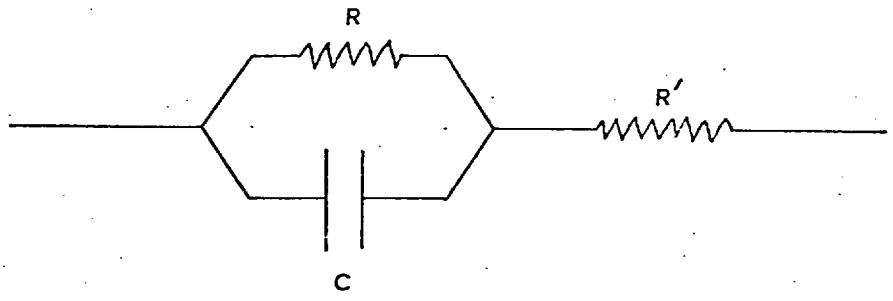

CAPACITOR WITH LEAD SERIES RESISTANCE R'

COMPLEX IMPEDANCE $Z = R' + \frac{R}{(1+jt)}$ where $j = \omega RC = \frac{1}{TAN\delta}$

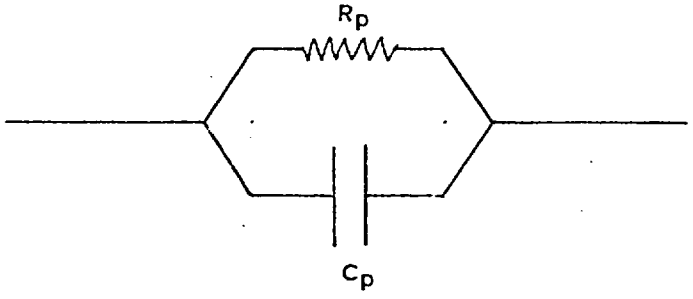

PARAMETERS MEASURED BY BRIDGE

COMPLEX IMPEDANCE $Z = \frac{R_p}{(1+jt_p)}$ where $j_p = \omega R_p C_p = \frac{1}{TAN\,\delta_p}$

EQUATING REAL AND IMAGINARY PARTS OF COMPLEX IMPEDANCES GIVES

$$TAN\,\delta_p = TAN\delta + \omega R'C + \frac{R'}{\omega R^2 C}$$

loss $\tan \delta_p$ is given by

$$\tan \delta_p = \tan \delta + \omega R'C + \frac{R'}{\omega R^2 C}$$

where $\tan \delta$ is the real loss of the dielectric and R is the A.C. resistance of the dielectric. The last term is negligible for reasonable values of R'. Clearly, the R' contribution will become significant at high frequencies due to its frequency dependence, eventually dominating the real loss.

2.4 Temperature Coefficient of Capacitance

The importance of keeping the temperature coefficient of capacitance to a minimum has already been stressed. There are five main contributions to γ_c (see Section (1.2.4)) and each of these will be derived and discussed in some detail. The significance of these contributions will then be related to dielectric materials of different permittivities and loss. We are generally concerned with the temperature coefficient of permittivity γ_p which has already been defined by the equation

$$\gamma_c = \gamma_p + \alpha_l$$

where α_l is the linear expansion coefficient.

2.4.1 γ_p Arising From Relaxation Phenomenon

A relaxation phenomenon with a single relaxation time is described by the Debye equations (see Section (2.3.3)). However, in order to keep the analysis general to begin with, we will use the Cole-Cole relationships[62] (see Section (2.3.4)). These will include all possibilities from the single, Debye relaxation time to an infinite distribution of relaxation times. Such unusual properties as skew-type relaxation peaks are not included.

In order to differentiate ε' with respect to temperature, it is first necessary to assume that the mean relaxation time τ_o is related to temperature by the Arrhenius relationship:

$$\tau_o = \tau_\infty e^{\frac{q}{kT}}$$

This defines a mean activation energy 'q' associated with the relaxation process.

The resulting equation for γ_p is:

$$\gamma_p = \frac{2q}{kT^2} f(\beta) \tan \delta$$

where

$$f(\beta) = (1 - \beta) \frac{1 + \sin \frac{\beta\pi}{2} \cos h(1 - \beta)x}{\sin \pi\beta + 2 \cos \frac{\beta\pi}{2} \cos h\ (1-\beta)x}$$

and $x = \log_e \omega \tau_o$.

The function $f(\beta)$ has been determined as a function of 'x' during the present work using a computer and is shown in Figure (14) for selected values of 'β'. It will be seen from this that certain approximations can be made to the function $f(\beta)$.

For frequencies well removed from the dispersion frequency $\omega = \frac{1}{\tau_o}$ i.e. $x \gg 1$:

$$f(\beta) \longrightarrow \frac{1 - \beta}{2} \tan \frac{\beta \pi}{2}$$

This implies that '$f(\beta)$' approaches a value independent of frequency or temperature. An additional approximation can be made for an extremely broad distribution of relaxation times, i.e. $\beta \longrightarrow 1$, when $f(\beta) \longrightarrow \frac{1}{\pi}$. For this limiting case γ_p is given by:

$$\gamma_p = A \tan \delta$$

where $A = \frac{2q}{\pi kT^2} = \frac{2}{\pi T} \log_e \frac{\tau_o}{\tau_\infty}$

This result, first obtained by Herspring[88], is similar to that obtained by Govers[77] where analysis was briefly outlined in Section (2.3.6). Their equations gave

$$A = \frac{2}{\pi T} \log_e \left(\frac{1}{\omega \tau_\infty}\right)$$

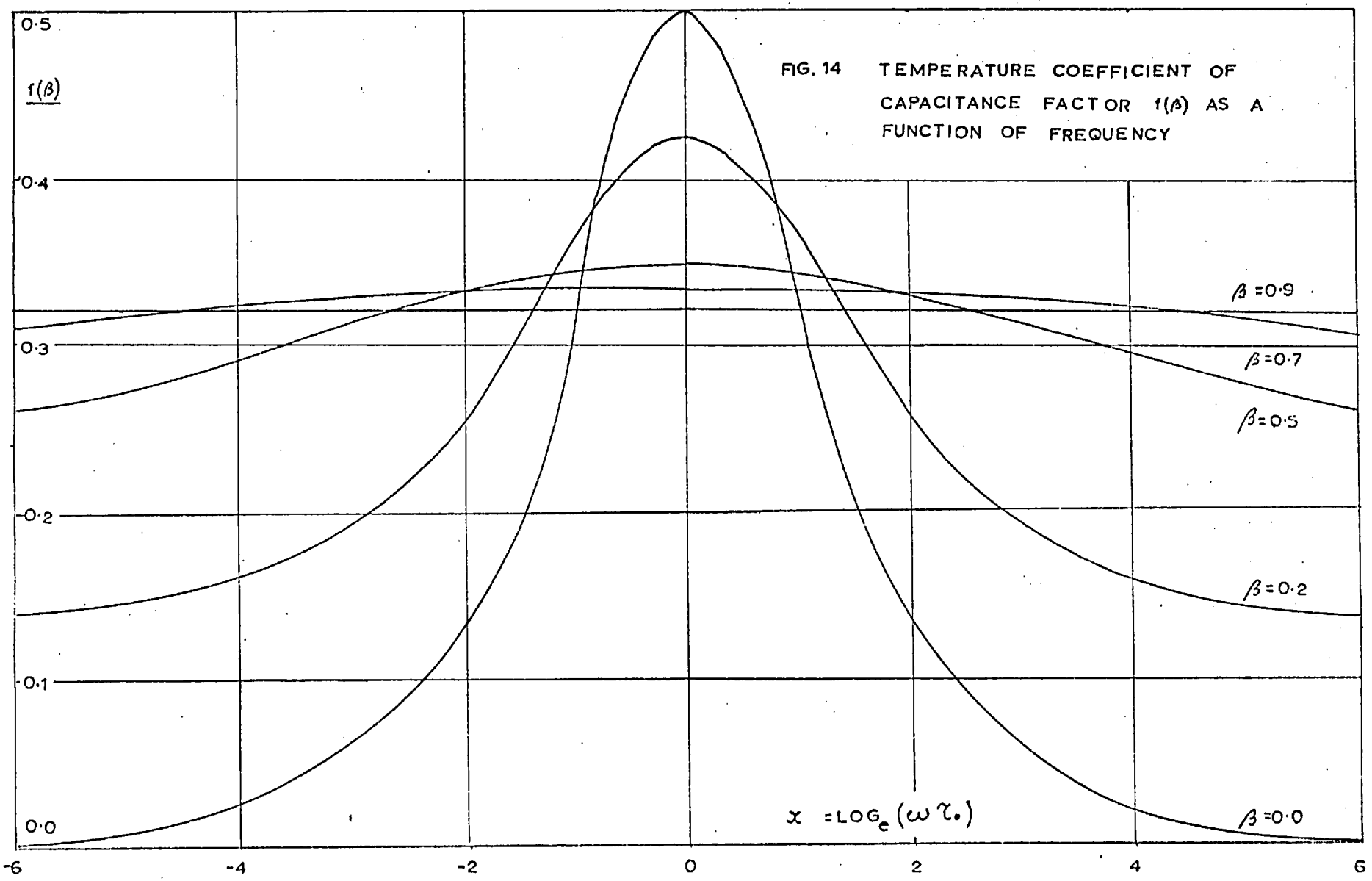

FIG. 14 TEMPERATURE COEFFICIENT OF CAPACITANCE FACTOR $f(\beta)$ AS A FUNCTION OF FREQUENCY

which has a small frequency dependence.

It is interesting to note that in the case of a single relaxation time, for the whole frequency range of dispersion, γ_p is given by

$$\gamma_p = A\,B\,\mathrm{Tan}^2\,\delta$$

where $$B = \frac{\pi\varepsilon'}{(\varepsilon_s - \varepsilon_\infty)}$$

In the general analysis of 'γ_c' we are not considering special cases where relaxation peaks appear in the loss (i.e. $\beta < 1$) but the frequency region where loss becomes near-invariant with frequency (i.e. $\beta = 1$). Therefore, the first contribution to γ_p is given by A Tan δ where $A = .05 \pm .01$ from experimental results[77, 88].

Although it is not relevant to the determination of γ_p, mention should be made of the temperature coefficient of loss, T.C. (Tan δ).

Since $\mathrm{Tan}\,\delta = \frac{\varepsilon''}{\varepsilon'}$

$$\text{T.C. (Tan } \delta) = -\gamma_p + \frac{1}{\varepsilon''}\left(\frac{\partial\varepsilon''}{\partial T}\right)$$

Again using the Cole-Cole[62] relationships, the second term is defined by

$$\frac{1}{\varepsilon''}\left(\frac{\partial\varepsilon''}{\partial T}\right) = \frac{2q}{kT^2}\,g(\beta)$$

where $g(\beta) = \frac{(1-\beta)}{2} \frac{\sin h(1-\beta)x}{\cos h(1-\beta)x + \sin \frac{\beta\pi}{2}}$

The function $g(\beta)$ has been machine-calculated in the present work and is shown in Figure (15). For frequencies well removed from the relaxation frequency $\omega = \frac{1}{\tau_o}$, i.e. $x \gg 0$, $f(\beta) \longrightarrow \frac{1-\beta}{2} \tan h(1-\beta)x \longrightarrow \frac{1-\beta}{2}$.

For an infinite distribution of relaxation times $\beta = 1$, $\frac{1}{\varepsilon''} \frac{d\varepsilon''}{dT} = 0$. Therefore the temperature coefficient of loss in the limiting case is equal to $-\gamma_p$.

2.4.2 γ_p Arising From Polarizability Considerations

Since the permittivity of a material is directly related to the polarizability of the contributing process by the 'Clausius-Mosotti' equation, differentiation of this equation will give us another contribution to the γ_c. This equation applies to most isotropic materials when the contributing particles or dipoles are effectively infinitely small (see Section (2.3.2.1)).

$$\frac{\varepsilon' - 1}{\varepsilon' + 2} = \frac{\alpha_m}{3V\varepsilon_o}$$

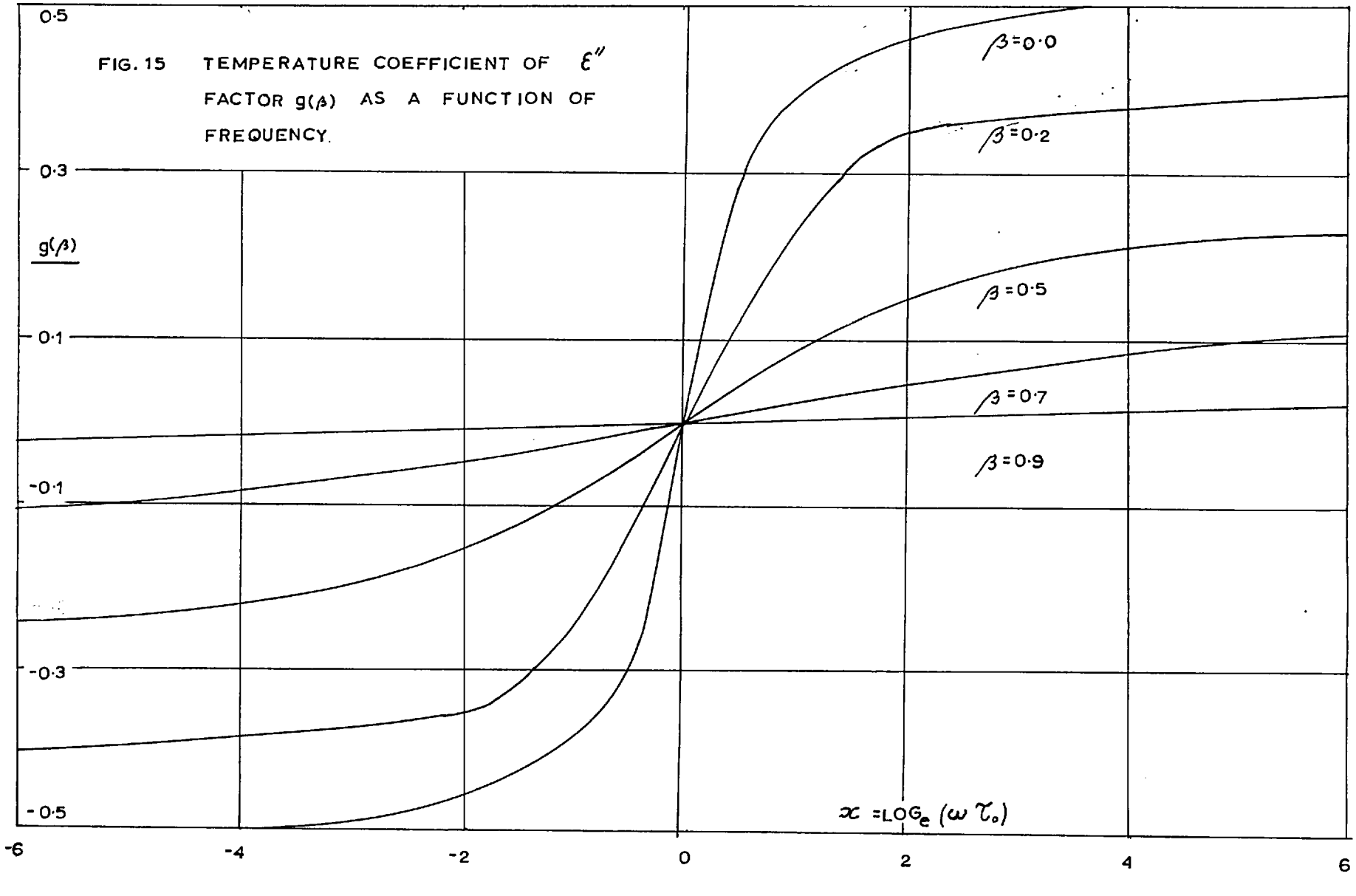

FIG. 15 TEMPERATURE COEFFICIENT OF ε'' FACTOR $g(\beta)$ AS A FUNCTION OF FREQUENCY.

where α_m is the polarizability of a macroscopically small volume V.

Differentiating with respect to temperature

$$\frac{1}{\varepsilon'}\left(\frac{\partial \varepsilon'}{\partial T}\right)_P = \frac{(\varepsilon' - 1)(\varepsilon' + 2)}{\varepsilon'} [A + B + C]$$

where $$A = -\frac{1}{3V}\left(\frac{\partial V}{\partial T}\right)_P = -\alpha_1$$

This term is the negative linear ~~comparison~~ expansion coefficient and represents the decrease in number of polarizable particles/unit volume because the volume is expanding with increased temperature.

$$B = \frac{1}{3\alpha_m}\left(\frac{\partial \alpha_m}{\partial V}\right)_T \left(\frac{\partial V}{\partial T}\right)_P$$

This term represents the increase of the polarizability of a constant number of particles with the increase in available volume as the temperature increases.

$$C = \frac{1}{3\alpha_m}\left(\frac{\partial \alpha_m}{\partial T}\right)_V$$

This term is the straightforward temperature dependence of the polarizability at constant volume. It is the intrinsic contribution of the electronic and ionic polarizability.

In Govers analysis he differentiated the 'Clausius-Mosotti' equation but omitted the contributions B and C. These three contributions were investigated by Havinga[89] and Bosman and Havinga[90] who found that they were applicable mainly to non-polar, isotropic materials of low loss. This meant that these were the only contributions to γ_c in their work. Experimentally, they were able to calculate the magnitudes of the various contributions by measuring:

$$\varepsilon', \quad \frac{1}{} \left(\frac{\partial}{\partial T}\right)_P, \quad \frac{1}{} \left(\frac{\partial}{\partial P}\right)_T, \quad \frac{1}{V}\left(\frac{\partial V}{\partial T}\right)_P \text{ and } \frac{1}{V}\left(\frac{\partial V}{\partial P}\right)_T$$

Very often, particularly in the case of thin films, it is difficult to ascertain the values of some of these parameters and different contributions become indistinguishable. Therefore, contributions 'B' and 'C' will be taken together:

$$B + C = D = \frac{1}{3\alpha_m}\left(\frac{\partial \alpha_m}{\partial T}\right)_P$$

The contribution $A = -\alpha_1$ will be taken together with the expansion term resulting from the capacitance-permittivity relationship of a parallel plate capacitor (see Section (1.2.4)). The resulting contribution will be

$$-\alpha_1 \left(\varepsilon' - \frac{2}{\varepsilon'}\right)$$

This term was obtained by Gevers[77].

For a general analysis, therefore, only three of the five contributions will be considered and the total temperature coefficient of capacitance can be written as:

$$\gamma_c = A \text{ Tan } \delta + \frac{(\varepsilon' - 1)(\varepsilon' + 2)D}{\varepsilon'} - \alpha_1 (\varepsilon' - \frac{2}{\varepsilon'}$$

Intrinsic contributions will arise through the term 'D', the polarizability contribution.

Although, at first sight, the general equation appears rather complex, it is possible to break it down for particular limiting cases.

There appear to be five important regions, illustrated in Figure (16).

REGION I $\varepsilon' = 1$

The permittivity of a vacuum is unity and clearly, 'γ_c' will be zero. This gives us a single point on the graph.

REGION II $1.5 < \varepsilon' < 2.5$

For such low permittivities the electronic contribution will dominate and $\varepsilon' \simeq n^2$, where n is the refractive index of the dielectric. Therefore, the term 'D' will be very small and for materials of very low loss, γ_c is given by

FIG. 16 ILLUSTRATION OF THE VARIOUS REGIONS OF T.C.C. VS. PERMITTIVITY

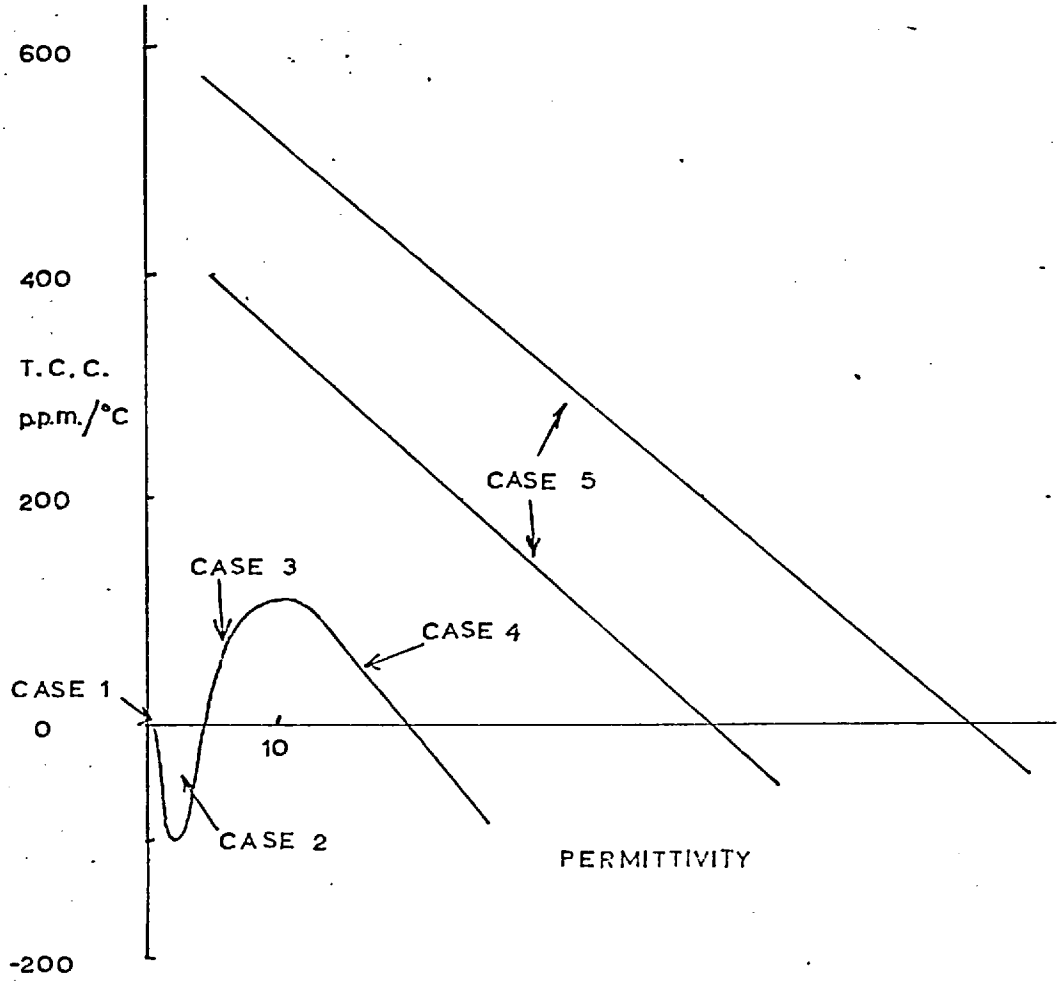

$$\gamma_p \simeq -\alpha_1 \left(\varepsilon' - \frac{2}{\varepsilon'}\right)$$

i.e. $$\gamma_p \simeq -\alpha_1$$

REGION III $2.5 < \varepsilon' < 10$

This is a poorly defined region where intrinsic and extrinsic components contribute to varying degrees and it is necessary to plot a spread of data. If 'γ_p' is negative then electronic polarizability dominates and if 'γ_p' is positive then the ionic contributions dominate.

REGION IV $\varepsilon' > 10$

For permittivities greater than ten, two cases may be considered. The first is the region of very low loss such that the 'A Tan δ' term is negligible. 'γ_c' is then given by

$$\gamma_c \simeq \varepsilon' D - \alpha_1 \varepsilon'$$

Herspring[88] and Cockbain and Harrop[91] have shown experimentally that the first term is a constant 'K'. Therefore:- $\gamma_c \simeq K - \alpha_1 \varepsilon'$.

This gives a straight line plot.

REGION V $\varepsilon' > 10$

The second region of large permittivities is that for high loss and 'γ_c' is given by

$$\gamma_c = A \text{ Tan } \delta - \alpha_1 \varepsilon'$$

This equation produces a series of straight lines of slope '$-\alpha_1$' and intercepts depending on the loss.

2.4.2 Experimental Verification of $\gamma_c - \varepsilon'$ Relationships

Figure (17) shows the $\gamma_c - \varepsilon'$ curves for a number of materials in both bulk and thin film form, for results taken from the literature[91]. Bulk data is included because of lack of thin film data and the lower losses often found in bulk materials.

Region V is discussed in detail with experimental verification by Gevers[77] and the straight line relationship of Region IV has been discussed adequately, both by Herspring[88] and Cockbain[92]. This region applies to a number of polycrystalline materials and ceramics as shown in Figure (17).

Region II applies mainly to organic plastics containing such materials as P.T.F.E. and polystyrene, with γ_c's varying from - 50 p.p.m./°C to - 300 p.p.m./°C.

FIG. 17 TEMPERATURE COEFFICIENT OF CAPACITANCE VS PERMITTIVITY FOR VARIOUS LOSSES.

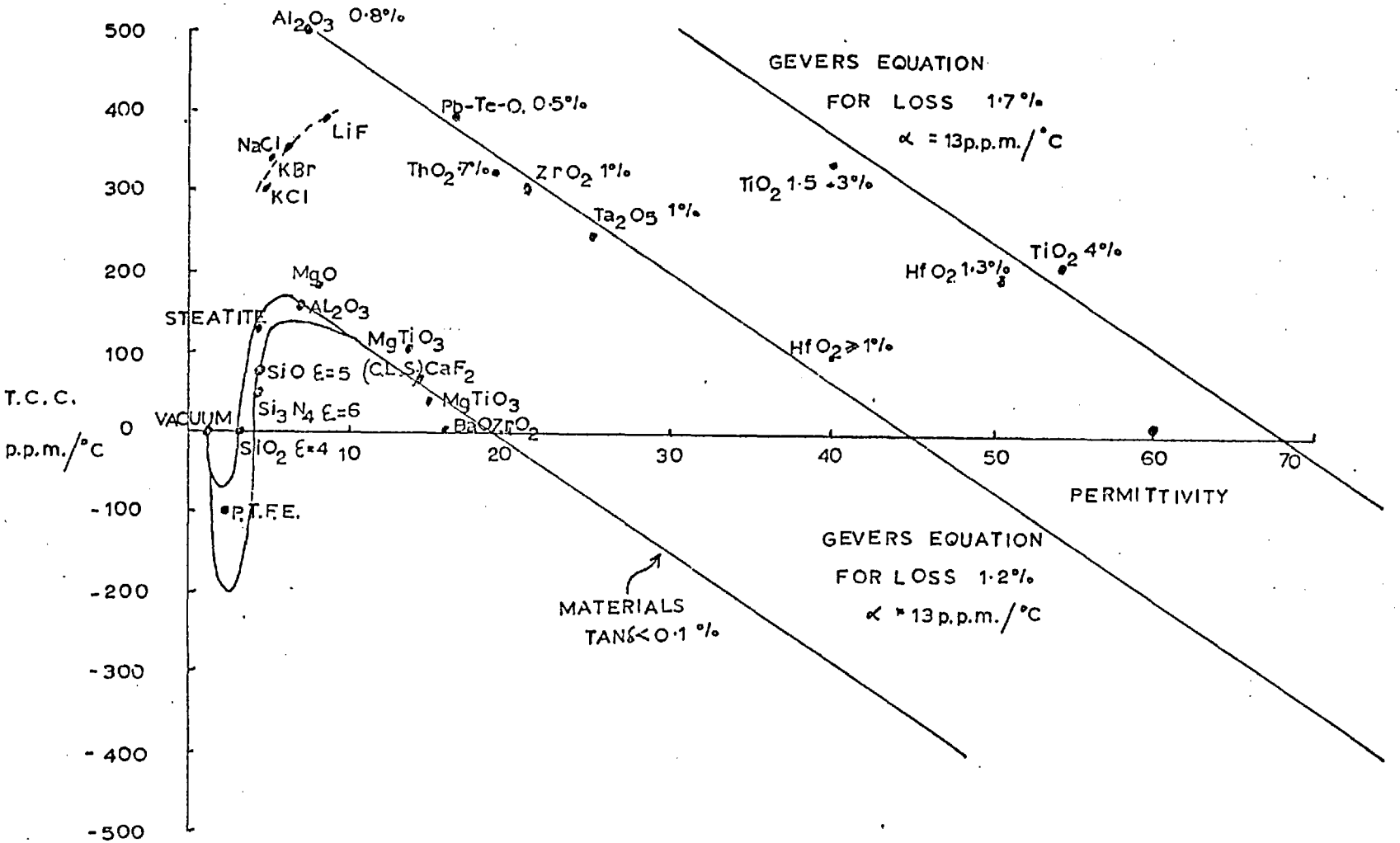

Region III contains silicon oxide which is the material chosen for study and results on this will be discussed later. This region also contains materials which have received much attention in their thin film form, such as Al_2O_3, SiO_2 and Si_3N_4. It is interesting to note that high permittivity materials in Region III will always have a high positive γ_c due to the dominating intrinsic contributions.

Certain results in the literature show an anomalous behaviour, but these can generally be explained by such features as high expansion coefficients, porosity and non-stoichiometry giving variable valency. The high 'γ_c's' of the alkali bolides are explained by Bosman and Havinga[90] as being due to high coefficients of linear expansion. A few results are plotted on the graph. In general, ferro-electric materials will fall into Region IV, giving large negative 'γ_c's'.

It is observed that this analysis will give a useful guide to the γ_c of a material when its loss and permittivity are known.

2.5 The Glassy (Amorphous) State

2.5.1 Introduction

Glass is the most widely used amorphous structure and its properties have been widely studied.

It is useful, therefore, in connection with the present work on amorphous thin films, briefly to describe the electrical properties of metal-glass-metal sandwiches.

2.5.2 Discussion

In order to explain the physical and electrical properties of a glass-like material, Zacharisiasen[93] proposed that the vitreous state was built up from a random three-dimensional network. A two-dimensional schematic representation of his picture is given in Figure (18).

Normal glasses are composed of inorganic oxides, constructed of polyhedra of oxygen ions attached around a multipally-charged ion, such as Si^{++}, called the network former. The oxygen ions present can either link polyhedra together and are called bridging oxygen ions, or can belong to only one polyhedra and are then called non-bridging oxygen ions. These three types of ions contribute to the physical structure of the glass. Network modifying ions can also be introduced and contribute very little to the structure but have more effect on the electrical properties. They are usually impurity ions and are located in the interstices of the network. Ions such as Li^{+}, Na^{+}, K^{+} will be highly mobile, whereas ions such as B^{++}, Pb^{++} can be considered as immobile,

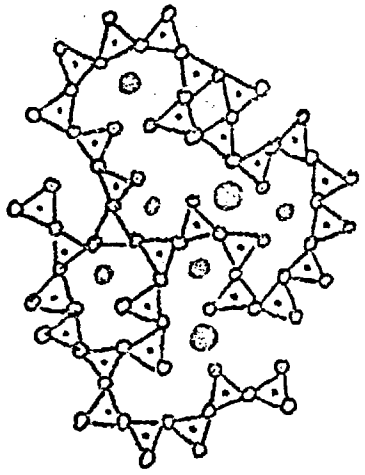

- NETWORK-FORMING ION
- NETWORK-MODIFYING ION
- BRIDGING OXYGEN ION
- NON-BRIDGING OXYGEN ION

FIG.18 SCHEMATIC TWO-DIMENSIONAL REPRESENTATION OF GLASS ACCORDING TO ZACHARIASEN'S THEORY.

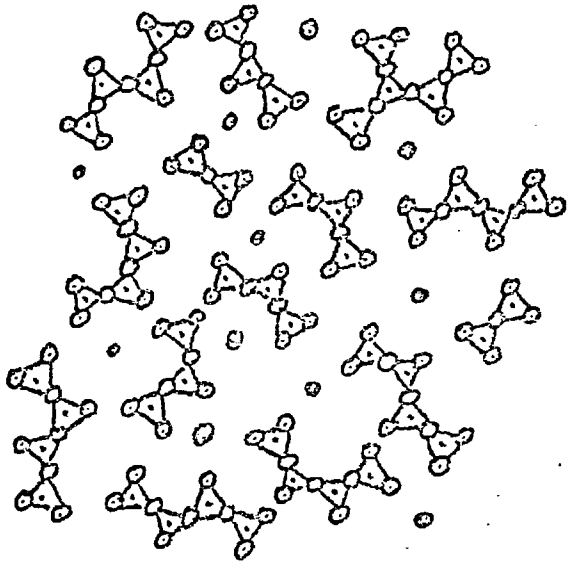

FIG.19 SCHEMATIC TWO-DIMENSIONAL REPRESENTATION OF THE INVERT GLASS STRUCTURE.

and therefore not contributing to the electrical properties to the extent of the lighter ions.

An important parameter used to define this structure is the number of bridging ions per polyhedra Y. If $Y < 2$ then spatial coherence is lost and the structure is built up of chains whose length will depend on how close 'Y' is to 2. These are called "invert glasses" and an example is given in Figure (19).

The concept of network imperfections, although mainly concerned with the crystalline state, is partially applicable to the vitreous state. Stevels[94] has shown evidence of grain boundaries and dislocations and, of particular importance, "point defects". These may be vacancies, interstitial atoms or foreign atoms.

Stevels[95] has made an attempt to give a general picture of the behaviour of glass in an alternating field and gives a qualitative picture of the spectrum of losses expected over a wide range of frequencies, as shown in Figure (20). He considers four contributions to the losses.

2.5.2.1 Conduction Losses

Under the influence of a field, the network modifying ions will move through the structure giving up part of the energy, thus obtained, in the form

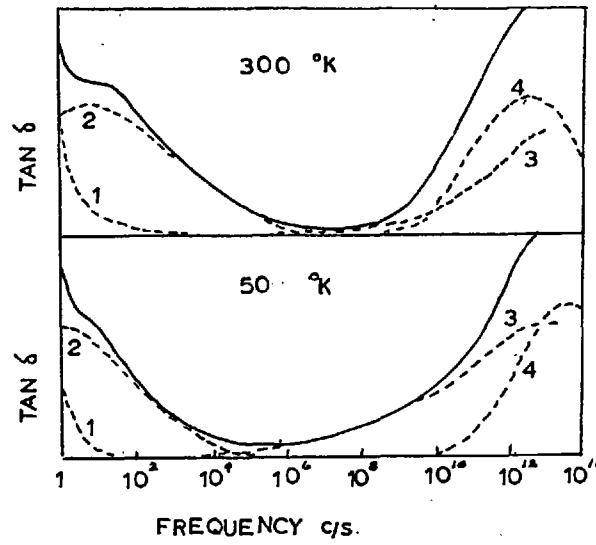

FIG. 20 DIAGRAMMATIC REPRESENTATION OF THE FREQUENCY SPECTRUM OF THE DIELECTRIC LOSSES IN GLASS.

1 CONDUCTION LOSSES 2 RELAXATION LOSSES

3 DEFORMATION LOSSES 4 VIBRATION LOSSES

FIG. 21 . POTENTIAL OF A NETWORK-MODIFYING ION ALONG AN ARBITRARY DIRECTION IN THE GLASS.

of heat which will constitute a loss. The conductivity σ is given by

$$\sigma = \tan \delta \, \omega \, \varepsilon' \, \varepsilon_o$$

For frequencies greater than 50 c/s the conduction losses are generally negligible compared to other losses.

2.5.2.2 Relaxation Losses

In this type of loss the transport of network modifying ions over atomic distances only is considered. Figure (22) shows the potential energy of an ion in an arbitrary direction. Due to the amorphous nature of the material, the potential barriers are randomly distributed. The application of an electric field alone is not usually sufficient to move the ions over the higher potential barriers, and energy must be obtained from either collision processes or Brownian Motion. Therefore, the ion will spend a certain time in each potential well, before moving into an adjacent well, called the relaxation time τ, and generally there will be a broad distribution of τ, but we can define an average relaxation time τ_o.

The losses will be frequency dependent and for a single relaxation time will be related by the Debye equation

$$\text{Tan } \delta \; \alpha \; \frac{\omega\tau}{1 + \omega^2 \tau^2}$$

In general the losses will occur over the range 10^{-3} to 10^{6} c/s but this will depend upon the particular material.

2.5.2.3 Deformation Losses

Another loss having similar characteristics of an after effect i.e. (of the movement lagging the change in applied field) is the movement of whole sections or chains of the network. The relaxation time involved will be very small and will have a large distribution. The frequency range is shown in Figure (21).

2.5.2.4 Vibration Losses

As a result of thermal agitation, network formers, network modifiers and oxygen ions will vibrate about their equilibrium position. The vibrations are always damped and will therefore be accompanied by loss. These will occur at very high frequencies and again with a large distribution of relaxation times.

Besides their obvious frequency differences, these losses may be differentiated by their temperature behaviour. Types 1, 2 and 3 will shift to higher frequencies with increased temperature, whereas the opposite effect happens to type 4.

Most work performed on glasses and amorphous in-

sulators has been at a frequency less than 10^8 c/s and therefore the deformation and vibrational losses are rarely investigated.

There is much published literature on the electrical properties of glasses. As far back as 1920, McDowell et al[96] investigated the behaviour of glasses as a dielectric in an alternating current circuit. Reviews on the electrical properties of glass have been published by Taylor[59, 97] and Owen[80]. The work of Sutton[73, 74] has already been discussed. Other interesting publications include work by many authors[98-103].

CHAPTER 3

PREVIOUS ELECTRICAL STUDIES ON SILICON OXIDE

3.1 Introduction

This chapter briefly outlines the electrical studies already performed on silicon oxide which are of importance to the present work. Figure (22) is a table indicating the D.C. properties and Figure (23) indicates the A.C. properties. The effects of deposition conditions and heat treatment are not discussed in any detail. Briefly, low deposition rates and high pressures produced the more desirable capacitor dielectrics, i.e. a high D.C. resistivity and a low loss.

3.2 Discussion of Previous Electrical Studies

The experimental results agree reasonably well, despite the fact that deposition conditions and post deposition heat treatment differ considerably. However, the interpretation of the results varies considerably, and some features still remain unsolved.

Very few authors attempt to study the low field D.C. conduction [107, 104], whereas the high field region has received much attention[44, 105, 106, 107]. Stuart[107]

Author	Low Field Properties	High Field Properties		
		Activation Energy	$\varepsilon^{*}_{S.E.}$	Proposed Mechanism
Hirose and Wada[104, 138]	E=.37eV, $\rho=5.10^{12}\Omega$cms. Diffusion of Si ions	0.54 eV	3	Poole-Frenkel Conduction
Johansen[44]	-	0.56 eV	3.8	Schottky Emission from small silicon islands into a silica matrix
Hartman, Blair and Bauer[105]	Ohmic region	0.43 eV	3.0	Model proposed by O'Dwyer[57] (see Section 2.2.7))
Stuart[106, 107]	Ohmic region E=0.5eV	-	-	Used model proposed by Simmons[58]
Argall[68]	Conducivity composed of both ionic and electronic contributions	-	-	-
Siddall[108]	Conductivity controlled by leakage paths	-	-	-

Figure 22 Previous Results on D.C. Conduction

* This column gives the value of permittivity assuming Schottky Emission. $\varepsilon_{SE} \times 4 = \varepsilon_{P.F.}$ the value, assuming Poole-Frenkel Conduction.

Author	Frequency Range	Dispersions at Room Temp.	Activation Energy	$\beta^{*'}$	γ_c p.p.m./°C	Reasons for Dispersions	General Behaviour
Argall[63]	10^{-2}-10^{7}c/s	Type A - 5.10^{-3}c/s	0.5eV(10Å/sec)	A.β=0	220	A-short range movement of impurity ions	Audio Frequency Tan δ f^{AT} > A.F. electron hopping conduction
		Type B - 5.10^{-7}c/s	0.8eV	B.β=0.5	25° 1Mc/s	B-blocking of charge carrier at electrodes	
Hirose and Wada[104]	10^{-2}-10^{7}c/s	l.f. 10^{-1} c/s	0.36eV	l.f.β>0	-	l.f. diffusion of Si ions	-
		h.f.>10^{7} c/s				h.f. local torsional vibrations of SiO chains	
Siddall[103]	1 Kc/s and 10 Kc/s	-	-	-	100<5Å/sec 400 10Å/sec	-	Loss initially controlled by leakage paths

Figure 23 Previous Electrical Results of A.C. Conduction

*' β - Distribution of Relaxation Times Factor as defined by Cole-Cole[62] (see Section (2.3.4))

attempts to explain the low field region using a model proposed by Simmons[58]. The basic assumption used is that the work function of the metal is greater than the work function of the insulator which requires that the fermi level of the insulator is shifted towards the conduction band (see Section (2.1)).

It is recognised by all the authors that high field conduction is not a straightforward Schottky Emission or Poole-Frenkel effect. However, since the current-voltage characteristics all show the logarithm of the current proportional to the square root of the voltage relationship, it is likely that some modification of these effects occur. However, Jonscher points out that the plotting of results can sometimes lead to confusion. If data covers only a small range in current then the current-voltage relationship might be mistaken for a power law of the form

$$I \alpha V^{n}$$

when 'n' is a high exponent. This makes it necessary to take results over a wide range of currents in order to distinguish between the two cases.

Hartman et al[105] produced an equation which applied at both low and high fields. The high field region was explained using the model of O'Dwyer[57].

Both Hartman et al[105] and Jonscher[25] point out an activation energy of .85 - .90 eV is obtained for the Schottky barrier heights ranging from 0.85 - 1.5 eV and also for any reasonable value of the disposable parameters in the theory. Hartman et al[105] obtained a value of $\emptyset$ = 143 eV which was slightly smaller than the values of Hirose and Wada[104] ($\emptyset$ = .56 eV) and Johansen[141] ($\emptyset$ = .54). It is difficult, therefore, to understand why Hartman et al used O'Dwyer's model.

Unlike the other authors, Johansen[44] plots the logarithm of the conductivity versus the square root of the applied voltage. According to Jonscher[25] this implies that once the electrons have been released from the traps, they drift a distance proportional to the applied voltage.

Qualitatively, the model of Simmons[58] appears to explain the results of Stuart's[106, 107] high field region analysis. The value of $\emptyset$ according to Simmons equals $\frac{E_t + E_d}{2}$. For values of $\emptyset$ = 0.5 to 0.6 eV, this requires that the fermi level of the insulator is shifted to within less than 1 eV of the conduction band.

The first authors to perform experiments over a reasonable frequency range were Hirose and Wada[104]. They showed the existence of the low frequency dispersion at 5.10^{-2} c/s at room temperature. The activation energy

of .36 eV was very similar to the low field D.C. conduction activation energy of .37 eV. However, Argall[66], using more sophisticated techniques, showed the existence of two low frequency loss peaks, the lower of the two probably corresponding to the peak of Hirose and Wada. Both Hirose and Wada and Argall show a loss increasing with frequency at high frequencies but again, different explanations were given.

CHAPTER 4

EXPERIMENTAL APPARATUS AND TECHNIQUES

4.1 Introduction

Figure (22) gives an overall view of the apparatus. The following sections describe the individual parts in detail and also the techniques and methods of preparation involved.

4.2 The Pumping System

An Edwards 4" fractionating diffusion pump, charged with a low pressure silicon oil, Ms 705, was backed by an N.G.N. rotary pump. A liquid nitrogen cold trap was placed between the diffusion pump and chamber to reduce contamination from the pump oils. The pressure obtainable overnight, using liquid nitrogen, was 5.10^{-6} Torr with baking up to 250°C. All seals were of Viton, greased with a low pressure vacuum grease and the presence of these seals restricted the baking temperature to 250°C. However, a very low pressure was not required and so the seals were not replaced.

Backing pressures were measured with 2 Pirani gauge heads, one to determine the backing pressure of the diffusion pump and the second to indicate the backing pressure when roughing out the chamber. The chamber

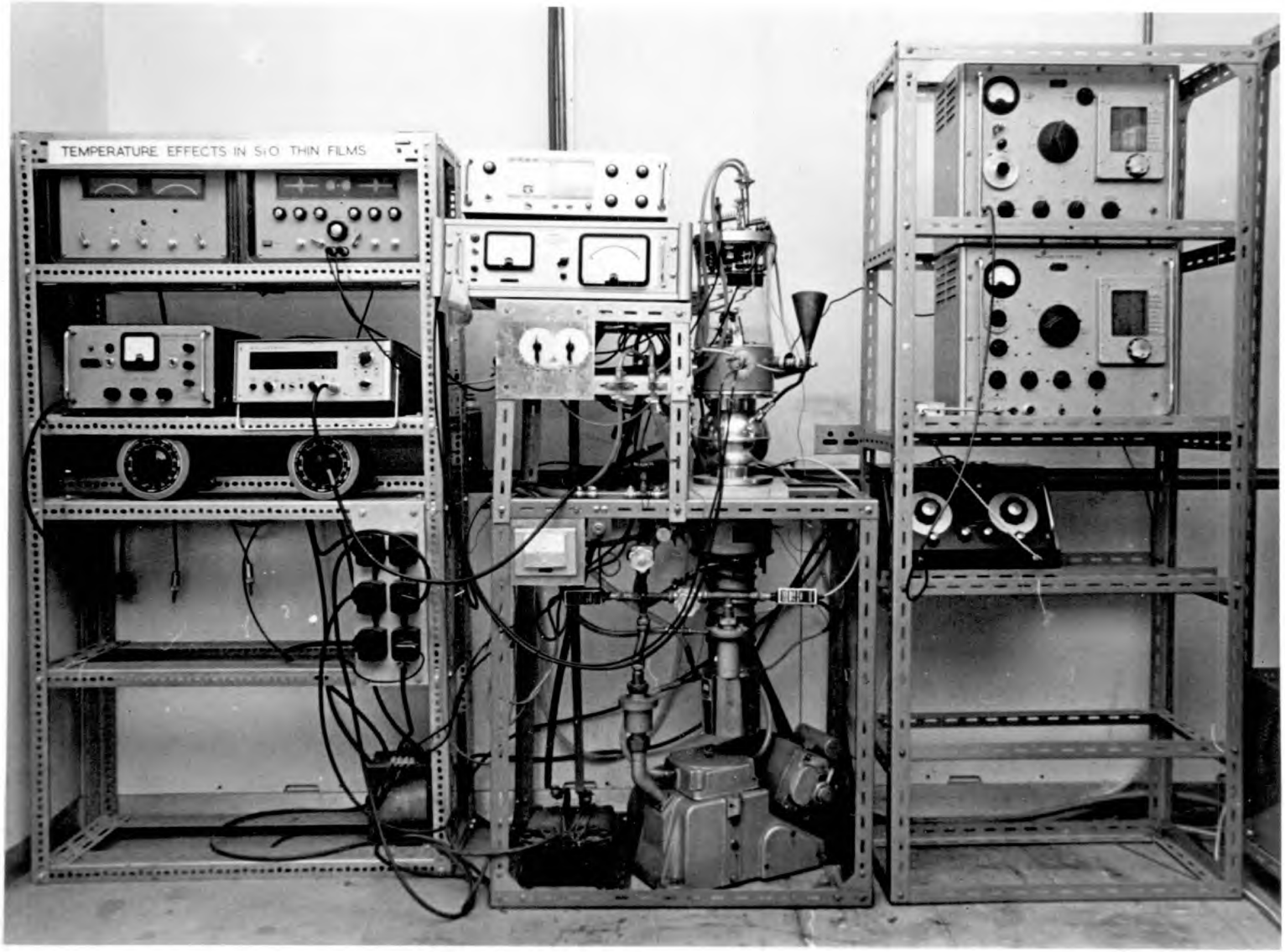

FIG. 22' OVERALL VIEW OF APPARATUS

pressure was measured using an ionisation gauge head type IOG 12 connected externally to an ionisation gauge. Outgassing was performed before any pressure readings were noted.

4.3 Sources

Figure (23) shows the arrangement of sources after the whole substrate assembly has been removed. Three sources are visible, the two aluminium sources being placed on either side of the silicon oxide source.

An aluminium source consisted of approximately .020 inch tungsten wire with aluminium wire hooked on to a number of loops. This arrangement was surrounded on five sides by a molybdenum box to prevent unnecessary contamination of the chamber.

The silicon oxide source was an inverted type Drumheller Source[109] as shown in Figure (24). The silicon monoxide charge was placed in the central cylinder such that the majority of the vapour steam suffered a reflection at the outer cylinder, reducing spitting of the larger lumps. The source was spot-welded from .002 ins. tantalum with .005 ins. tantalum leads. Copper contacts were used to clamp the leads, preventing over-heating in the leads.

For an evaporation rate of 11Å /sec at the substrate,

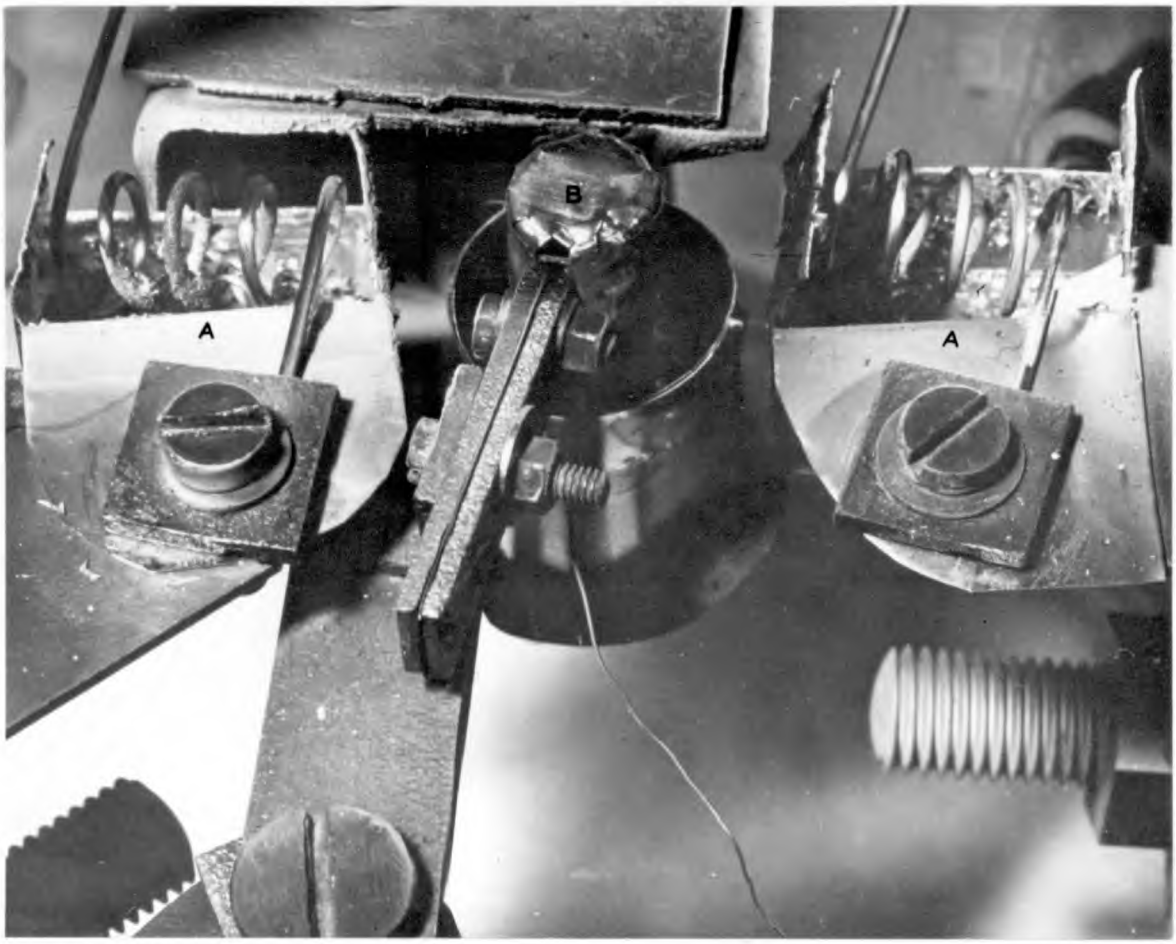

FIG. 23' SOURCE ARRANGEMENT

A ALUMINIUM SOURCES
B SILICON MONOXIDE SOURCE

FIG. 24

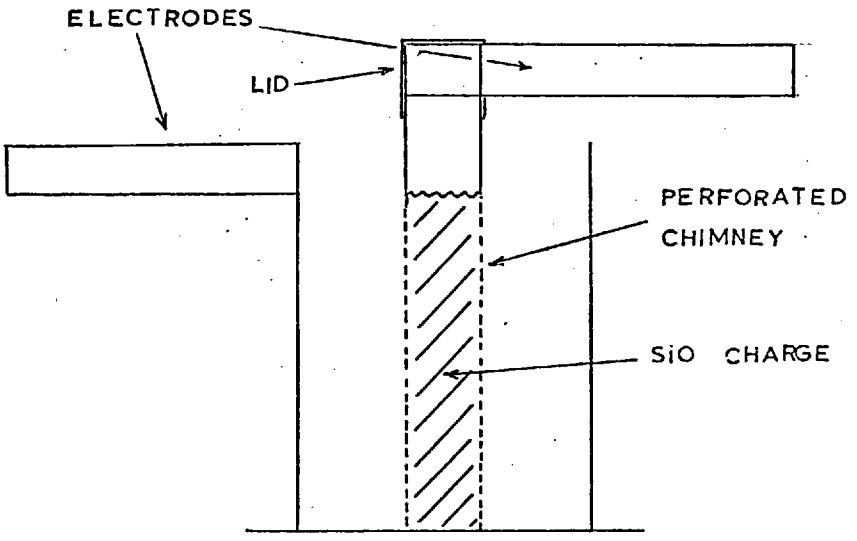

TANTALUM SiO SOURCE

FIG. 26

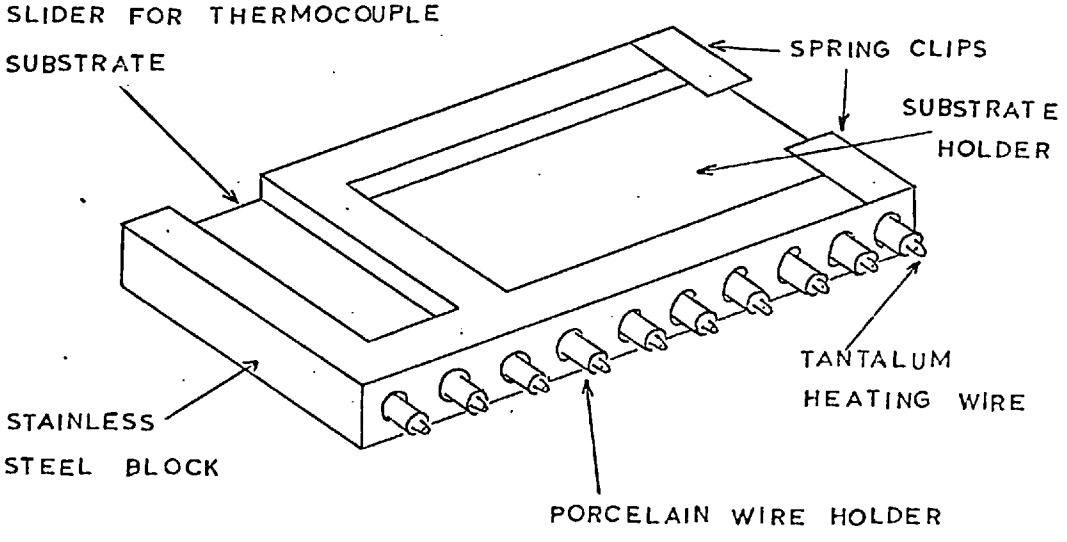

SUBSTRATE HOLDER AND HEATER

the outer cylinder temperature was 875°C compared to 1205°C of the inner cylinder. These temperatures were measured with Pt/PtRh thermocouples, spot-welded to the source.

The electrical connections to the source and thermocouples were made through a section of 0.5 ins. thick dural pipe. The gas leak inlet and the ionisation gauge head also passed through this pipe section.

4.4 Head Plate

To enable the substrate mechanics to be handled more efficiently, the remainder of the chamber requirements were fitted on to a head plate. This could be easily removed and was used in preference to the conventional system of a bell-jar with all connectors passing through a base-plate. The 1.0 ins. thick dural head-plate was supported on a 9 ins. length of 6 ins. quartz pipe section, which fitted directly on the source support. Figure (25) shows the underside of the head plate.

4.4.1 Substrate Heater

The substrate heater is shown schematically in Figure (26). The former consisted of a stainless steel block through which holes were drilled. Porcelain

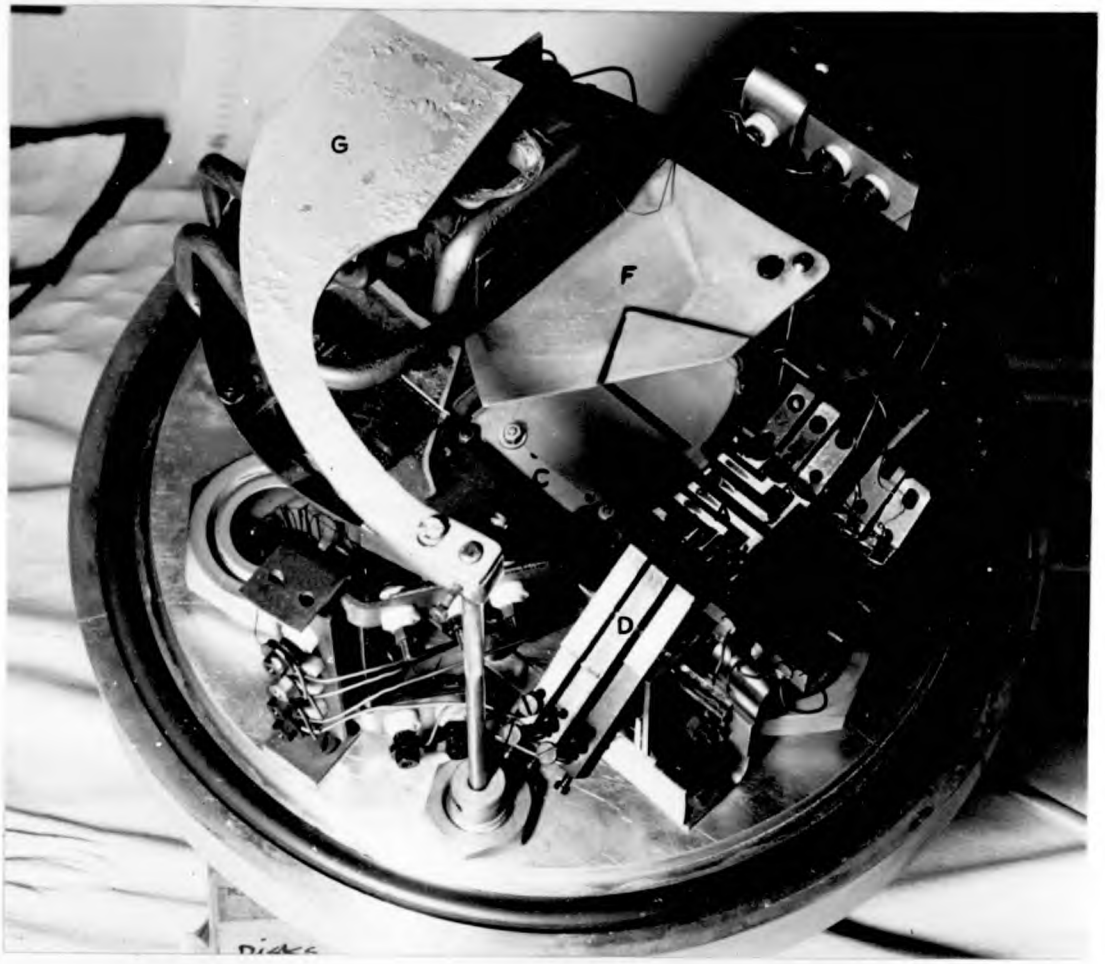

FIG. 25 UNDERSIDE OF HEAD PLATE

A	SUBSTRATE
B	THERMOCOUPLE
C	ROTARY MASK HOLDER
D	PRESSURE CONTACTS
E	CRYSTAL RATE MONITOR
F	SUBSTRATE SHUTTER
G	RATE MONITOR SHUTTER

insulating carriers were inserted in these holes with .010 ins. tantalum wire passing through and back along each element, reducing the effect of the heating current. Stainless steel strips were spot-welded into the block to locate both the substrate and thin film thermocouple support, shown in Figure (25). These substrates were held in position in the inverted state by spring clips spot-welded into the strips and also by the pressure contacts for the electrical measurements. A chromel/alumel thermocouple junction was inserted into one of the porcelain carriers to indicate the temperature of the heating wire.

4.4.2 Mask Changer

The mask changer, shown in Figure (27), locates over the substrate by the screws holding the masks on to the changer. These fit either side of the heater block. The rotary control is sprung so that in order to change a mask, the rotor is depressed and rotated and located with the next set of screws. There are four possible settings of the mask changer, three for capacitor production and the fourth for encapsulation. The masks could be fitted on to either side of the changer for close or shadowing contact. A close contact mask produced a well defined edge of the evaporated

FIG. 27 SUBSTRATE HOLDER AND MASK CHANGER

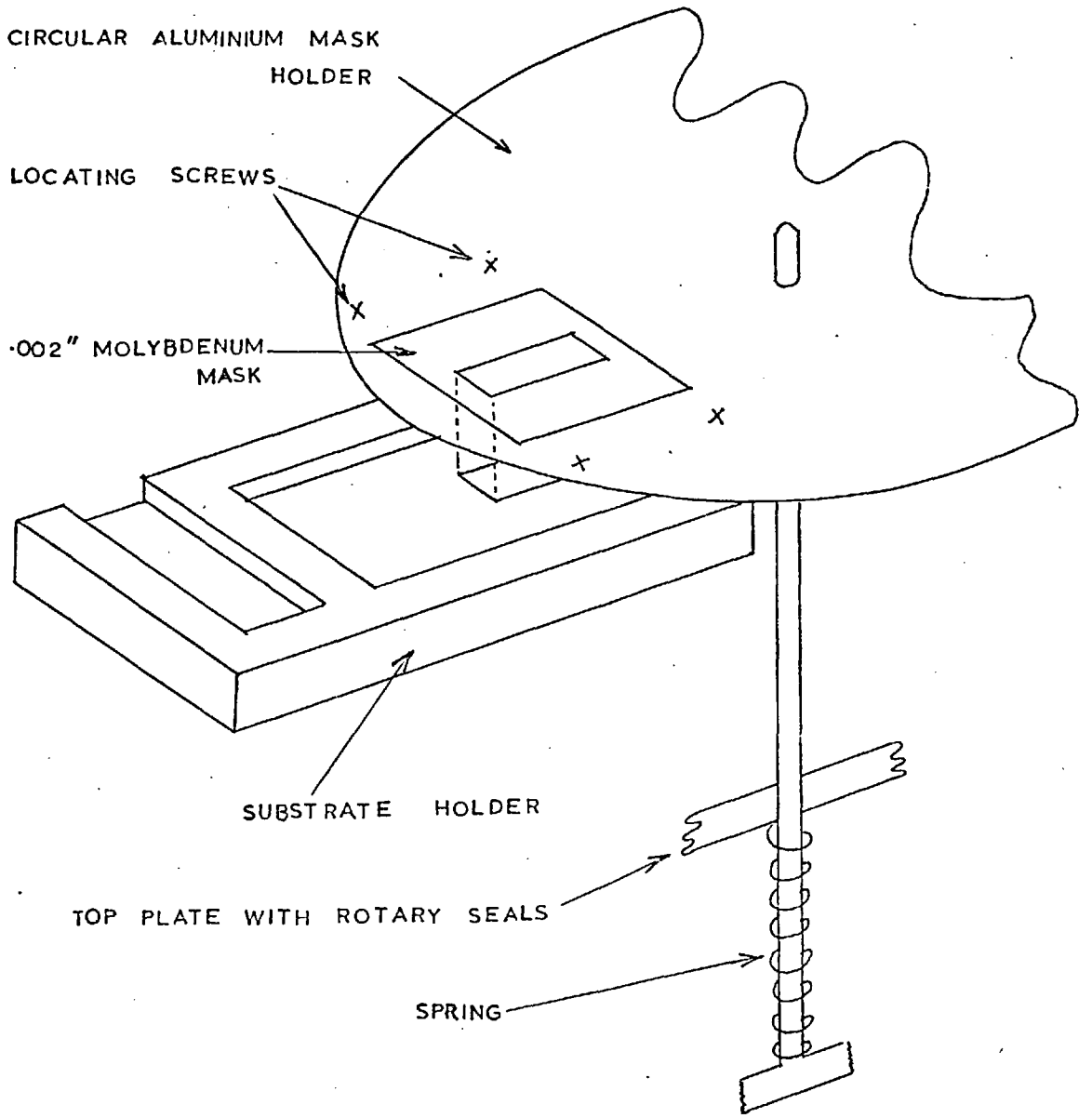

film. A shadowing contact mask produced a diffuse edge which was less likely to produce breakdown in the capacitor edge of the top aluminium electrode (see Siddall[108]).

4.5 Mask Production

Two methods of mask production were tested, a spark erosion process[110] and a photo-etching technique[110]. The latter was found to be a superior technique due to a better edge definition.

4.5.1 Spark Erosion

In order to produce a hole in a sheet of molybdenum, a copper block was produced with a cross-section identical to the shape of hole required. Immersed in a paraffin bath, the block was brought into contact with the molybdenum sheet and a direct current passed through the system. The molybdenum was eroded away at the point of contact. The accuracy to which a slit could be made was $\pm$ 0.1 mm. The optical microscope showed that the edge definition was poor compared to the photo-etching technique.

4.5.2 Photo-Etch Technique

When this technique was first tried, several difficulties were encountered and the following para-

graphs give the method which was finally used for producing masks.

A drawing of the required pattern was produced, ten times the actual mask size. Black tape was stuck to the part to be removed from the mask and a negative produced the reduced size, by photographing the drawing.

The mask material used was .002 ins. molybdenum sheet. This was prepared by roughening one of the surfaces with emery cloth and ultrasonically cleaning it in "R.B.S. 25" to remove grease. The sheet was then clamped at the centre of a centrifuge table which was rotated at maximum speed. While spinning, the sheet was sprayed with iso-propyl alcohol to clean it. When dry, the photo-resist (Kopierlack-P) was sprayed on and five minutes spinning motion ensured even coverage of resist. After allowing to dry, the molybdenum sheet was removed and placed in an oven to harden at 80°C.

The negative was then placed over the molybdenum sheet and clamped with a glass slide to prevent crinkling of the negative in the heat. This assembly was exposed to ultra-violet light for about five minutes.

The resist was developed in Ozalid K.E.P. developer for about one minute and washed. It was then baked in an oven at about 250°C for fifteen minutes. This

had the effect of changing the colour of the resist and making it resistive to the subsequent etch.

As much of the surface as possible, except close to the masking edges, was coated with Lacomit, an etch resistant material. An etch developed by Fisher[111] was used, made up as follows:-

60 cc HNO_3
35 cc H_2O
5 cc H_2SO_4
50 cc Acetic acid

When the etch appeared to have removed the unwanted molybdenum, the metal sheet was left a further 30 secs. in the etch solution before removing and washing.

Finally the Lacomit and resist were removed with acetone and the mask cleaned and cut to the required shape.

4.6 Temperature Measurement

A thin film thermocouple enabled the actual temperature of a thin film capacitor to be determined reasonably accurately. Two identical thermocouples were produced in one operation on separate $\frac{1}{2}$" x 1" Corning 7059 glass substrates, in order to investigate the temperature gradient across the heater block.

Copper/manganese contact pads were first evaporated on to the glass substrates which adhered well to the glass and were not removed by the pressure contacts. Copper and nickel were the materials used and the two films crossed at the centre of the block. A silicon oxide protective layer was deposited over the thermocouple

In order to eliminate the e.m.f.'s produced at other junctions, copper or nickel wire was wrapped around the pressure contacts and made direct connection to the electrode terminal.

The thermocouples were calibrated by immersion in oil and measuring the oil temperature with Cromel/Alumel thermocouples. The oil was mechanically stirred and the whole system allowed to reach an equilibrium temperature by taking readings every hour. The e.m.f.'s of the two thermocouples agreed to within less than $1^{o}/o$. The calibration curve is shown in Figure (28).

The temperature gradient across the heater block was determined by placing one thermocouple in its correct position and the other at various positions along the block, corresponding to the positions of the evaporated capacitors. There was found to be only $1^{o}/o$ deviation across the block, if the block was allowed to reach an equilibrium temperature. Due to the large

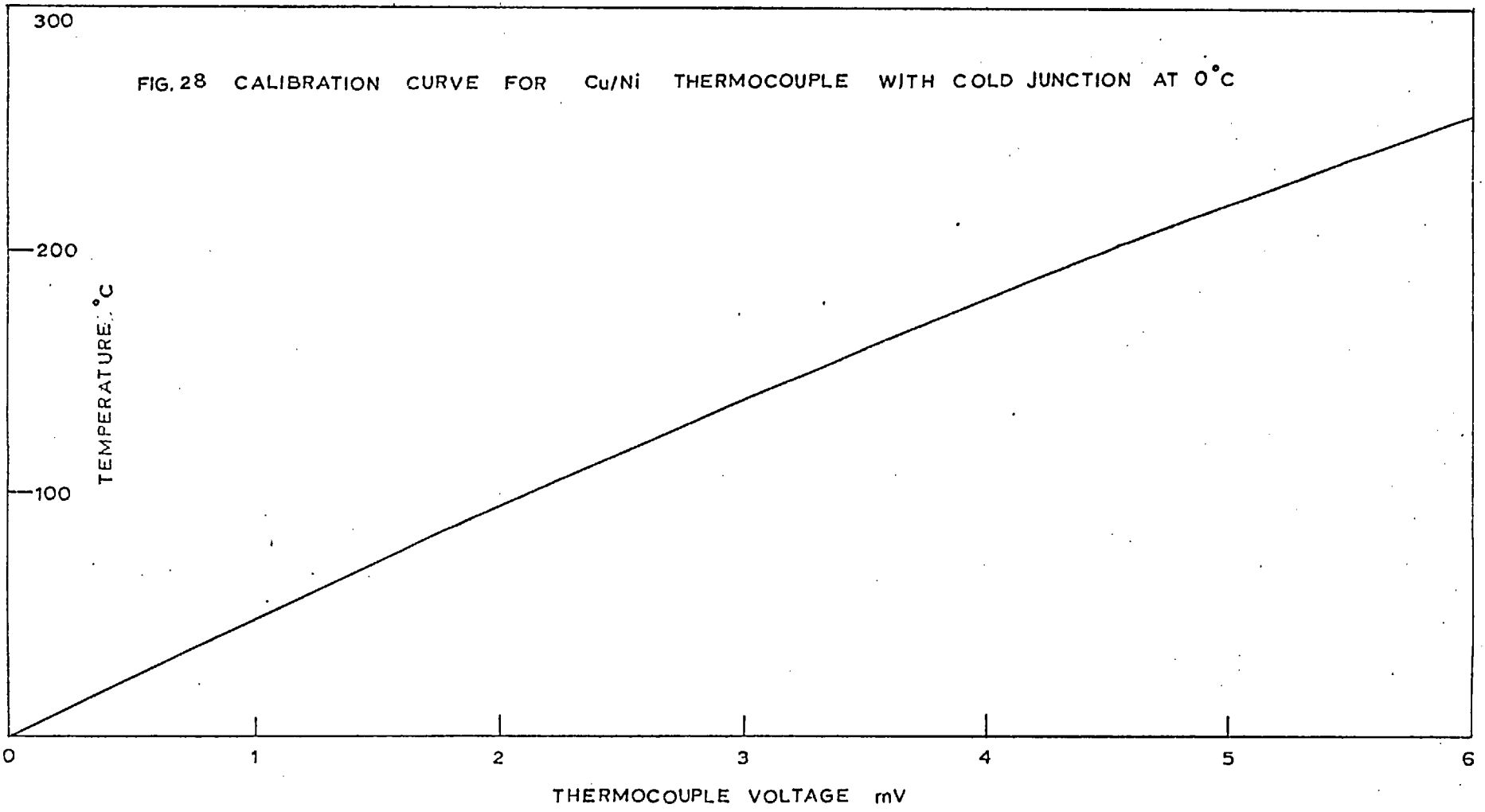

FIG. 28 CALIBRATION CURVE FOR Cu/Ni THERMOCOUPLE WITH COLD JUNCTION AT 0°C

thermal mass of the block this took about $1\frac{1}{4}$ hours. In all experiments when the temperature was varied, readings were taken every $1\frac{1}{4}$ hours so that the temperature indicated by the thin film thermocouple was very nearly that of the capacitor. The only occasion when this was not true was during an evaporation, when local heating took place due to radiation from the silicon oxide source.

Heat transfer by radiation and conduction also heated the head-plate assembly and the quartz pipe section. Because of the viton seals in the assembly, the ultimate temperature at the substrate was restricted to 250°C.

4.7 Pressure Contacts

Connections to the copper/manganese electrode contact pads were made by means of spring contacts, made from nickel silver relays having spherical contact tips. These leaves were spot-welded on to steel arms which were pivoted on a quartz rod axle. Good contact was achieved by tightening screws against a glass plate. Three pressure contacts were made on each side of the heater block for electrical measurements and two contacts to the thin film thermocouple.

4.8 Electrode Design

For the initial experiments, it was decided to evaporate five capacitors which would fully utilise the six contacts available. The electrode area was made small to reduce the effect of pin-holes. Because the mask changer always covered part of the substrate, it was necessary to use long thin film electrodes to the contact pads.

In the frequency variation experiments where the resistance of the electrodes becomes an important factor at high frequencies, it was decided to monitor the resistance of the electrodes. This was made possible by making contact at each end of the electrodes. With six contact pads available, only two capacitors could be evaporated at once.

Figure (29) shows the electrode design for both five and two capacitor production before the aluminium electrodes were evaporated and also after the capacitors had been produced.

4.9 Mechanical Disc Rate Monitor

4.9.1 Introduction

A disc-type rate monitor was developed, having the advantages of economical construction and being bakeable.

FIG. 29 ELECTRODE CONFIGURATIONS

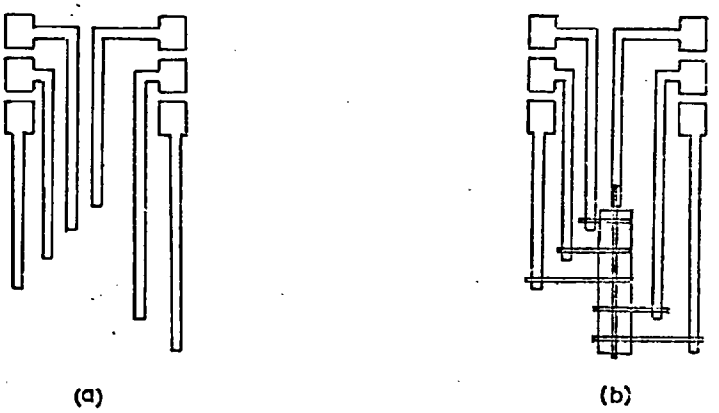

5-CAPACITOR ELECTRODE CONFIGURATION. (a) INITIAL Cu-Mn ELECTRODES. (b) (a) + Al. ELECTRODES AND DIELECTRIC.

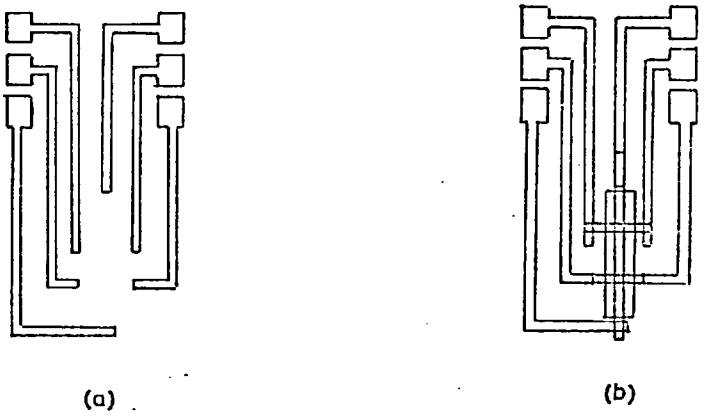

2-CAPACITOR ELECTRODE CONFIGURATION (a) INITIAL Cu-Mn ELECTRODES. (b) (a) + Al. ELECTRODES AND DIELECTRIC.

Measurement of rate using the momentum of the incident vapour stream was first developed by Campbell and Blackburn[114], who used a modified milliammeter movement attached to a vane . The current required to produce zero deflection in the vapour stream was measured. On completion of the practical work on the disc rate monitor, Beavitt[115] published a paper discussing both a cylindrical and disc-type rate meter, giving the relevant theory.

4.9.2 Theory

Figure (30) defines the parameters required to give the theory. The disc was used to indicate rate and not to monitor thickness and so was suspended from a fine suspension wire. Thus a constant flux of particles would give a constant angle of rotation. A magnetic circuit was used for damping purposes.

The turning couple 'α' produced by the incident flux is given by

$$\alpha = 2nm\bar{c} \cos \phi \sin \phi \int_0^{\frac{\pi}{2}} \int_0^{r} \cos \theta \, r^2 \, d\theta \, dr$$

$$= \frac{2}{3} nm\bar{c} \, r^3 \cos \phi \sin \phi$$

where '$\bar{c}$' is the average particle velocity, 'n' the particle density and 'm' the mass of a particle.

FIG. 30 MECHANICAL DISC RATE MONITOR

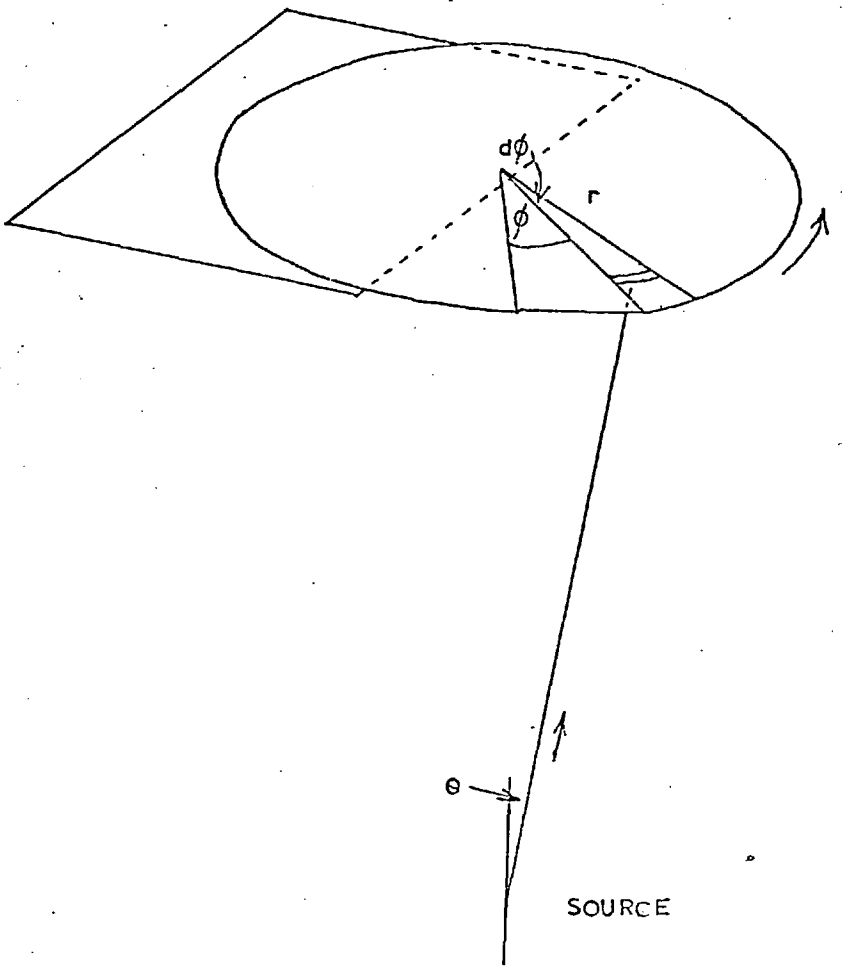

n PARTICLE FLUX mols. per sec per unit area

$\bar{c}$ AVERAGE PARTICLE VELOCITY

m PARTICLE MASS.

This couple is balanced by the torsion in the suspension wire '$c\theta$' where 'c' is the torsional constant of the suspension.

If 'p' is the density of the deposit, then the rate of deposition is given by

$$\frac{3c\theta}{2p\,\bar{c}\,r^3\cos\phi\sin\phi}$$

The important result is that the rate is proportional to 'θ'.

4.9.3 Experimental Arrangement

The 2" diameter disc was made of aluminium foil, dished between two watch glasses to improve rigidity and to improve balance by lowering the centre of gravity below the point of suspension. The disc was marked in sections so that with the use of a pointer, the number of revolutions could be determined.

The disc was suspended by an aluminium mounting into which the gold alloy suspension wire was clamped. About 12 cms. of .002 ins. x .0002 ins. gold alloy suspension wire was used, which was soldered to a manoeuvrable gold wire at its other end. A magnetic circuit was introduced to produce damping and also to smooth out the effect of irregularities in the rotor.

The air gap of the magnetic circuit was varied to give a response time of about 2 seconds. The experimental arrangement is shown in Figure (30(a)).

4.9.4 Disadvantages

The size of the vacuum chamber in which the rate monitor was used put severe restrictions on its use. The usual sensitivity was about 180° rotation for a rate of 1Å/sec at the substrate. The high sensitivity was caused by the proximity of the disc to the silicon oxide source, but this also meant that the thickness of deposit on the disc would build up very quickly. The stresses set up in the film would sometimes cause the disc to crumple.

The fineness of the suspension wire made it extremely difficult to handle, so that control of the length of wire was difficult. This had the effect of altering the sensitivity for each run and hence the final thickness and rate could not be predicted accurately.

Spitting on to the disc from the source caused the disc to spin so that the number of revolutions could not be determined.

Due to the large number of disadvantages it was decided that an Edwards Crystal Rate Monitor should be

FIG. 30(a) DISK RATE MONITOR SHOWING POSITION RELATIVE TO SILICON MONOXIDE SOURCE

A DISK
B MAGNETS
C SUSPENSION WIRE
D SILICON MONOXIDE SOURCE

used. This had none of the disadvantages listed above.

4.10 Crystal Rate Monitor

The resonant frequency of a crystal is a function of its mass. If its mass is altered by a film forming on one of its surfaces, its resonant frequency will change. Theory shows that the change in mass or thickness of deposit is proportional to the change in its resonant frequency. This principle is incorporated in the quartz crystal rate monitor which indicates both rate and total thickness.

The instrument was calibrated by measuring the thickness of a film using a T lysurf (see Section (4.11)) for a measured time of evaporation. The average calibration factor was 2.2 c/s frequency change for a deposit of 1Å at the substrate.

Despite the crystal having an A/T cut[116] to reduce temperature sensitivity, the crystal's resonant frequency was altered by the hot source. Therefore a system of water cooling was used.

The crystal can holder was inserted into a copper box with walls .25 ins. thick, surrounded by copper piping carrying the water. A molybdenum shield, .002 ins. thick, allowed just enough evaporant to cover the crystal so that the copper box was not exposed

directly to the vapour stream. The water-cooled copper box is seen in Figure (25). The molybdenum shield was attached to another shield which stopped the sources contaminating the substrate machinery. With no material in the source and the source at the temperature of evaporation, there was about a 1°/o change in the resonant frequency of the crystal with the water cooling.

The rate monitor was used as a rate controlling device and also to give a guide to the thickness required. The actual average rate was determined by measuring the thickness with a Talysurf and dividing by the time of evaporation. This meant that no accurate calibration was required as this was dependent to a small amount on the thickness of deposit already on the crystal.

4.11 Thickness Measurements

4.11.1 Talysurf Method

Film thickness measurements were performed using the Talysurf[117, 118], a product of Taylor-Hobson Limited, Leicester.

The principle of operation is that a reference skid and a free stylus transverse a surface. Vertical motion of the stylus is electrically sensed and after amplification, displayed on a moving chart by an

electrical discharge on carbon backed starch-iodide rectilinear paper. However, the Talysurf is not an absolute intrument and is calibrated using optically determined step heights. It is basically a surface profile instrument but, by knowing the magnification, the height of a step can be determined. The runs were made per film so that an average could be determined. For films of 2000Å thickness, the highest magnification range of x 100,000 could be used. With 0.5 mm. being the smallest distinguishable measurement, an accuracy of $\pm$ 50Å or better could be obtained. Such accuracy was only feasible if the substrate and film surfaces were smooth. Corning '7059' glass has surface irregularities of less than 25Å and this was used in preference to soda glass microscope slides. Another requirement for accurate measurements is that the stylus does not scratch the surface of the film. The film thickness being measured was silicon oxide which, being a glassy material, was very hard.

It was necessary to remove any dust particles from both sides of the substrate. Dust on the underside caused rocking and dust on the film showed on the trace if traversed.

A typical trace is shown in Figure (31). If the surface were parabolic, the relative motion of the

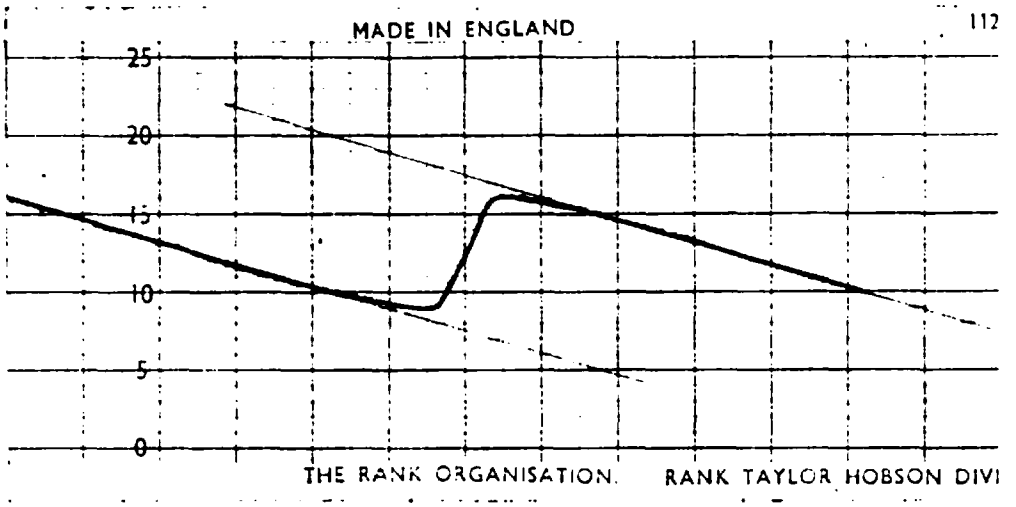

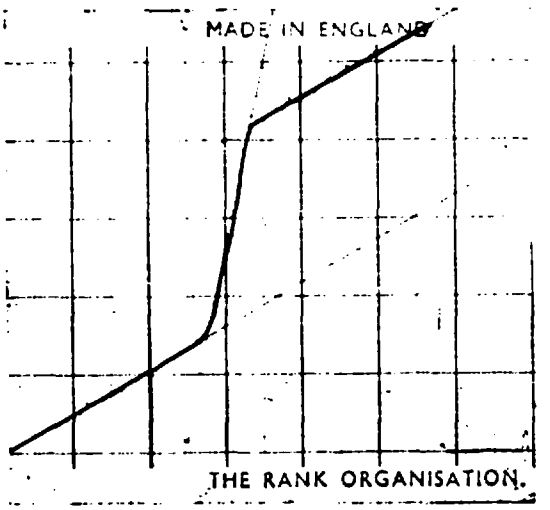

FIG. 31 EXAMPLES OF TALYSURF TRACE. VERTICAL MAGNIFICATION x 100,000 , STEP HEIGHT MEASURED IS VERTICAL SEPARATION OF LINES

skid and stylus resulted in a slope on the chart. However, this did not impede measurements if the distance between traces at 90^{o} to the direction of motion were measured.

Knowing the horizontal magnification, the width of a film could be determined accurately using this method.

4.11.2 Optical Method

The optical method of determining film thicknesses is an absolute method and involves the formation of Fizeau fringes using an interferometer. Of the three variable parameters involved, approach angle and wavelength of light are kept constant, so that the thickness of the film is the only variable. In order to obtain a reasonable fringe definition, at least a $94^{o}/o$ reflectivity on both surfaces of the edge is required. Therefore it was necessary to deposite a reflective coating of aluminium on the step.

The optical flat of the interferometer was brought into contact with the top film surface and the interference fringes viewed through an eye-piece. The shift in crosswire in the eye-piece was calibrated so that the fringe spacing and fringe offset could be measured.

The equation for determining the step height is

$$\text{Step Height} = \frac{\text{Fringe Offset}}{\text{Fringe Spacing}} \times 2946\text{Å}$$

2946Å is one half the wavelength of the sodium vapour light source.

An average of three vernier readings was taken for each position of the hair line. Step heights taken at three different points along the step agreed to within $\pm$ 30Å.

4.11.3 Summary

The accuracies of the two methods for determining film thicknesses were similar. However, it should be pointed out that Taylor-Hobson have now produced an instrument called a Talystep which produces a vertical magnification of one million. The Talysurf method was preferred as it did not involve the deposition of a reflecting coating over the step.

The electrode pattern was so designed that both the skid and the probe of the Tolysurf were in contact with the substrate only before the step was transversed. However, with more complex circuits this would not be possible and it becomes advantageous to use the interferometric method.

4.12 Head Plate Connections

Figure (32) shows an overall picture of the top side of the head plate.

There were three rotary seal connections, one to the mask changer, one to the substrate shutter and one to the crystal shutter. The thermocouples' connecting plate was attached directly to multicore wire which plugged into a switching box. All the thermocouples had a cold junction in ice.

Contact to the capacitors was made by attaching crocodile clips on to the appropriate points on the connecting plate.

P.V.C. tubing carried the water supply to and from the cooling system. The copper piping was one continuous piece, being soldered into a large blank inlet electrode.

4.13 Substrate Material and Preparation

Capacitance and conduction measurements, at high frequencies in particular, can be influenced by conductivity of the substrate material. Soda glass microscope slides were initially tried as a substrate, but the stray capacitance and conductance was found to be quite significant, especially at elevated temperatures. It was decided to use a barium-alumino silicate glass, type 7059 manufactured by Corning Glass. This glass

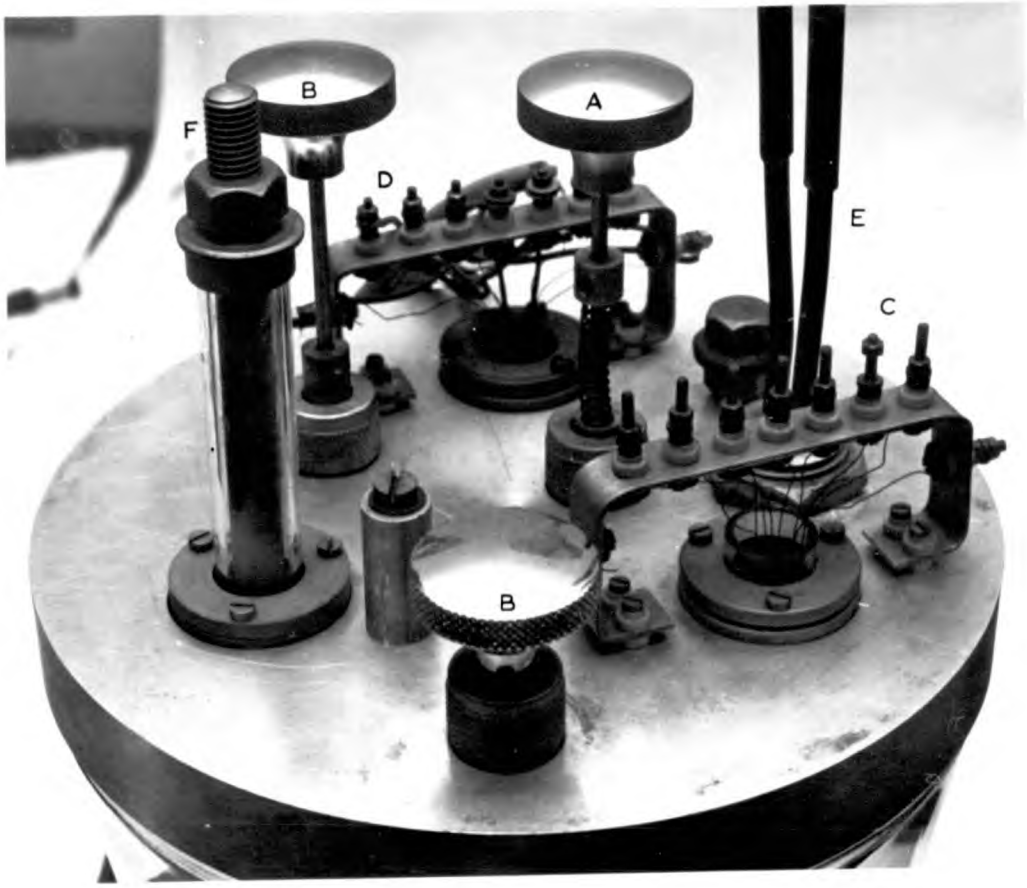

FIG. 32 TOP SIDE OF HEAD PLATE

A MASK ROTATOR

B SHUTTER OPERATORS

C CAPACITOR CONNECTIONS

D THERMOCOUPLE CONNECTIONS

E WATER COOLING

F SUBSTRATE HEATER ELECTRODE

was developed for micro-electronic circuit fabrication. It has a very low ionic conductivity at elevated temperatures and also a very smooth finish. The latter consideration gives a greater accuracy in film thickness determinations.

The substrates were supplied by the manufactuers in a "clean" condition, except for a layer of dust. However, it was still thought necessary to give them an additional clean.

Various methods were tried but it was difficult to assess the advantages of different methods. The method which was finally decided upon began with wiping the substrate using a hot Stergene solution to remove grease. After rinsing in distilled water, the substrate was ultrasonically cleaned in a solution of R.B.S. 25, an organic decontaminant, for about fifteen minutes. The substrate was again rinsed in distilled water and after drying, ringed in iso-propyl alcohol vapour which was continually redistilled in iso-propyl alcohol for several hours.

The copper/manganese electrodes were deposited in a separate vacuum chamber, the substrate being heated during evaporation to give better adhesion. The substrate plus electrodes was again placed in the refluxing system for several hours, before finally being introduced

into the vacuum chamber. Pieces of dust which adhered to the substrate were removed by a jet of air. At all times the substrates were handled with tweezers.

4.14 Film Preparation

The two electrode and dielectric evaporations and all electrical measurements were performed in one pump-down. This reduced to a minimum contamination from the atmosphere and enabled the dielectric to be evaporated on to a clean aluminium surface without introducing the complication of having an Al_2O_3 layer at the interface.

Both the aluminium electrodes were deposited on to a room temperature substrate, the common electrode being deposited first. The electrodes for a 5-capacitor evaporation were made by evaporating a standard amount of aluminium wire and assuming the resistance was constant for every evaporation. The electrodes for 2-capacitor preparation were monitored by measuring their resistance during evaporation. The resistance of the electrodes was accounted for in the computer program (see following section).

Except when rate was the parameter being varied, it was kept constant during all evaporation at about $10\text{Å/sec.} \pm 1\text{Å/sec.}$ As the current through the silicon

oxide source was increased, the temperature was maintained, which gave an indication when to expose the quartz crystal to the evaporant by operating a shutter. The crystal was not exposed unnecessarily, as the sweep of the thickness indicating needle was almost the complete traverse of the scale. By knowing the rough calibration of the rate meter, the approximate rate was obtained. Five minutes were allowed for the rate to become steady, when the substrate shutter was operated and the time taken for the crystal frequency to change a precalculated number of c/s. For a film of 2000Å thickness the time of evaporation on to the substrate was 3 mins. 20 secs. The average rate was determined using the Talysurf as explained in Section (4.11.1). Because the film thickness could be measured to $\pm$ 50Å, the average rate could be determined to within an accuracy of $\pm$ 3°/o. During the evaporation the rate fluctuated only a small amount which was compensated for by increasing or decreasing the current through the source.

The pressure in the chamber was measured both before and during evaporation.

Measurements were not performed until at least one hour after evaporation in order to allow the dielectric to cool to room temperature.

The substrate and film were not removed from the chamber until the end of each experiment or unless the film was to be oven-annealed at 400°C. In the latter case, the film was always annealed at 240°C in the chamber before being exposed to the atmosphere. Subsequent measurements were performed after replacing the substrate in the chamber and evacuating the system.

4.15 Calibration of Apparatus

Two types of calibration were performed on the apparatus, both as functions of temperature and frequency.

The first calibration determined the stray capacitance and conductance existing between the two measuring terminals when there were no capacitors on the substrate. The system was prepared as for an evaporation with the copper/manganese electrodes deposited. The stray capacitance and conductance were then measured with the various bridges as functions of temperature and frequency.

The stray capacitance for the audio frequency arrangement was less than 1 p.F. and was neglected, as was the conductance, both being independent of temperature and frequency.

Long leads were used for the radio frequency

calibration having a stray capacitance of 8 p.F. and negligible stray conductance. The stray capacitance was accounted for before the results were programmed.

The second type of calibration was to determine the lead resistance in the 5-capacitor case. This was done by evaporating a known amount of aluminium wire from each source, without the dielectric layer separating the electrodes. The resistance of the levels as a function of temperature was determined using an avometer. The value was 30 ohms indpendent of temperature.

In the 2-capacitor case the resistance of the leads was determined in each experiment since the resistance of the leads could be monitored. This meant that at high frequencies, an accurate value of resistance could be determined.

4.16 Electrical Measurements

4.16.1 A.C. Measurements

All the initial experiments on variation of evaporation parameters and annealing work were performed on a Wayne Kerr B221 bridge, together with the AA221 auto-balance adapter. The bridge had a fixed internal frequoncy source of 1592 c/s ($\omega = 10^4$ rads/sec). It gave both capacitance and conductance

values to four figures. The first two figures were manually set up on the B221 and the last two figures displayed automatically on the AA221 adapter. So that continuous readings of capacitance could be made, an A.E.I. 10 ins. potentiometer recorder, type 10S, was connected to an output of the adapter via an alternating and smoothing circuit. The block diagram is shown in Figure (33) with only the quadrature component detection illustrated.

The B221 bridge was also used for frequency variation measurements in the audio frequency range. An Advance Signal Generator, type H1, was used to generate a sinusoidal signal with a frequency range of 15 c/s to 50 c/s. The out of balance signal from the bridge was detected using a Radiometer, Copenhagen wave analyser, type FRA2, with a maximum sensitivity of less than 1 μV. The frequency range was 10 c/s to 16 Kc/s. The minimum frequency for accurate measurements was 300 c/s.

The bridge used for the radio frequency range was the Wayne Kerr type B601, with a frequency range of 15 Kc/s to 5 Mc/s, with an accuracy of $\pm$ 1%. The R.F. signal generator was an Airmec instrument with with a frequency range 30 Kc/s to 30 Mc/s. The out of balance detector was an Airmec wave analyser, type 853, with the same frequency range as the signal generator.

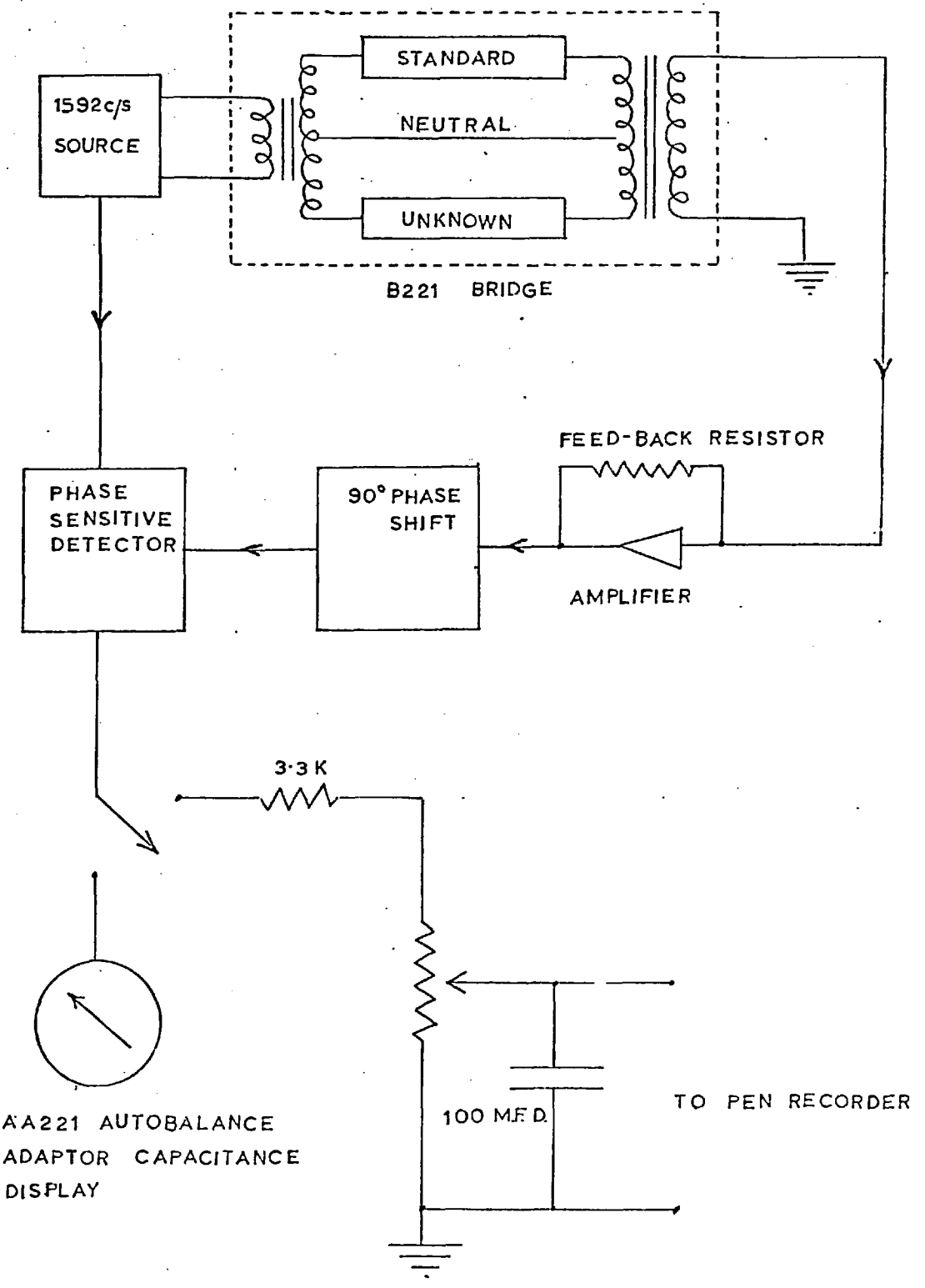

FIG. 33 BLOCK DIAGRAM OF WAYNE KERR B221 UNIVERSAL BRIDGE COUPLED TO THE AA221 AUTOBALANCE ADAPTOR SHOWING EITHER PEN RECORDER OR DIRECT CAPACITANCE READOUT

The bridge arrangement was unsuitable for measurements of frequency greater than 1 Mc/s.

4.16.2 D.C. Measurements

A Solatron transistor power supply, type A57572, was used as a stable D.C. voltage supply. The voltage drop across the dielectric was taken as the output voltage of the power supply. This was so if the voltage drop across the current measuring instrument was made negligibly small. The current was measured using a Model 610B Keithly electrometer which was capable of measuring a current of 10^{-14} amps to an accuracy of $\pm$ 4%. During the investigation of the transient current as a function of time, the Keithly was used in conjunction with a Bryan X-Y coordinate plotting table.

4.17 Elimination of Lead Resistance

Because the series resistance of the leads was known, it was possible to calculate the real parallel resistance and loss of a capacitor knowing the measured capacitance and loss.

If we let 'R_p' and 'C_p' be the measured components and 'R' and 'C' be the true values and 'R'' the series resistance of the leads, then the complex impedances

of the equivalent circuits can be calculated.

If $t_p = \omega C_p R_p$ and $t = \omega R C$

$$C = \frac{C_p (1 + t_p^2)}{1 + t_p^2 + A^2 - 2A} ,$$

$$R = \frac{C_p}{C} \frac{R_p}{(1 - A)}$$

where $A = \frac{R'}{R_p} (1 + t_p^2)$ and $t = \frac{t_p}{(1 - A)}$

The true loss = $\tan \delta = \frac{1}{t} = \frac{1}{\omega RC}$

Measurements were made on five capacitors at eight different temperatures which made it necessary to produce a computer program to calculate the required parameters.

Because the five capacitors were very nearly equal in thickness and area, average values of the parameters were determined.

For high loss, the power dissipated is proportional to sin δ rather than tan δ, so this parameter was determined also.

A first order approximation of the γ_c and T.C. (tan δ) was computed by the following method. From

Figure (34) the slope of the curve at a point $C = \frac{C_1 + C_2}{2}$ was taken as $\frac{C_2 - C_1}{T_2 - T_1}$ at a temperature of $\frac{T_2 + T_1}{2}$ which was a first order approximation when the curvature in the range investigated was only small.

An average value of γ_c was computed by two methods. Firstly, from the average of all the γ_c's and secondly, from the value of γ_c's for the average values of capacitance. The difference between these two derivations was a guide to the initial spread in capacitor values. The program and an example computer result sheet are shown in the Appendix.

FIG. 34 FIRST ORDER APPROXIMATION OF TEMPERATURE COEFFICIENT OF CAPACITANCE.

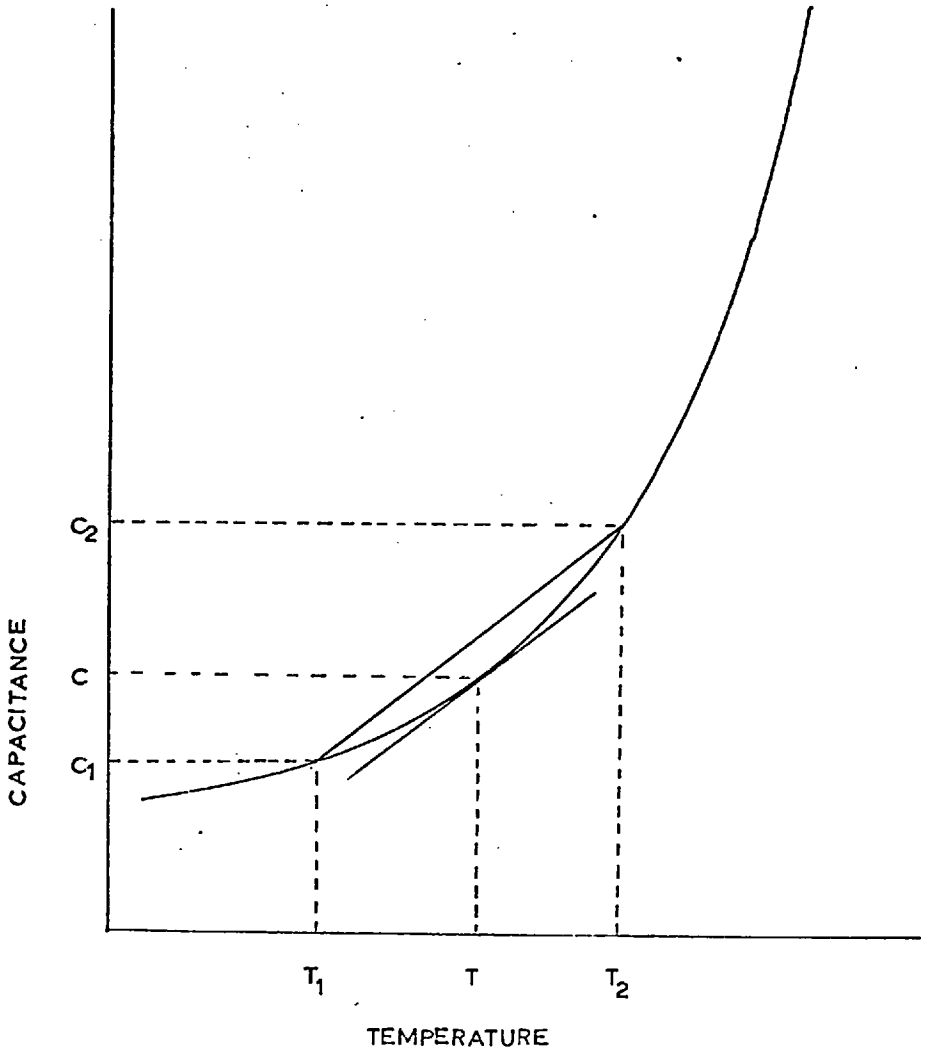

$$\text{T.C.C. AT } T=\frac{T_2+T_1}{2} \simeq \frac{2(C_2-C_1)}{(C_2+C_1)(T_2-T_1)}$$

CHAPTER 5

EXAMINATION OF FILMS

5.1 Electron Microscopy

Specimens were prepared for electron microscopy by evaporating the silicon oxide films directly on to Corning 7059 glass substrates. The films were removed by immersing the substrate into diluted hydrofluoric acid and floating the films off in distilled water. Fragments of the films were picked up on microscope grids and dried before examination.

Electron microscopy showed no indication of structural features such as pin-holes. However, films deposited on to aluminium showed a dome-like structure[12] which has been shown to be replicated from the surface of the aluminium. It is not clear how these domes originate but they do not appear to affect the electrical properties.

5.2 Electron Diffraction

Specimens for electron diffraction were prepared by evaporating about 200Å of silicon oxide directly on to freshly cleaved rock salt. This enabled the film to be floated off in distilled water and picked up on to microscope grids. Figure (35) shows the resulting diffraction pattern. Determination of the radial

FIG. 35 DIFFRACTION PATTERN OF SILICON OXIDE FILM

distribution function, $4\pi r^2 u(r)$ was made by Bicknell of the Allen Clark Research Laboratories, of the Plessey Company. The diffracted intensity was determined using a microdensitometer with a linear output and scanning the photographic plate along a radius. Figure (36) shows the radial distribution function.

The interpretation of the radial distribution function is the subject of some controversy. However, one result which is generally accepted is the existence of Si-O tetrahedra in silicon oxide. The first peak at 1.62Å corresponds to the Si-O peak as observed in vitreous silica. The second peak at 2.65Å corresponds to the O-O peak. The coordination number of about 4 suggests that silicon and oxygen exist in a tetrahedral bonding with the Si-O-Si bond at an angle of about 145°C. This will not account for the structure of SiOx where x is intermediate between one and two. Coleman and Thomas[19] suggest the 'extra' silicon exists as small islands within a silica matrix which would be given by a peak at 2.35Å. In the present work there is not sufficient evidence for the introduction of such a peak, and it is considered that the silicon-oxygen tetrahedra are interlinked with some combination of Si-O bonds (see also infra-red evidence, Section 5.3).

FIG. 36 THE RADIAL DISTRIBUTION FUNCTION OF SILICON OXIDE DEPOSITED AT 10 Å/SEC AT A PRESSURE OF 2.10^{-5} TORR

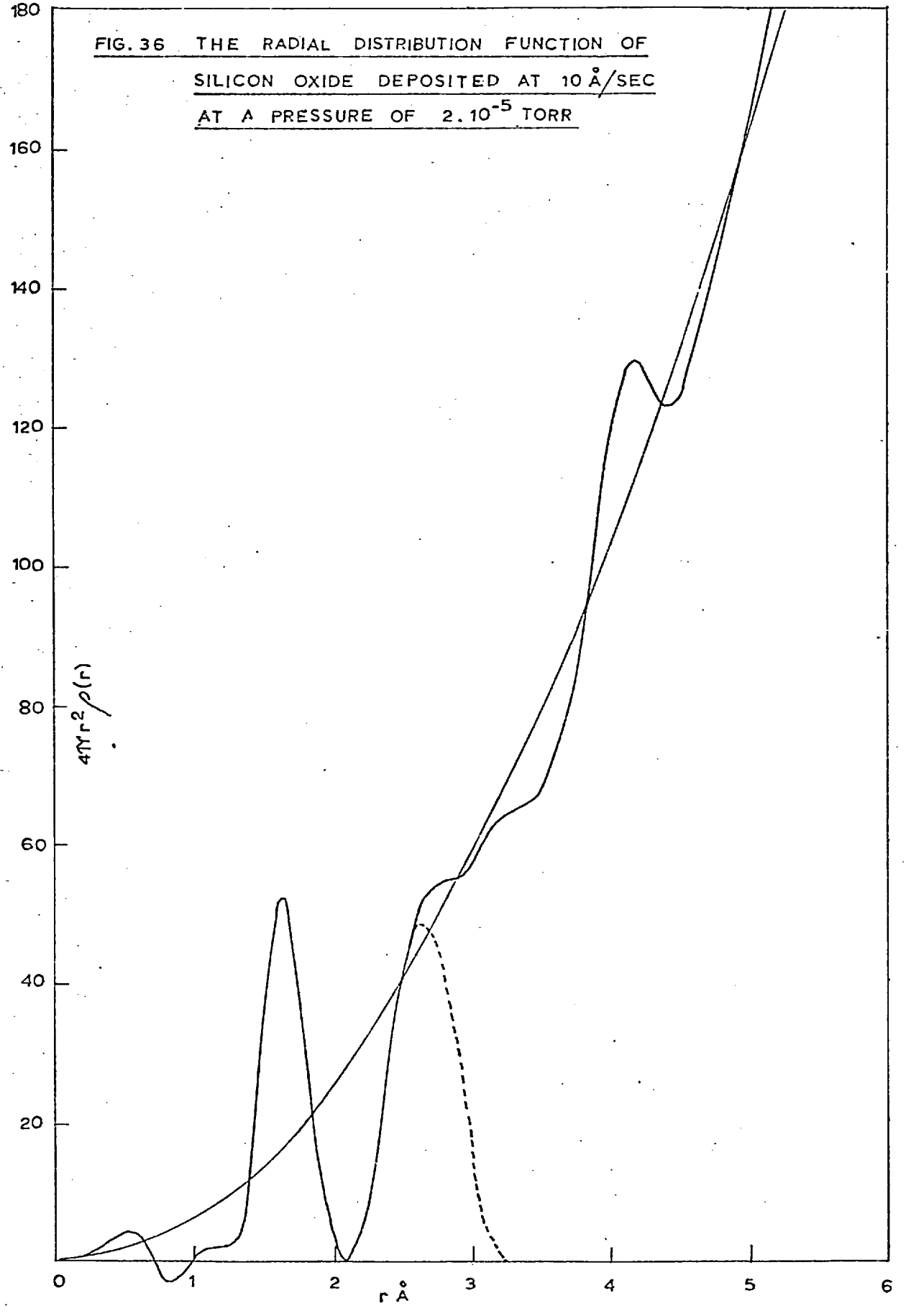

5.3 Infra-Red Spectroscopy (I.R.S.)

In this work I.R.S. was used to give an indication of the degree of oxidation of silicon oxide and also to detect either water or hydrogen present in the film before annealing.

The silicon oxide was evaporated directly on to a potassium bromide disc, pressed from the powder. A control disc was placed in the vacuum system so that it received the same treatment except that no film was deposited on to it. Measurements were then performed on each disc and on both using a two beam method, eliminating the effect of absorption due to the KBr substrate. The machine used was a Perkin-Elmer spectroscope.

Silicon oxide showed the usual Si-O stretching band peak, occurring very near to 10 microns wavelength, as shown in Figure (37). This indicated a value of x in the formula SiOx close to unity. The peak for the Si-O stretching band occurs at 9.2μ for SiO_2 and about 10μ for SiO.

The presence of a small peak at about 5.6μ indicated an Si-H stretching band. This would be due to either the presence of hydrogen or water. Peaks at 2.9μ and 6.1μ indicated the presence of water as a result of a stretching frequency and a deformation frequency respectively. However, the latter three peaks existed in

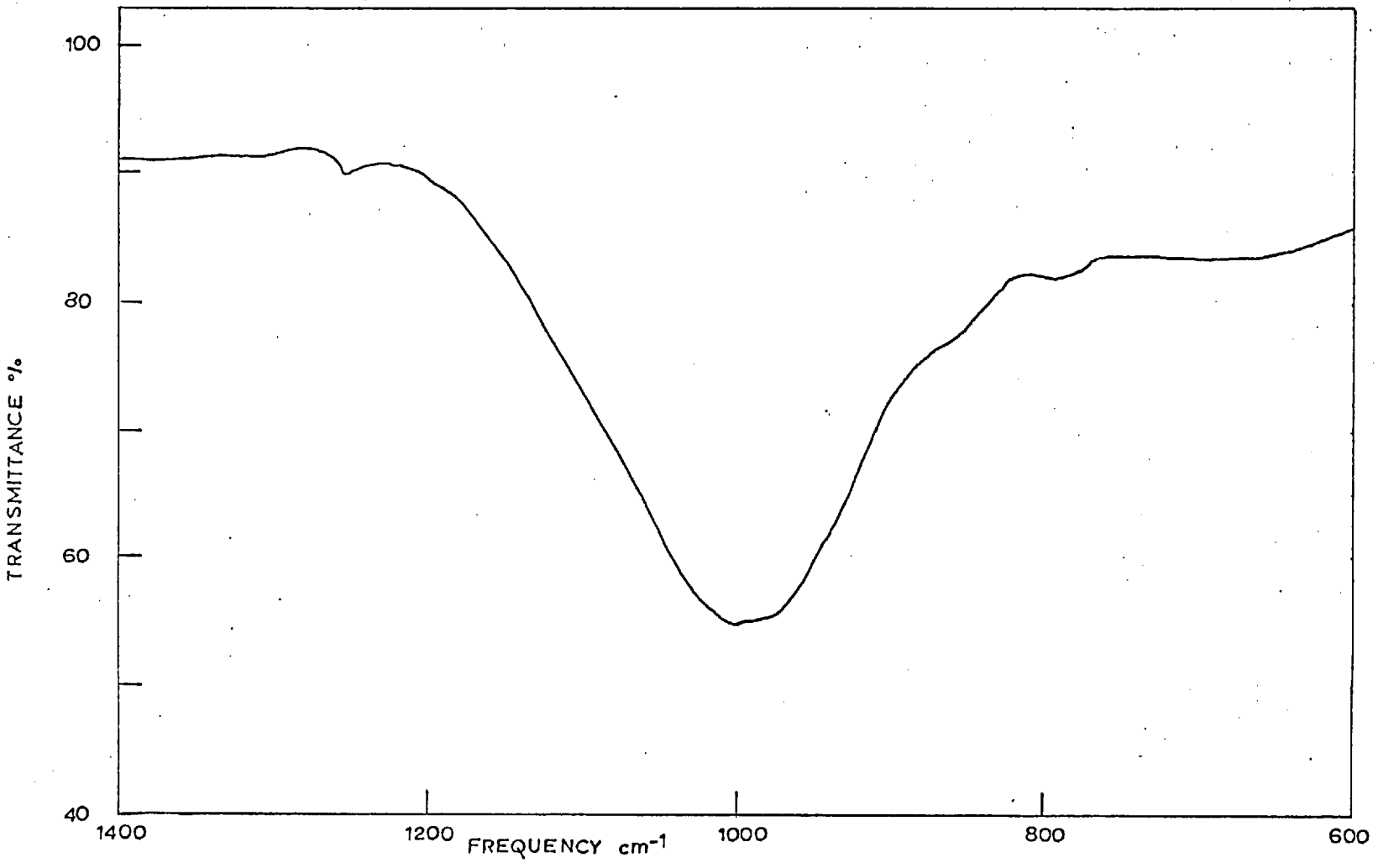

FIG.37 INFRARED ABSORBTION SPECTRUM OF SILICON OXIDE ON A KBr DISK RUN AGAINST A BLANK DISK

the control disc also and the two beam method almost eliminated them, indicating that it was not a feature of the film only. This result is unexpected since Pliskin[119], using I.R.S., sputtered on to substrates at low temperatures, i.e. < 100°C, picked up several times as much water as films deposited at high temperatures > 300°C.

No structural change could be determined by shifts occurring in the Si-O stretching peak on annealing the film. This indicated that there was no detectable oxidation process occurring during annealing.

Pliskin and Lehman[119] interpreted their results as indicating the existence of an intermediate oxide, Si_2O_3, its absorption band occurring near 11.5μ. They suggested that films deposited at high pressures and low rates of evaporation probably consisted of a mixture of the three oxides, SiO, Si_2O_3 and SiO_2, but this has not been fully substantiated.

Allam and Pitt[120] also investigated silicon oxide films by means of I.R.S. They found no conclusive evidence for oxidation on annealing, but suggested that a number of different localized structures may exist. The type and density of these would be dependent on the film preparation conditions and subsequent treatment.

5.4 Chemical Method

Another method of determining the parameter x in SiOx is to determine the weight of silicon in a known weight of silicon oxide. Various chemical methods have been developed such as that described by Morrison and Wilson[136]. The silicon oxide is deposited on a platinum underlayer so that the film can be removed chemically. It is fused with sodium carbonate to form sodium silicate. The silicon content of the sodium silicate is determined by absorption methods as reduced α-molybdosilicic acid. Accuracies of less than 1% are quoted but this will depend on the amount of original silicon oxide. This method was not used in the present work.

5.5 Electron Micro-Probe Analysis

An electron micro-probe equipment was used to determine the percentage of silicon in silicon oxide. The analysis was performed by the analytical services laboratory of Imperial College. A film of 1μ thickness was deposited on to an aluminium underlayer on a Corning 7059 glass slide. A thick film was required so that the electron beam used in the micro-probe did not detect the silicon of the substrate material and higher beam energies could be used. The value of x in the formula

SiOx was determined by taking counts from the SiKα radiation on Si, SiOx and SiO_2 in turn and comparing counts. The resulting formula was $SiO_{1.01}$. A film of 2μ thickness had the formula $SiO_{1.05}$. These films were prepared at the standard rate and pressure of 10Å/sec and 2.10^{-5} Torr during deposition, respectively.

5.6 X-Ray Powder Photograph of 'Silicon Oxide'

The original material before evaporation was investigated by taking a powder photograph. The silicon monoxide supplied by the Kemet Company of the Union Carbide Corporation was a grey powder but when crushed existed as a finely divided brown powder. The film was exposed to the reflected X-radiation for 10 hours. Figure (38) is a table of the detectable lines occurring on the photograph as measured with a direct reading angstrom rule, and the corresponding elements or compounds taken from the A.S.T.M. book of X-ray powder diffraction data, corresponding to these lines. Some of the lines were determined by comparing the photograph with a photograph for pure silicon.

5.7 Silicon Oxide Residue Evaluation

After evaporating the SiOx from the tantulum source, there remained a residue of various colours and this

FIG. 38

LINE	ORIGIN	COMMENTS
4·1	UN.	EXTREMELY FAINT
4·3	α-QUARTZ	
3·35	α-QUARTZ	STRONGEST LINE
3·13	Si	
2·45	UN.	
2·28	UN.	
2·14	UN.	
1·93	Si	
1·82	α-QUARTZ	
1·64	Si	
1·54	UN.	
1·25	Si	BY COMPARISON WITH Si
1·11	Si	BY COMPARISON WITH Si

RESULT OF X-RAY POWDER PHOTOGRAPH ON SILICON MONOXIDE STARTING MATERIAL. LINES CORRESPOND TO POSISTIONS ON DIRECT READING ANGSTROM RULE

UN. - UNKNOWN

was analysed by X-ray fluorescence in order to establish what impurities had been co-evaporated with the silicon oxide. The table in Figure (39) shows the detectable constituents. One column of the table gives the original concentration of these impurities as given by Union Carbide, from whom the starting material was obtained. There were two main constitutents in the residue, one black and the other brown. Each was tested separately.

Aluminium and molybdenum, although present in the original material, were not detectable in the residue but it may not be concluded that these elements therefore appear in the evaporated film. However, even if they were present in the film, their effect on the electrical properties would be negligible due to their low mobility in the silicon-oxygen network, and also the negligible effect of acceptors or donors in low concentrations (see Section (2.1)).

5.8 Summary of Silicon Oxide Film Structure

Both electron diffraction and infra-red absorption analyses indicate that silica tetrahedra are present in all evaporated silicon oxide films. However, the ratio of silicon to oxygen necessitates that extra silicon is taken up in the structure. There is still

FIG. 39

ELEMENT	CONTENT IN SiO POWDER	RESIDUE CONTENT	
		BLACK	BROWN
	%		
Fe	·04 - ·07	M	M
Ni	·05	H	L
Al	·02 - ·05	N.D.	N.D.
Mo	·01 - ·06	N.D.	N.D.
Cu	·02 - ·04	M	H
Mn	·01	L	M
Mg	< ·01	N.D.	N.D
Ti	< ·01	TR.	TR.
B	< ·01	—	—
Cr	< ·01	L	TR.
Ca	< ·01	M	L
Sn	N.D.	N.D.	N.D.
Na	N.D.	—	—
V	N.D.	N.D.	TR.
Si	0·1	MAJOR	MAJOR

L - LOW < 0·1 %

M - MEDIUM 0·1 – 1·0 %

H - HIGH > 1%

N.D. - NOT DETECTABLE

TR. - TRACE

THE ORIGINAL SiO POWDER ALSO CONTAINED 1·0 – 1·5 % α-QUARTZ, 95% SiO AND THE BALANCE WAS AMORPHOUS SiO_2

not sufficient evidence to indicate whether the extra silicon exists as silicon islands or as Si-O-Si or O-Si-O bridges[120]. The latter suggestions of inter-linking bridges will result in a distribution of small groups possessing localised structure. Probably the most important result is the existence of short range order similar to that of silica. This will affect energy band considerations as discussed in Section (2.1).

The small amounts of metallic impurity which would be present in evaporated films probably have negligible effect on the electrical properties.

CHAPTER 6

DEPOSITION PARAMETERS AND POST-DEPOSITION TREATMENT

6.1 Introduction

This section describes the more important parameters which can be controlled during the evaporation of silicon monoxide. In order to obtain stable films, the effect of heat treatment on the deposited films was also investigated.

The electrical parameters measured were capacitance and loss tangent. The latter quantity is a ratio and is independent of the area and thickness of the dielectric, providing the conductivity and permittivity are independent. However, the capacitance is a function of both thickness and area so that in order to calculate permittivities to compare different films, additional errors are introduced due to uncertainty in the dimensional measurements. A parameter that is not dependent on accurate area or thickness measurements is the temperature coefficient of capacitance γ_c. Furthermore, it has already been shown (see Section (2.4)) that between permittivity values of 4 and 10, γ_c increases as 'ε' increases. Thus γ_c is a useful measure of the behaviour of 'ε' for the case of silicon

oxide (where ε' is in the range 4-6). In the case of the variation of rate and pressure, therefore, ε'_c is the parameter determined, together with the loss tangent.

The section initially presents the experimental results of both deposition conditions and post-deposition heat treatment and finally discusses these results. The results for deposition conditions are for unannealed capacitors deposited on to substrates at about 200°C.

6.2 Results of Rate and Pressure Variation

The parameter which is plotted in this set of experiments is the ratio '$(\frac{P}{R})$', where 'P' is the pressure during evaporation in Torr, and 'R' is the rate of evaporation in Å/sec. The reasons for plotting this ratio are given in Section (6.5) and were first suggested by Anastasio[121] and Hill and Hoffman[122].

Figure (40) shows the variation of loss tangent, plotted on a log scale with $\frac{P}{R}$. For temperatures above room temperature there is greater spread in loss with temperature for low values of $(\frac{P}{R})$.

Figure (41) shows ε'_c plotted as a function of $(\frac{P}{R})$. Again there is greater spread with temperature for low values of $(\frac{P}{R})$.

The forms of the 'ε'_c' and loss tangent curves are reasonably similar, suggesting a relationship between

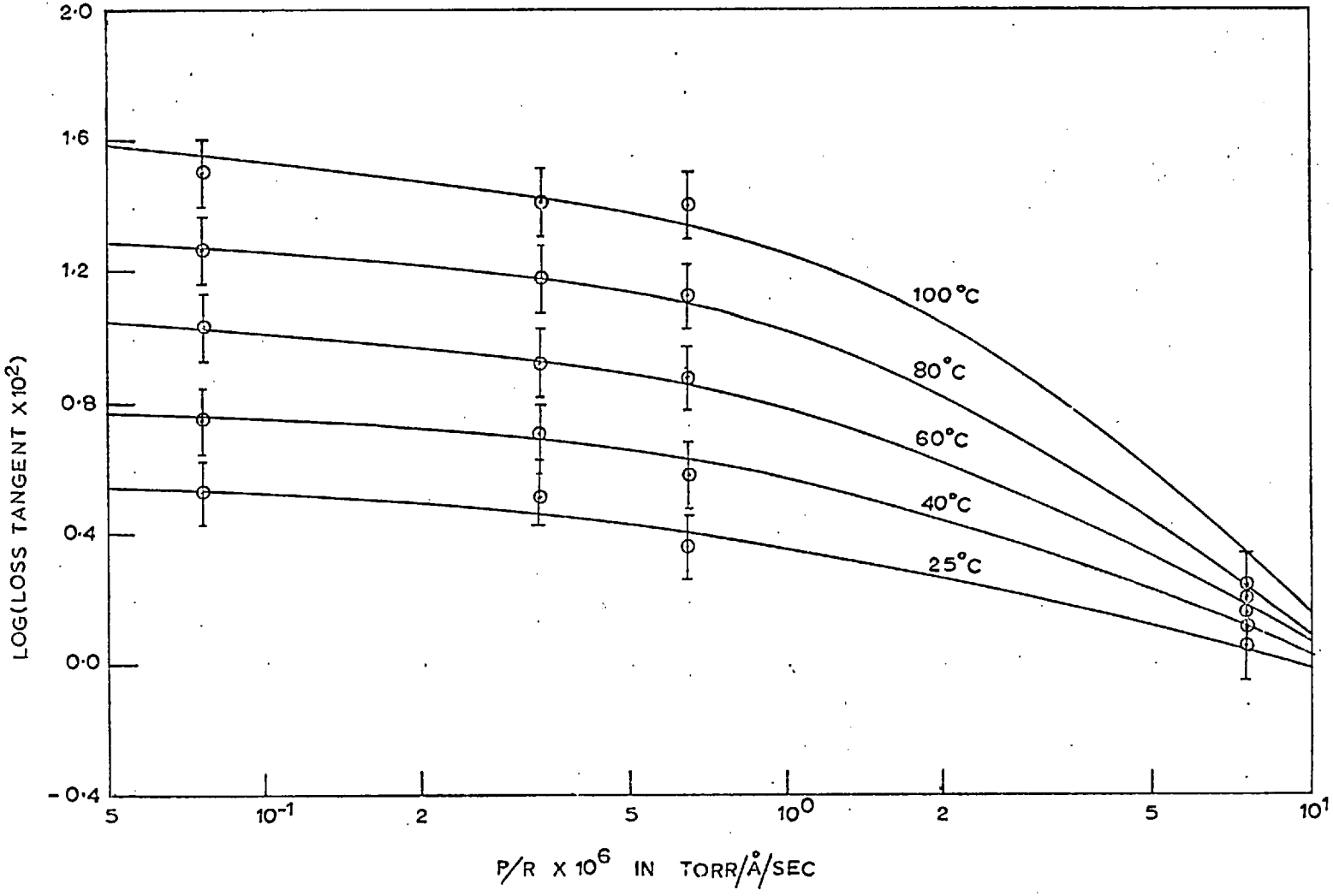

FIG.40 DEPENDENCE OF LOSS TANGENT ON THE RATIO P/R AT DIFFERENT TEMPERATURES.

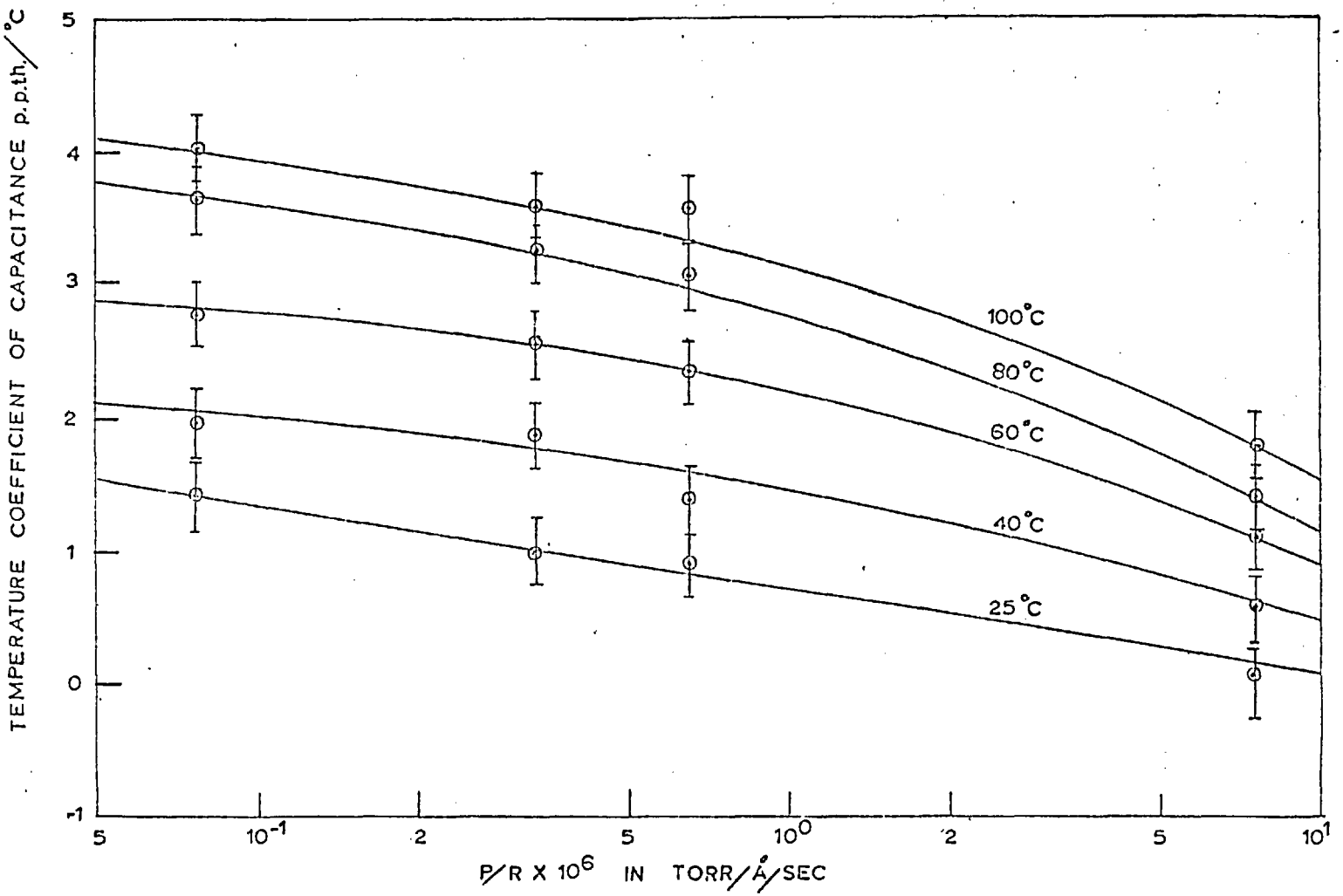

FIG. 41 DEPENDENCE OF TEMPERATURE COEFFICIENT OF CAPACITANCE ON THE RATIO P/R

these two terms. The average value of $A = \frac{\gamma'_c}{\text{Tan } \delta}$ for all measured temperatures is 0.03 ± 0.015, apparently indpendent of $(\frac{P}{R})$ but decreasing with increased temperature.

6.3 Results of Residual Gas Variation

Figure (42) shows the effect on the loss tangent of introducing various gases into the vacuum chamber during deposition. Except in the case of air, the pressure was increased by two orders of magnitude by the introduction of the gas. Figure (43) shows the effect of annealing the films for 24 hours at 240°C in the vacuum chamber. The loss tangents were considerably reduced and also the spread for different gases was reduced. There does not appear to be any correlation between different gases except that oxygen was more effective in reducing the loss, both before and after annealing.

6.4 Annealing Results

In the case of annealing experiments, films were deposited on to substrates which were at room temperature at the onset of deposition. The rate of evaporation was 11Å/sec $\pm$ 1Å/sec at a pressure of 1.10^{-5} Torr during deposition.

FIG. 42 LOSS TANGENT AS A FUNCTION OF TEMPERATURE FOR DIFFERENT GASES INTRODUCED DURING DEPOSITION FOR UNANNEALED CAPACITORS

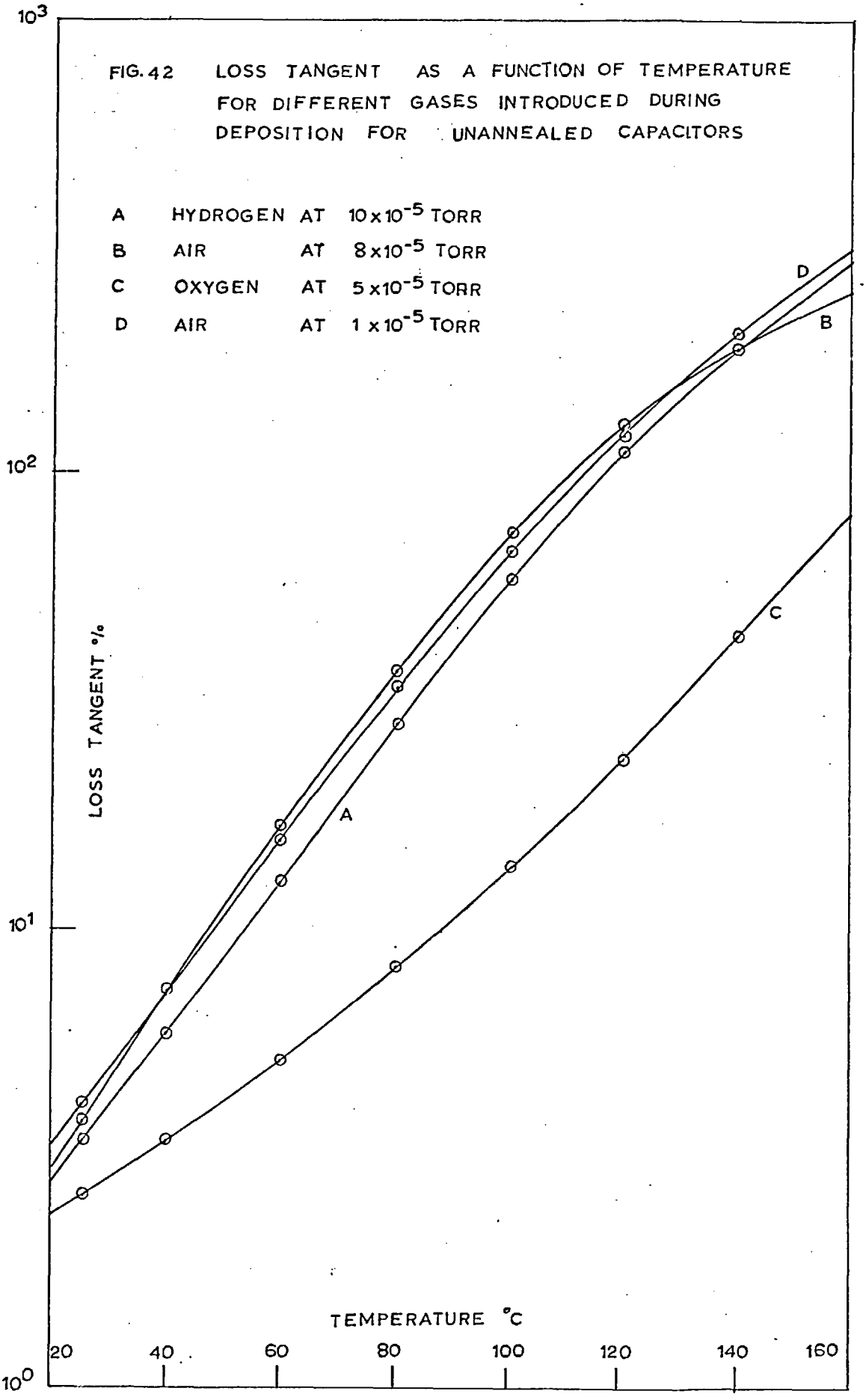

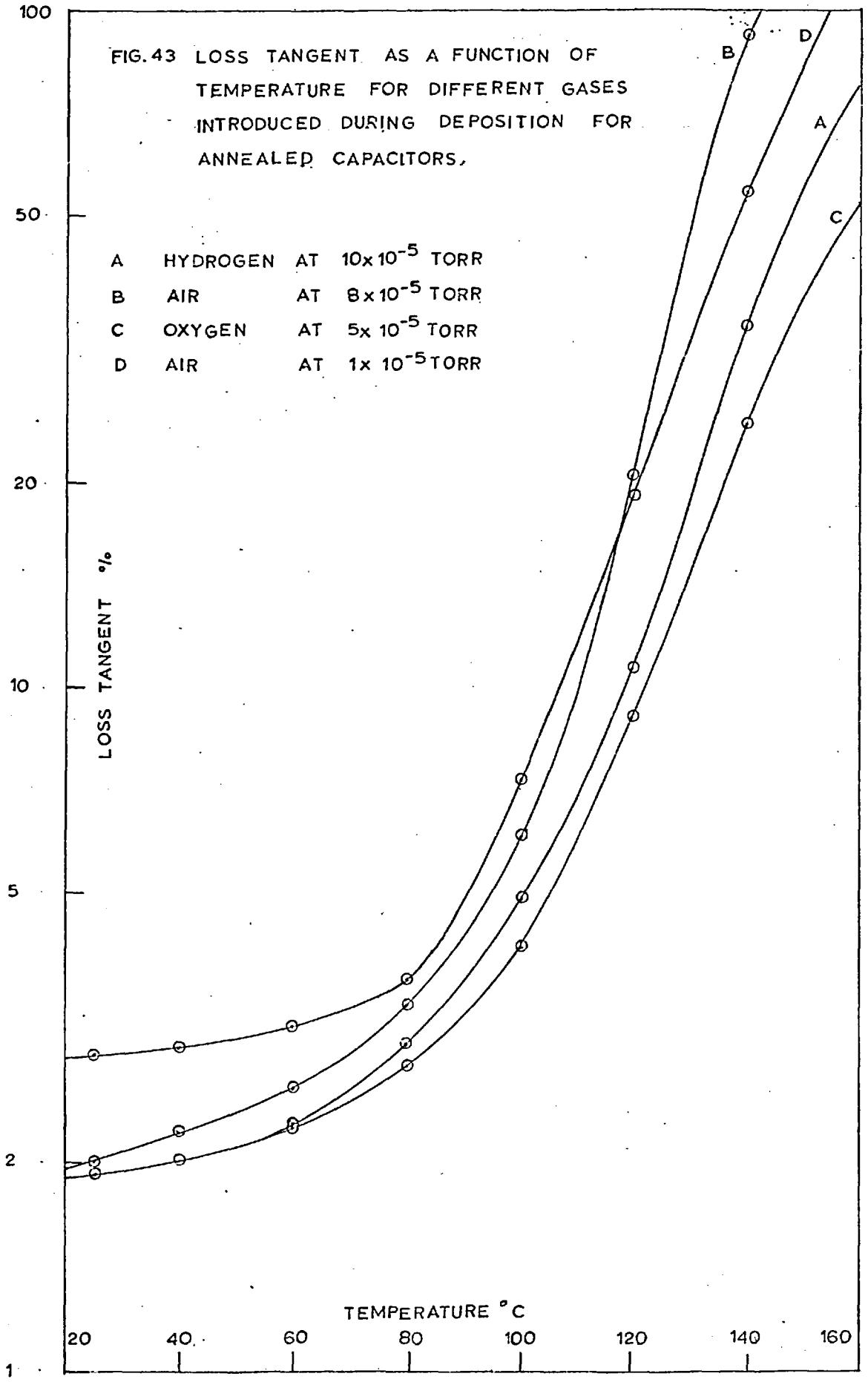
FIG. 43 LOSS TANGENT AS A FUNCTION OF TEMPERATURE FOR DIFFERENT GASES INTRODUCED DURING DEPOSITION FOR ANNEALED CAPACITORS.
A HYDROGEN AT 10x10⁻⁵ TORR
B AIR AT 8x10⁻⁵ TORR
C OXYGEN AT 5x10⁻⁵ TORR
D AIR AT 1x10⁻⁵ TORR
LOSS TANGENT %
100
50
20
10
5
2
1
TEMPERATURE °C
20
40
60
80
100
120
140
160
A
B
C
D

As the annealing was a function of time as well as temperature, the standard procedure adopted was to take readings every $1\frac{1}{4}$ hours (the time taken for the temperature to reach equilibrium). Figures (44) and (45) show the first two heating and cooling cycles on the capacitance and loss tangent. The initial increases in these parameters, as shown on the graphs, were time dependent. The capacitance was monitored with a pen recorder between points with $1\frac{1}{4}$ hours separation. It was observed that towards the end of this period the capacitance had reached a maximum value and was beginning to fall, although the temperature had not reached an equilibrium value. However, the decrease in capacitance was small compared to the initial increase in the same period and the overall effect is shown in Figures (44) and (45). Above 80°C the decrease in these parameters becomes significant and the overall effect is a decrease with temperature. Finally both parameters increase with temperature. Figures (44) and (45) also show the fully annealed values obtained after heating the capacitor, in vacuum at about 250°C for several days and then in air in an oven at about 400°C for half an hour. The process was irreversible as the peaks could not be reproduced even after letting the capacitors up to air for several days.

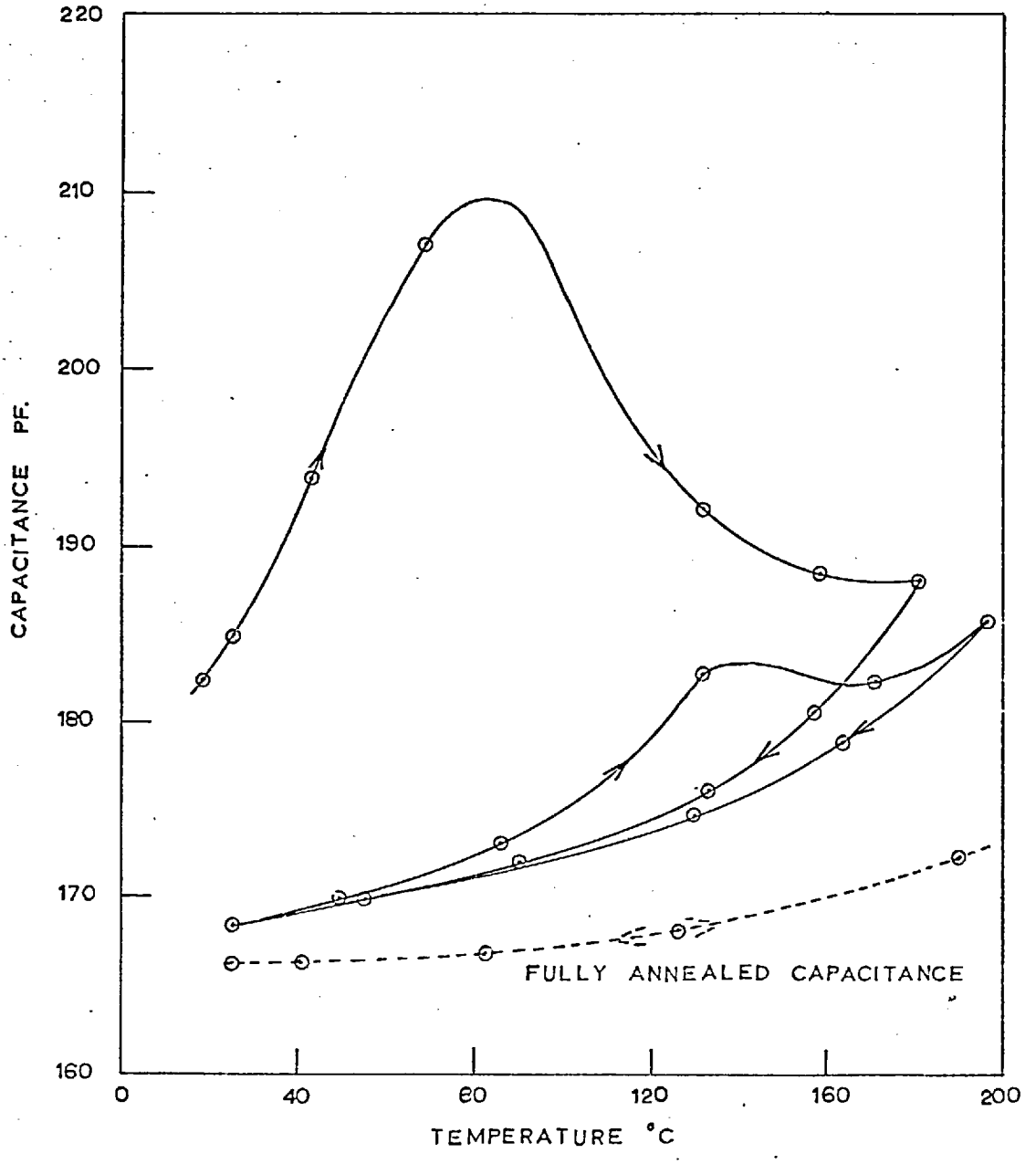

FIG. 44 FIRST TWO ANNEALING CYCLES ON A CAPACITOR DEPOSITED ON A SUBSTRATE AT ROOM TEMPERATURE. EFFECT ON CAPACITANCE

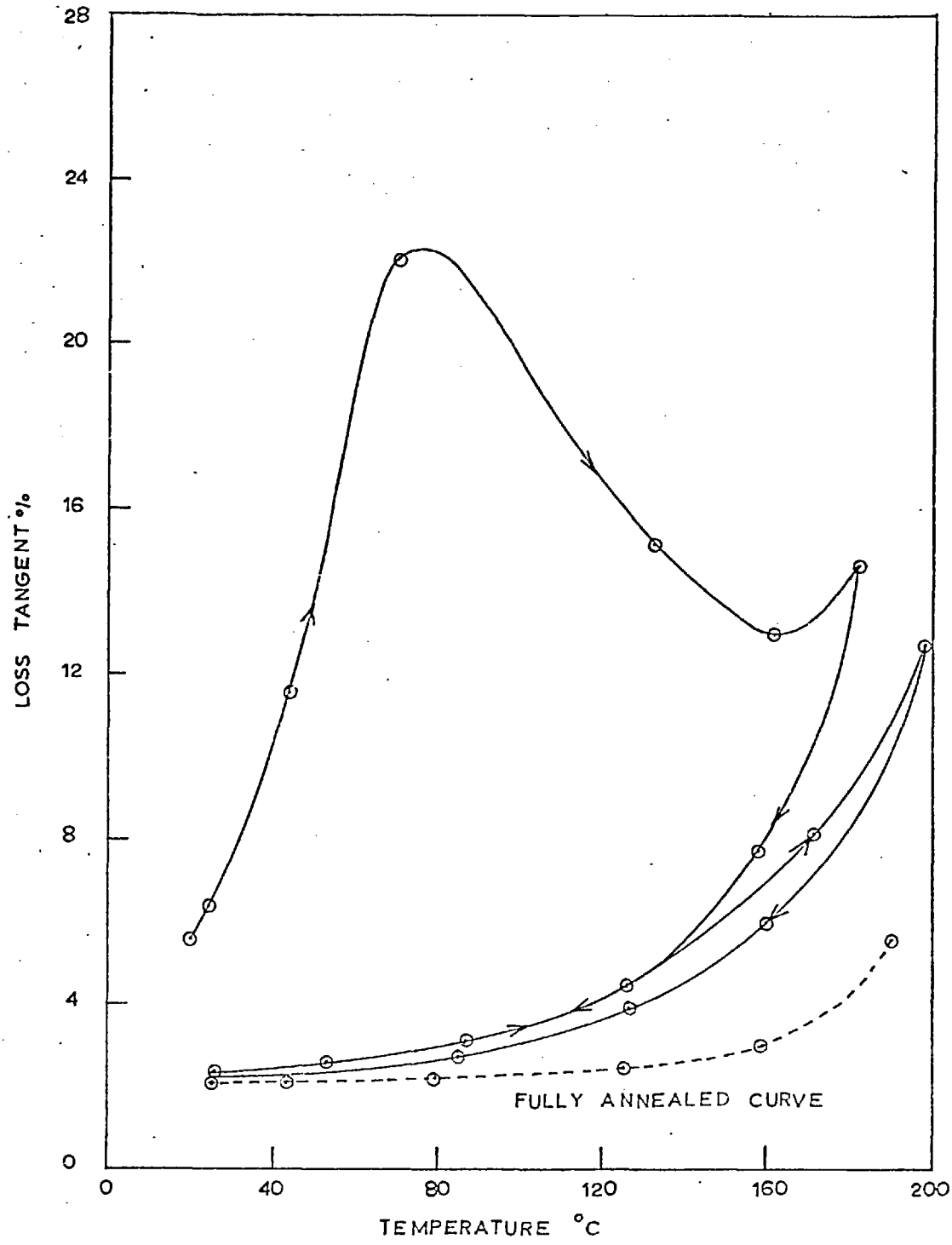

FIG.45 FIRST TWO ANNEALING CYCLES ON A CAPACITOR DEPOSITED ON A SUBSTRATE AT ROOM TEMPERATURE EFFECT ON LOSS TANGENT

Subsequent to the large initial changes in capacitance and loss tangent, small changes in these parameters were investigated both as functions of temperature and time.

6.4.1 Capacitance Anneal

The decrease in capacitance was observed as a function of time and Figure (46) shows a sample change in capacitance at 225°C. An exponential decrease in capacitance was assumed of the form

$$C(T, t) = C(T, \infty) \exp\left(\frac{\tau_c(T)}{t}\right) \qquad (1)$$

This would not be valid at or very near to $t = 0$.

Since it was not possible to determine the onset of annealing it was necessary to determine $C(T, \infty)$ the fully annealed value of capacitance at 'T'°C. The fully annealed γ_c is then $\gamma_c(T)$.

$$\gamma_c(T) = \frac{1}{C(T, \infty)} \frac{\partial C(T, \infty)}{\partial T}$$

A straight line plot was then made to determine $\tau_c(T)$ by putting $t = t_o + t'$

$$\therefore \log_e \frac{C(T, t)}{C(T, \infty)} = \frac{\tau_c(T)}{t_o + t'}$$

FIG. 46

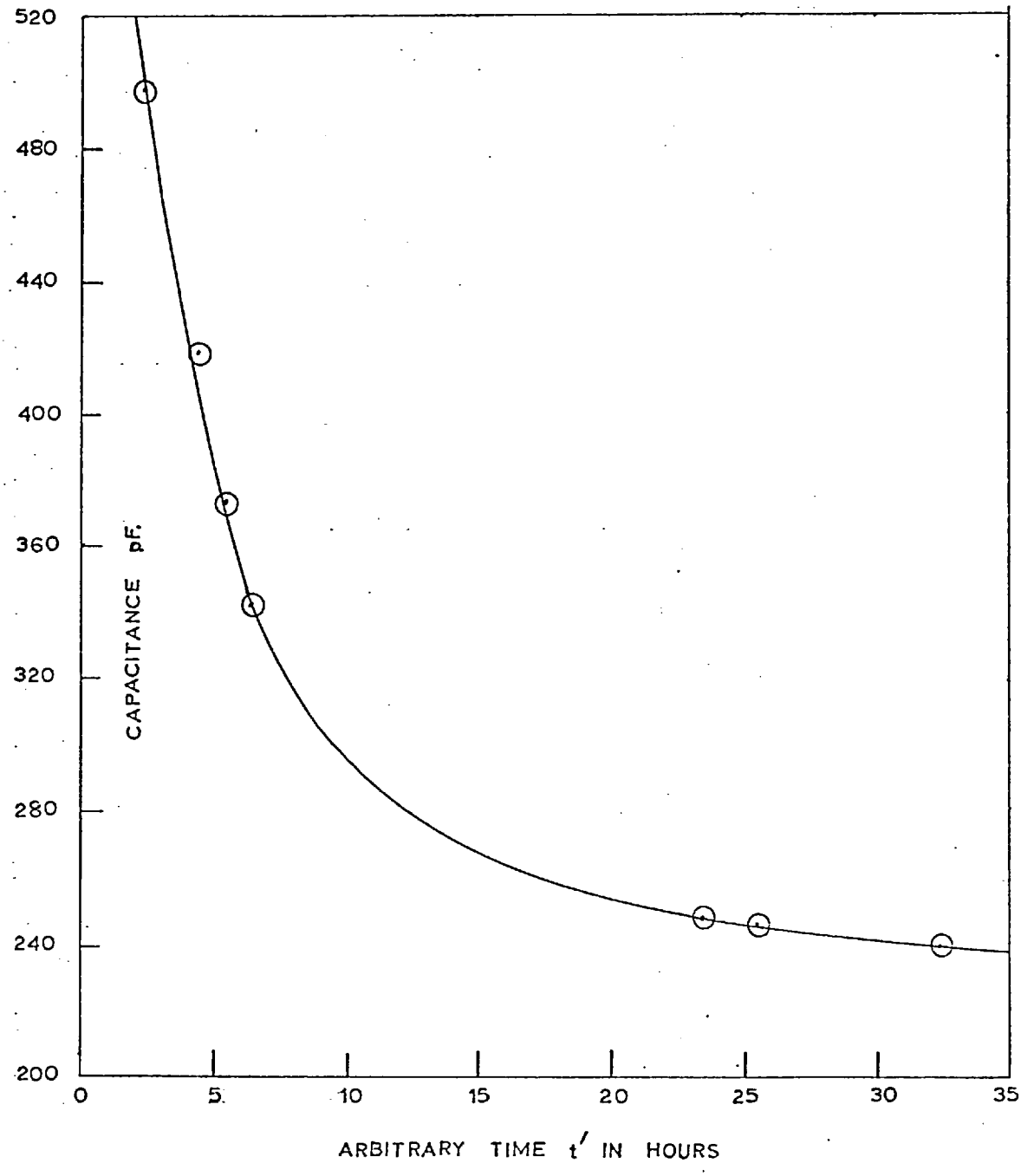

CAPACITANCE VARIATION DURING ANNEAL AT 225 °C

$$\left[\log_e \frac{C(T, t)}{C(T, \infty)}\right]^{-1} = \frac{t'}{\tau_c(T)} + \frac{t_o}{\tau_c(T)}$$

This plot at 225°C is shown in Figure (47).

'$\tau_c(T)$' was determined at several temperatures. However, a large spread in experimental results permitted only a crude estimation of $\tau(T)$ as a function of temperature. Averaging the results on several samples gives the following two values:

$T^\circ C$	$\tau_c(T)$ hours
150 ± 20	11.5 ± 0.5
232 ± 7	3.7 ± 0.2

If the annealing process was an activated one, then an Arrhenius relationship could be assumed. This gives an activation energy of $.23 \pm .05$ eV.

Figures most often quoted in the literature[108] give an annealing time of approximately 30 minutes at about 400°C. The above relationship gives $\tau_c(427^\circ C) \simeq$ 1 hour. However, $\tau_c(T)$ represents the time to reach e x the fully annealed value.

6.4.2 A.C. Resistance Anneal

Figure (48) shows a sample increase in A.C. resistance as a function of time at 225°C. This also

FIG. 47

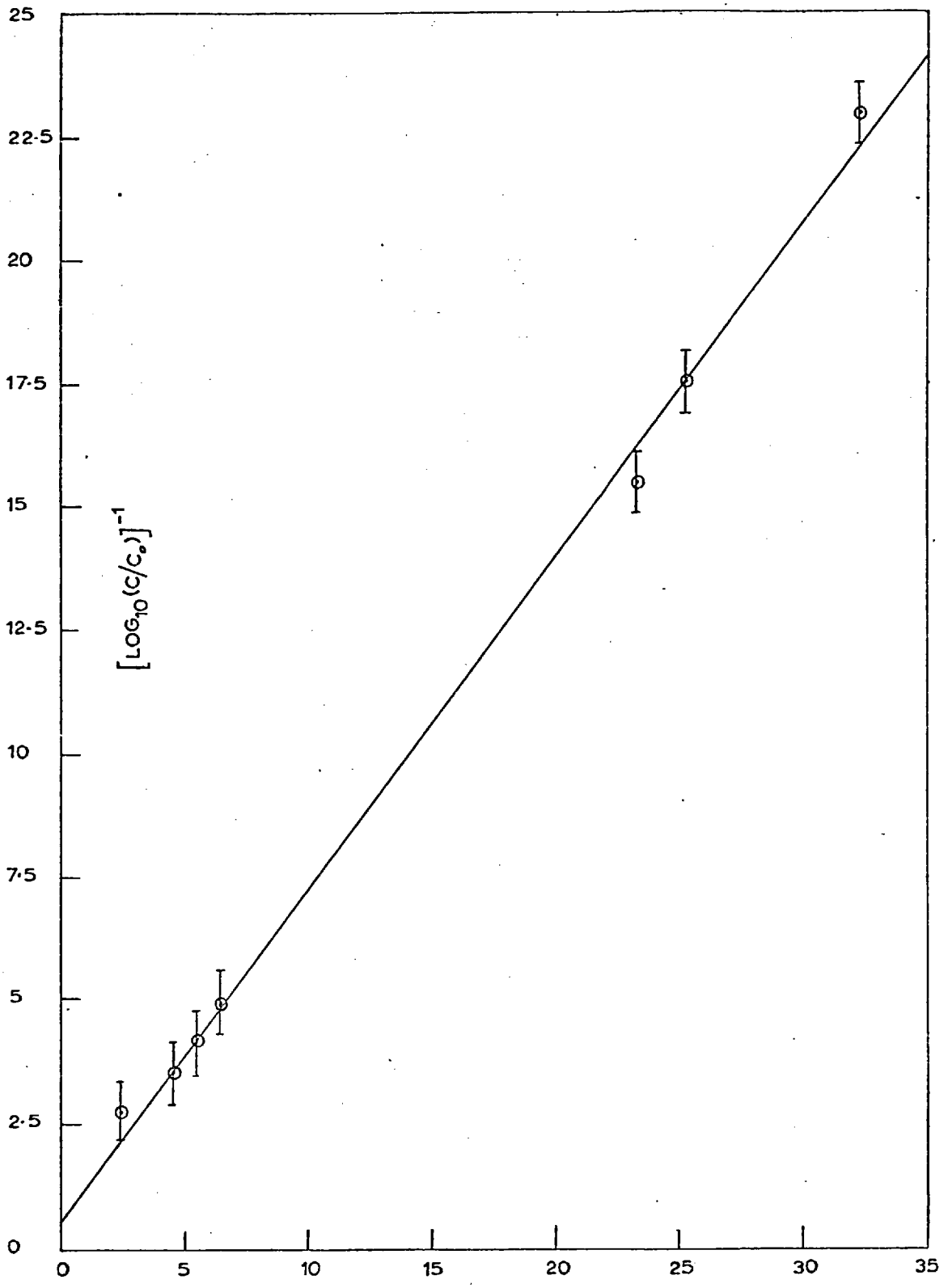

PLOT TO DETERMINE RELAXATION TIME τ_c AT 225°C

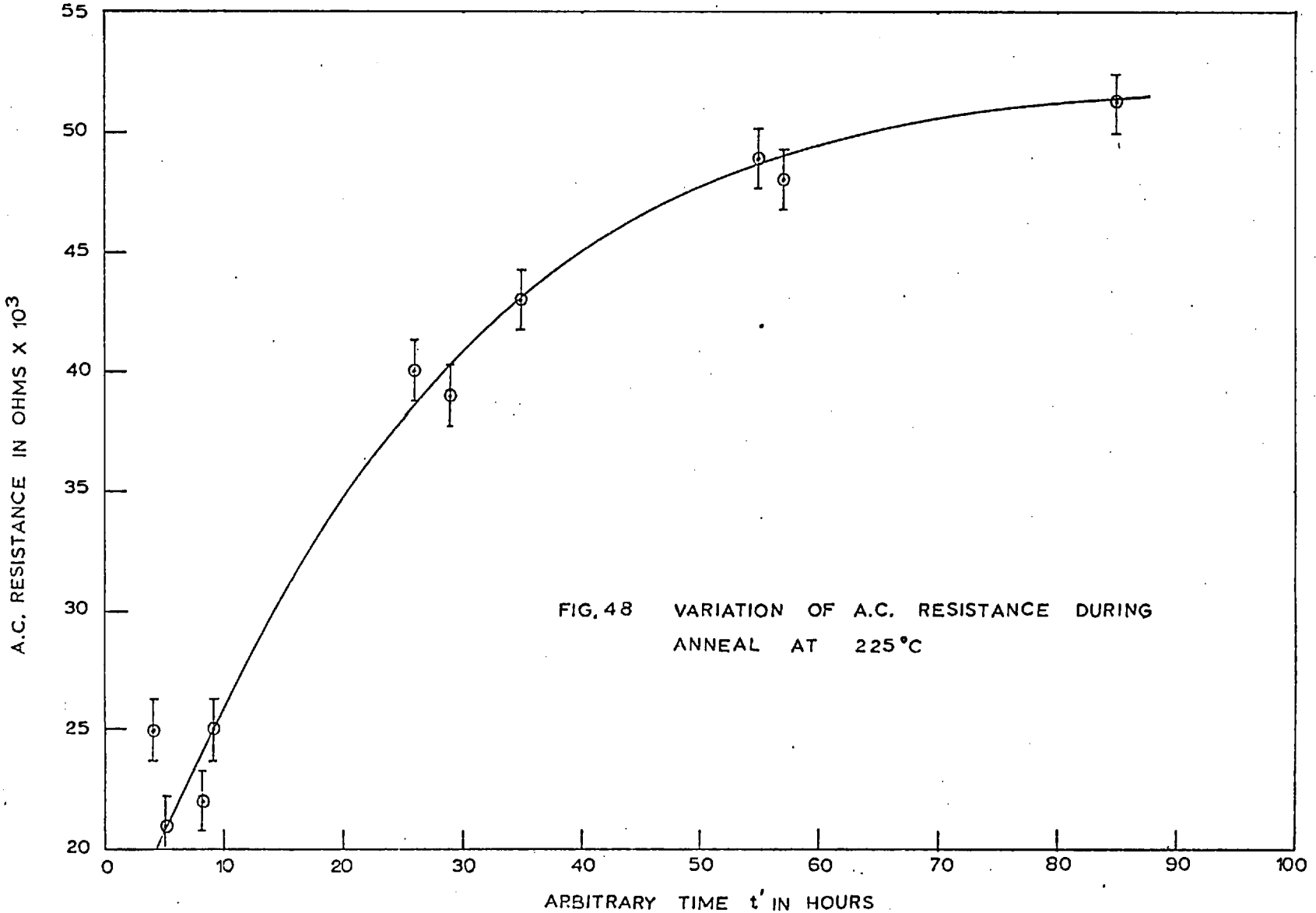

FIG. 48 VARIATION OF A.C. RESISTANCE DURING ANNEAL AT 225°C

follows an exponential relationship, of the form

$$R(T, t) = R(T, \infty)\left[1 - \exp\left(\frac{-t}{\tau_R(T)}\right)\right] \qquad (2)$$

This again is not valid at or very near to $t = 0$.

It is necessary to determine the fully annealed value of resistance in order to evaluate $\tau_R(T)$ from the following plot, putting $t = t_o + t'$

$$\log\left[1 - \frac{R(T, t)}{R(T, \infty)}\right]^{-1} = \frac{t'}{\tau_R(T)} + \frac{t_o}{\tau_R(T)}$$

Figure (49) shows this plot for a capacitor annealing at 225°C. Averaging the results of several experiments gives the following two values of $\tau_R(T)$:

T^oC	$\tau_R(T)$ hours
106 ± 18	42.5 ± 3
225 ± 5	11.7 ± 0.5

Assuming an activated process gives an activation energy of $0.18 \pm .04$ eV.

The change in loss tangent during annealing was not determined but clearly it will have annealing times similar to the A.C. resistance anneal.

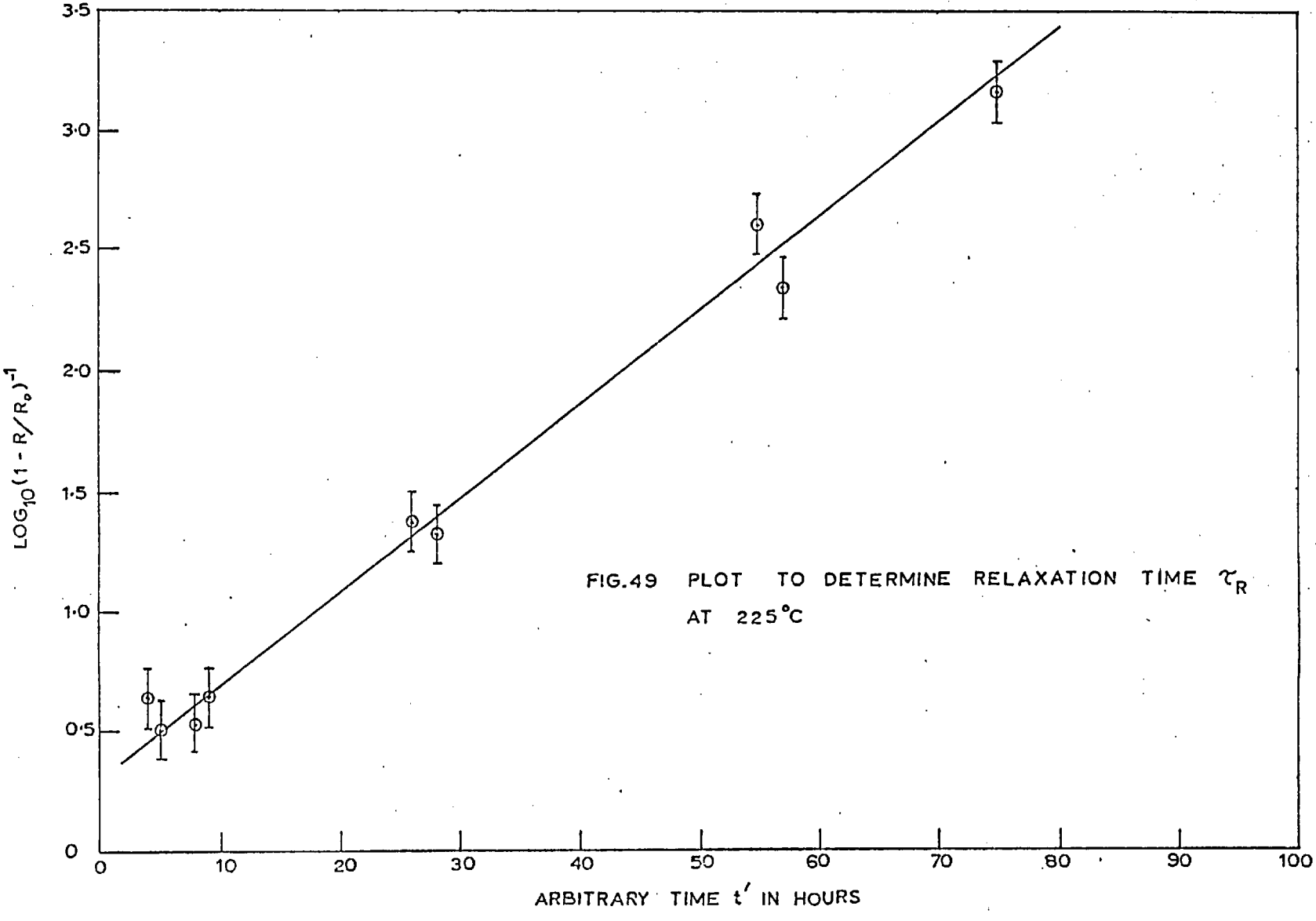

FIG.49 PLOT TO DETERMINE RELAXATION TIME τ_R AT 225°C

6.4.3 Frequency Behaviour

The frequency behaviour of the first annealing cycle on a freshly prepared capacitor is shown in Figure (50). The loss tangent showed a similar type of variation. The initial increase in capacitance and loss is more pronounced at low frequencies and would appear to disappear at high enough frequencies.

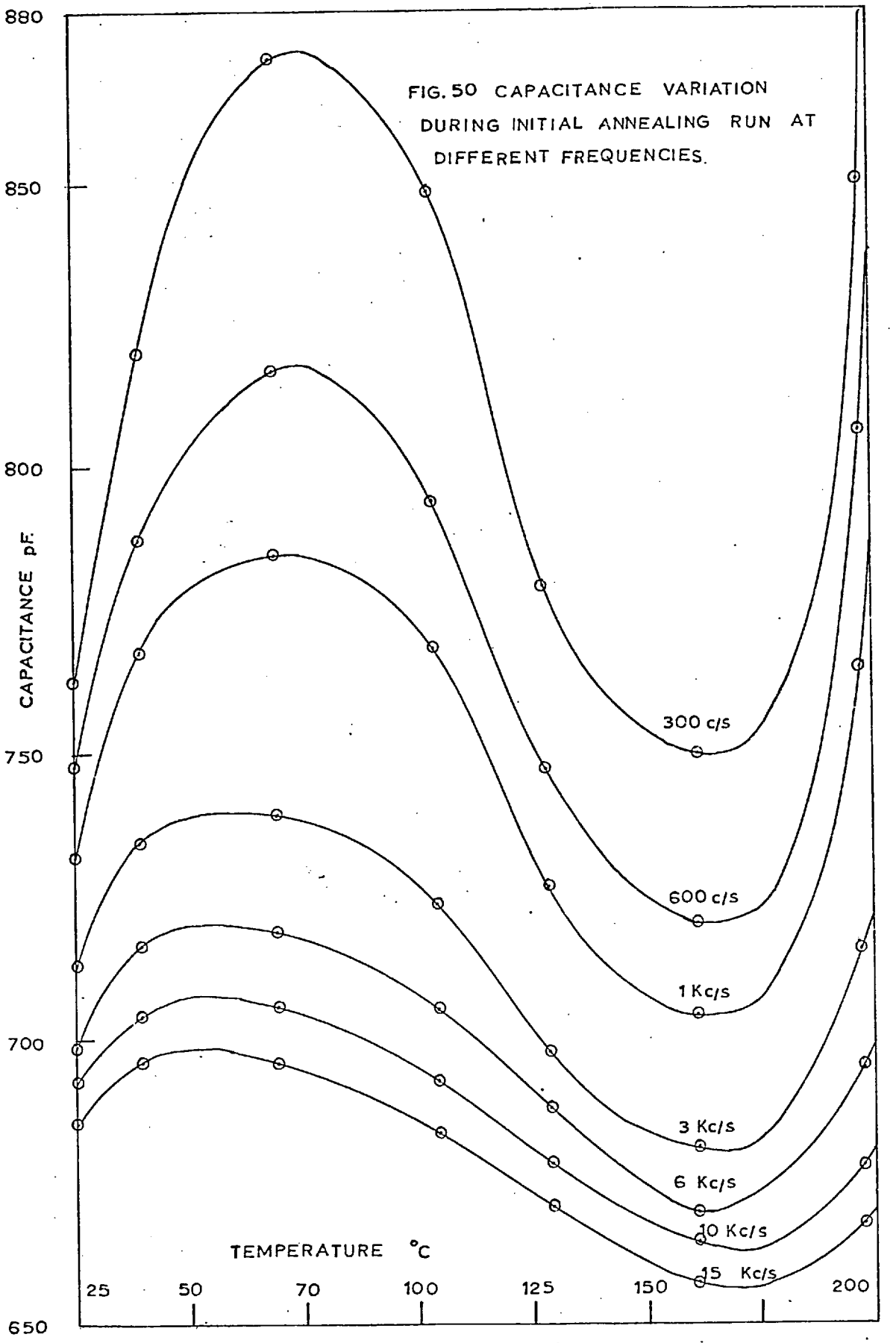

FIG. 50 CAPACITANCE VARIATION DURING INITIAL ANNEALING RUN AT DIFFERENT FREQUENCIES.

6.5 Discussion of Rate and Pressure Variation

The rate and pressure variation will affect the process of reaction of the residual gas with the silicon monoxide. This will be predominantly an oxidation reaction so that the finally deposited film will have an overall composition of the form SiOx where $1 < x < 2$. Reduction processes, such that $x < 1$, are not considered.

There are three ways in which a reaction with the original source material can occur. Before the charge evaporates a reaction could take place with the residual gas so that the evaporant is not silicon monoxide. This process is thought unlikely.

Secondly, the reaction could be a gas phase reaction as suggested by White[123] who calculated the mean free path of a molecule of silicon monoxide, before a collision occurred, using free energy data. Assuming a collision diameter of 2Å, an oxygen pressure of 10^{-4} Torr and a temperature of 1500°C, he calculated a mean free path of $3{\cdot}9.10^{-2}$ cm. He suggested, therefore, that the reaction was predominantly a gas phase reaction. However, it is considered that there is probably an error in these calculations. Assuming a Maxwellian distribution of velocities, the mean free path 'λ' is given by[124]

$$\lambda = \frac{kT}{\sqrt{2}\,\pi\, d^2\, P}$$

where 'd' is the collision diameter and 'P' and 'T' are the pressure and temperature respectively. Using $T = 300^{o}K$, $P = 10^{-4}$ Torr and $d = 2\mathring{A}$ results in a mean free path of 175 cm. It is considered, therefore, unlikely that any reaction occurs in the gas phase as values of temperature and pressure used in the experiments produce mean free paths, greater than the source to substrate distance of 18 cms.

The most likely place of the reaction is therefore at the substrate, within a very small time of arrival of both the oxide and oxygen. The work of Poat[125], using a rotating substrate holder so that the evaporation was pulsed, showed that oxidation was independent of the time the substrate was blind to the source.

The rate of the oxide-oxygen reaction is determined by two energies which can be considered as life-times, using the A rhenius relationship. Firstly, there is the life-time 'τ_a' of an oxygen atom on the substrate before re-evaporation, which is determined by the absorption energy 'E_a' and the life-time 'τ_o' related by the equation

$$\tau_a = \tau_o \, e^{\frac{E_a}{kT}}$$

The life-time 'τ_a' will determine the substrate surface coverage 'θ' defined by the fraction of the area

covered by the oxygen atoms. The surface coverage is related to the pressure of the residual gas 'P' by a Langmuir isotherm[126], by the equation

$$\theta = \frac{aP}{1 + aP}$$

where 'a' is a constant.

At low pressures 'θ' will be proportional to the pressure and at high pressures will become independent. The temperature dependence is given by[126]

$$\frac{\theta}{1 - \theta} = \text{const. } e^{\frac{E_a}{kT}}$$

As the temperature approaches absolute zero the surface becomes saturated and at high temperatures practically no oxygen atoms will reside on the surface.

The second process determining the amount of oxidation occurring is the reaction between the oxide and the oxygen at the substrate. The rate of this reaction increases with increased temperature.

The rate of the oxide-oxygen reaction as a function of temperature is, therefore, the resultant of two opposing terms: the increasing rate per atom of the reaction and the decreasing number available for the reaction.

At the low pressures used in the experiments it is

assumed that the coverage is proportional to the pressure. At a constant pressure the number of oxygen atoms available for reaction is fixed. Therefore, as the number of oxide atoms is increased, there will be less oxidation per oxide atom. The effect of the rate of arrival of the oxide will be to reduce oxidation as the rate is increased. The parameter $\frac{P}{R}$ which was plotted to determine the effect of temperature, therefore, represents the state of oxidation of the silicon monoxide. The value of P used was the total pressure during evaporation since, according to Anastasio[121], for pressures greater than 2.10^{-5} Torr, the partial pressure of the remaining gases constituted less than 10°/o of the oxygen partial pressure.

Similar quantities were used by Anastasio[121] and Hill and Hoffman[122] for investigating the effect of rate and pressure. The parameter determined by Anastasio was $p/r = 1{\cdot}06.10^{6} \frac{P}{R}$, whereas Hill and Hoffman determined $\frac{R}{P}$. These authors were mainly concerned with stress measurements but made correlations with electrical measurements.

The trend of loss tangent with $\frac{P}{R}$ is consistent with Anastasio, except that at low values of $\frac{P}{R}$ the loss is less than suggested by him. There are two possible reasons for this. Anastasio omits mention

of substrate temperature during deposition. The above discussion shows how the temperature can affect the state of oxidation. All measurements were performed with the capacitors in vacuum. If Anastasio's experiments were performed in air, there would probably be an increase in loss due to moisture absorption.

The trend of permittivity as indicated by the δ_c variation is similar to that of Anastasio. However, the permittivity did not vary to the extent found by him but varied from 4-6 at room temperature.

The effects of pressure and rate on the electrical and mechanical properties of silicon oxide have been discussed by many authors[46, 47] and similar conclusions were reached. Caswell[127] pointed out that water vapour was an order of magnitude more effective in promoting oxidation than oxygen. This was further magnified by the fact that in unbaked systems, water vapour was an order of magnitude more prevalent than oxygen. Caswell gave the two reactions involved in promoting oxidation:

$$SiO + (x - 1)\ H_2O \quad \longrightarrow \quad SiOx + (x - 1)\ H_2$$

$$SiO + \tfrac{1}{2}(x - 1)\ O_2 \quad \longrightarrow \quad SiOx$$

As has already been pointed out in Section (1.2.2), the mechanical stress in a film affects the electrical properties. In a review by Campbell[130] he showed that films which incorporate oxygen, etc., in the structure generally have a compressive stress, the higher the concentration of additional atoms, the higher the compressive stress. Since $\frac{P}{R}$ will affect the number of additional atoms incorporated in the film, and since a compressive stress will give a low loss (see Figure (4)), it follows that a high value of $\frac{P}{R}$ will be conducive to low loss. This is consistent with the work of Hill and Hoffman[122] who suggested that incorporation of oxygen and water vapour within the structure produced a compressive stress. Jackson[12] suggests that $\frac{P}{R}$ will also determine the pin-hole concentration as determined by an etch-pit method. It seems likely, therefore, that there is a relationship between the stress of a film and the number of pin-holes, both being determined by $\frac{P}{R}$.

6.5.1 Effect of Substrate Deposition Temperature

It has been shown in the previous section that an increase in the substrate temperature can either promote or inhibit oxidation. It is not possible to say in this work which was the dominating process for

the pressures and temperatures involved.

The substrate temperatures given define the temperature of the substrate prior to deposition. However, due to heat radiation from the source, the substrate temperature will rise, probably tens of degrees. Blackburn and Campbell[118] calculated the increase in temperature of a carbon substrate due to the latent heat of lithium fluoride. They determined an equilibrium temperature increase of 47°C.

This shows the difficulty in determining the effect of substrate temperature and also the difficulty in defining a substrate temperature. Section (6.4) showed an effect only observed in films deposited on substrates at or near to room temperature, which suggests that the absorption of gases during deposition accurs only at low temperatures. Further discussion on this phenomenon will appear in Section (6.7).

6.6 Discussion of Residual Gases

Introduction of gases during deposition appeared to have little affect on the loss tangents when the films received post-deposition heat treatment, except in the case of oxygen. Water vapour was not introduced into the system. Increasing the air pressure over an order of magnitude did not appear to make any significant change.

6.7 Discussion on Annealing Behaviour

The annealing behaviour can be considered as occurring in three stages which are probably inter-related. These are:

1) Initial increase of capacitance and loss tangent up to about 80°C
2) Decrease in capacitance and loss tangent with increasing temperature
3) Long term increase in A.C. resistance and decrease in capacitance at a constant temperature.

6.7.1 Initial Increase of Capacitance and Loss Tangent

An indication as to the cause of the initial increase in both capacitance and loss during the first heating cycle is that the effect disappears on heating the substrate above 80°C prior to deposition. As mentioned in the previous section, it is considered that gases are absorbed at the substrate during deposition. The increase in capacitance is then a temperature coefficient effect of the dielectric and absorbed gas molecules, being dominated by the latter. Gröbner[128] studied the effect of the absorption of different gas molecules in alumina powder and found that the increase

in capacitance was proportional to the number of absorbed gas molecules. Figure (50) shows the effect of the measuring frequency on the capacitance variation with temperature. The effect of the absorbed gas molecules is less pronounced at high frequencies. The low frequency behaviour suggests that the gas molecules would show a dispersion at low frequencies if they were not desorbed by heating.

It is thought that the gas responsible for the increased capacitance and large temperature coefficient of capacitance is hydrogen, desorbed from the tantalum source used for the silicon oxide evaporation. Siddall[129] showed that during the evaporation of silicon oxide at 10^{-7} Torr, the partial pressure of hydrogen increased by a factor of 10^{3} compared to very small increases in the partial pressures of the remaining gases such as N_2, H_2O and CO_2. Although the pressures used in these experiments were about 10^{-5} Torr, it is expected that there would still be a significant increase in the partial pressure of hydrogen. Allam and Pitt[120] using infrared spectroscopy, showed the presence of hydrogen in freshly prepared films of silicon oxide. Their films were deposited on to a substrate at 150°C during deposition.

The increase in capacitance and γ_c and the

frequency behaviour can be explained in terms of a Maxwell-Wagner type model (see Section (2.3.5)), assuming that an interfacial polarization mechanism is occurring. However, the model proposed by Sutton[74] gives a more useful, qualitative understanding of the process occurring. He explains the polarization mechanism in terms of a Debye relaxation with a single relaxation time (see Section (2.3.3)). This model will be discussed further in the following section.

6.7.2 Decrease in Capacitance and Loss Tangent with Increasing Temperature

It is suggested that the absorbed gases which produced an inflated δ_c during the initial temperature increase, were being desorbed faster at temperatures above 80°C. The overall effect was a decrease in capacitance until the increase in capacitance due to the dielectric took over. The desorption process was taking place during the increase in capacitance as discussed in the previous section, but by an insignificantly small amount. The position of the peak in Figure (50) is therefore a function of the time taken to record results. Allam and Pitt[120] showed that hydrogen was removed during ageing of silicon oxide films.

It is evident that the first two stages in the annealing process were due to the presence of hydrogen and the following discussion refers to both stages.

From the diffusion data of Bell et al[139] it is possible to calculate the approximate distance a molecule of hydrogen will diffuse in amorphous silica in a given time. The diffusion constant at a temperature T is given by

$$D = 9{\cdot}5.10^{-4} \exp(-.68/kT) \text{ cm}^2 \text{ sec}^{-1}$$

where k is Boltzman's constant equal to $8{\cdot}63.10^{-5}$ eV/°K. An estimate of the average distance a molecule will diffuse in a time t is given by $\sqrt{Dt}$. At room temperature a hydrogen molecule will diffuse only a few angstroms in one hour. At 80°C, however, a hydrogen molecule will diffuse a distance the order of 2000Å, the silicon oxide film thickness. Calculations were also performed on the diffusion of other gases that could be absorbed during the silicon oxide deposition. These calculations showed that water vapour and oxygen would diffuse distances much less than an angstrom over a period of several hours and at the highest temperatures of measurement.

The effect of the increase of the diffusion constant with temperature and the reduction in hydrogen concen-

tration due to diffusion out of the system becomes evident from Sutton's equations[74]. The Debye equation for the permittivity is:

$$\varepsilon' = \varepsilon_\infty + \frac{\varepsilon_s - \varepsilon_\infty}{1 + \omega^2 \tau^2}$$

According to Sutton the approximations for ε_s and τ are:

$$\varepsilon_s \simeq \frac{\varepsilon_\infty t}{L_D'} \quad \alpha \sqrt{\frac{p_o}{D}}$$

and

$$\tau \simeq \frac{t\, L_D'}{2\, D} \quad \alpha \sqrt{\frac{1}{D\, p_o}}$$

where t is the film thickness, L_D' is a Debye length equal to $\sqrt{\frac{D}{p_o}} \sqrt{\frac{\varepsilon_\infty}{8\pi e \mu}}$, p_o is the concentration of diffusing species. The effect of temperature is too complex to perform quantitative calculations, but the most significant effects are the increase in the diffusion constant resulting in a reduction in the concentration p_o. This will have the effect of reducing ε_s and increasing τ, so that the contribution to ε' from the hydrogen is significantly reduced. The increased frequency dependence at low frequencies is explained if it is assumed that $\frac{1}{2\pi\tau}$ is less than 300 c/s. The

analysis of Section (2.4.3) showed that the contribution to ε_c from the loss mechanism increased as the frequency approached the relaxation frequency $\frac{1}{2\pi\tau}$ and this effect is illustrated in Figure (50).

6.7.3 Long Term Increase in A.C. Resistance and Decrease in Capacitance

It is emphasised that processes mentioned in the previous section will still be relevant to this discussion, but that it is not possible to distinguish which processes are the more important.

Equations (1) and (2) given in Section (6.4) are purely empirical and give no guide to the mechanism of annealing. It has been shown by Stanworth[130] that stress in glass is relieved as an exponential function of time with the time constant τ related to temperature by the Arrhenius relationship. He pointed out that the resulting activation energy was also a function of temperature. It was suggested in the previous section that desorption of a gas or gases occurred. Barrer[131] determined the activation energy of hydrogen diffusion along flaws in new silicon glass to be 0.2 eV. Prolonged heating reduced the flaw diffusion and increased the activation energy of diffusion.

It is not possible to relate the experimentally

determined values of activation energies (given in Section (6.4)) to any particular process. However, from the above discussion it appears that if stress relief and gas desorption are the dominating processes, then the activation energy involved will be a function of temperature. It is dangerous, therefore, to extrapolate to temperatures outside the experimentally determined range in order to determine annealing times.

Hirose and Wada[104] suggested that local structural changes occurred during annealing with changes in the bonding of oxygen atoms. Such a process is probably related to the stress relief already discussed.

The permittivity appears to reach a fully annealed value before the loss, which is to be expected since loss will be more sensitive to such extrinsic properties as flaws.

Summary

An initial increase in capacitance and loss was probably due to the presence of hydrogen absorbed during deposition. Heating caused desorption of the hydrogen. The empirical equations evolved (see Section (6.4)) defined an activation energy but it was difficult to give an exact interpretation as it probably involved a number of processes occurring together. The main

processes occurring were probably gas desorption, stress relief and local rearrangement of structure.

In order that for subsequent experiments the capacitance and loss should have reached stable values, a standard form of anneal was used. The capacitors were annealed at 240°C for 24 hours before letting them up to air and then annealed in an oven up at air at 400°C for about an hour. The best annealing procedure for different capacitors probably depends on the deposition conditions and it is thought that longer times are required to produce stable capacitors than have previously been suggested.

CHAPTER 7

ELECTRICAL RESULTS

7.1 D.C. Results

7.1.1 Introduction

This section presents the results of applying D.C. voltages across annealed capacitors. Unannealed capacitors produced results which were difficult to analyse because of their properties changing as a function of temperature. The results are considered in four parts: firstly the time-dependent part of the current resulting at low fields, then the steady state currents which can be considered as two distinct regions at low and high fields and lastly, breakdown occurring at fields in excess of 2 MV/cm.

The low field region gave an ohmic characteristic for fields less than 0.05 MV/cm, of the form:

$$I = B V \qquad (1)$$

where 'B' is a constant, which is the low field conductance of the capacitor.

At high fields (> 0.3 MV/cm) the current-voltage relationship was similar to that of Schottky Emission and Poole-Frenkel conduction (see Section (2.2.2)).

i.e. $$I = A \exp(a V^{\frac{1}{2}}) \qquad (2)$$

where 'a' and 'A' are constants for a fixed voltage, temperature and material.

An expression which describes the current-voltage relationships for these experiments over the whole voltage range can be written:

$$I = C\,[\cos h\,(a V^{\frac{1}{2}}) - 1] \qquad (3)$$

For low fields this approximates to:

$$I = \frac{C}{2} a^2 V$$

Comparing this equation with Equation (1) gives:

$$B = \frac{Ca^2}{2}$$

For high fields, Equation (3) approximates to:

$$I = \frac{C}{2} \exp(a V^{\frac{1}{2}})$$

Comparing this with Equation (2) gives:

$$A = \frac{C}{2}$$

7.1.2 Absorption Current

The absorption current was investigated in order to obtain an indication of the low frequency behaviour (< 0.1 c/s). Figure (51) shows the decay in current on applying a voltage of 0.5 volts across a capacitor. The steady state current level obtained after

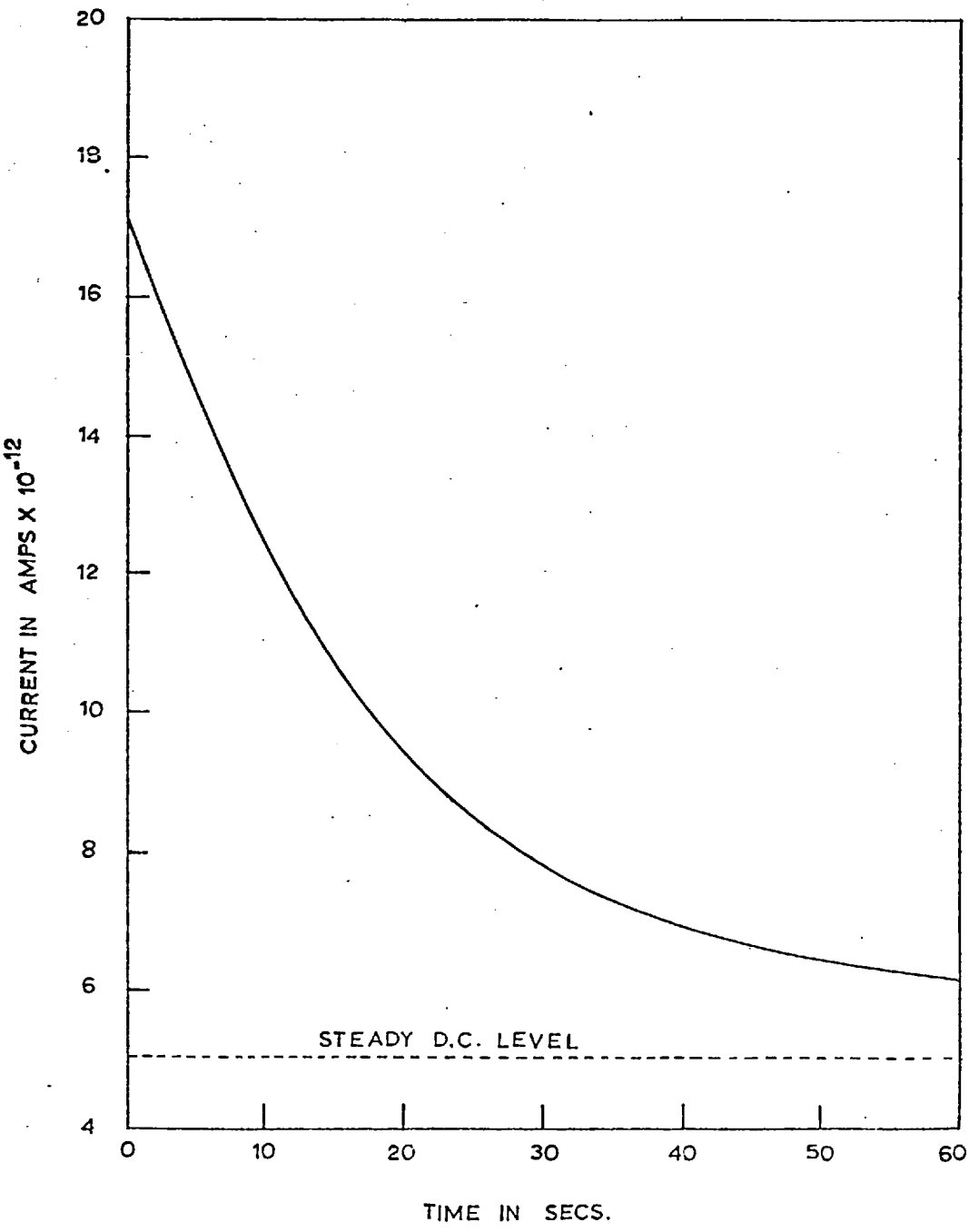

FIG. 51 DECAY OF ANOMALOUS ABSORPTION CURRENT AS A FUNCTION OF TIME SHOWING STEADY D.C. LEVEL

30 minutes is shown. The analysis of Hamon[76], as discussed in Section (2.3.5.1), was used to determine the behaviour of the loss 'ε''' as a function of frequency. This is shown in Figure (52) and indicates a loss peak, having a maximum in the region 5.10^{-3} c/s. Itis emphasised that this is only a crude approximation to the position of the loss peak (Hamon quotes an error of $\pm$ 15%). There is an additional error due to the value of 'n', defining a linear dielectric ($I \propto t^{-n}$), being outside the range of $0.3 < n < 1.2$. However, the experiment indicates the presence of a loss peak occurring at very low frequencies.

7.1.3 Steady State Low Field Conduction

Due to the time dependent nature of the low field, current readings were noted 5 minutes after applying the voltage. Before each voltage was applied the capacitor was short-circuited for a similar period. This was not necessarily the time taken to reach equilibrium, but gave a good approximation. Figure (53) shows the current-voltage characteristics, plotted on a log-log scale to emphasise the low field ohmic region. The conductances determined from Figure (53) are plotted as a function of reciprocal temperature in Figure (54). The slope of this curve indicates an activation energy

FIG. 52 DIELECTRIC LOSS ε'' CALCULATED FROM ABSORPTION CURRENT VS. FREQUENCY.

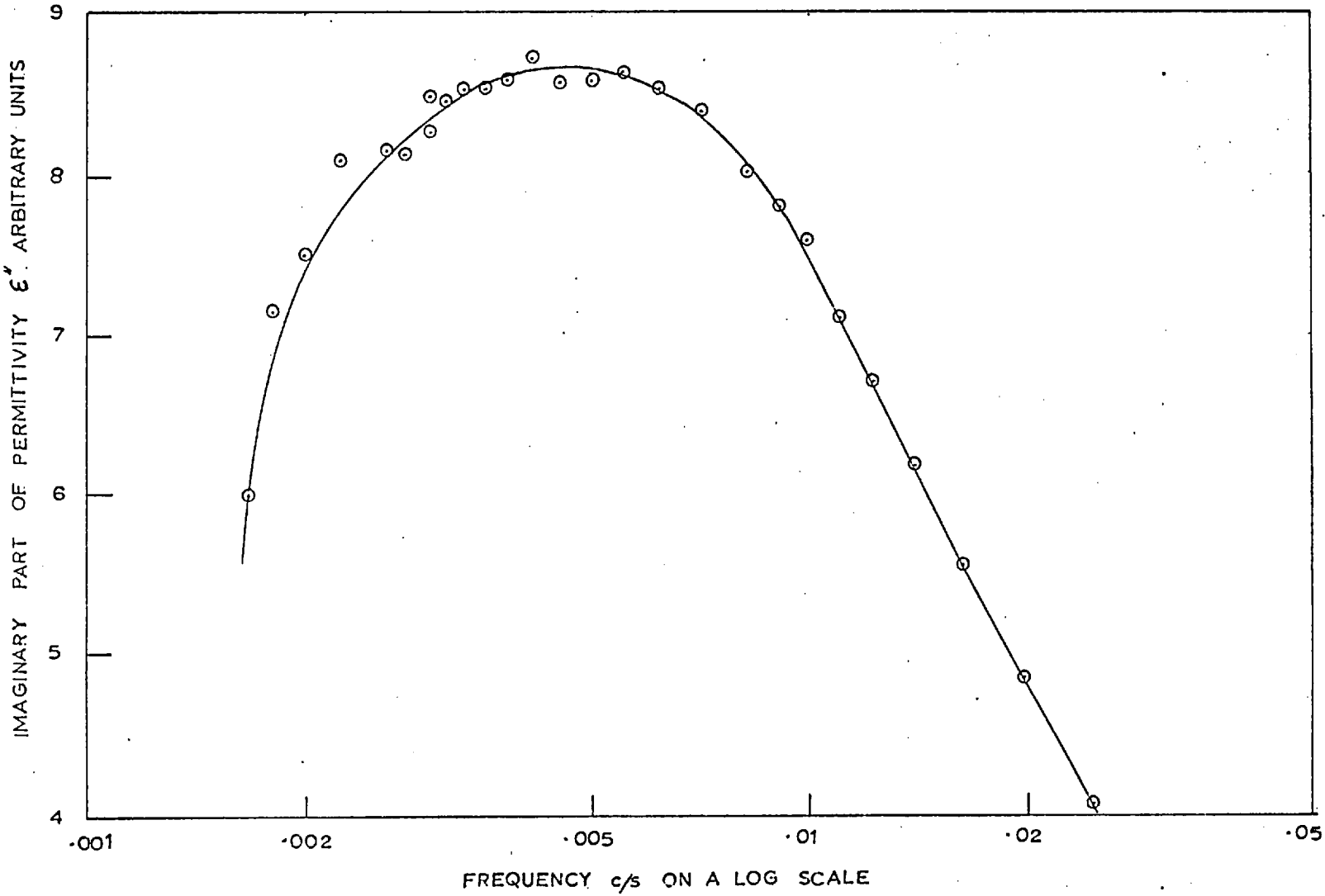

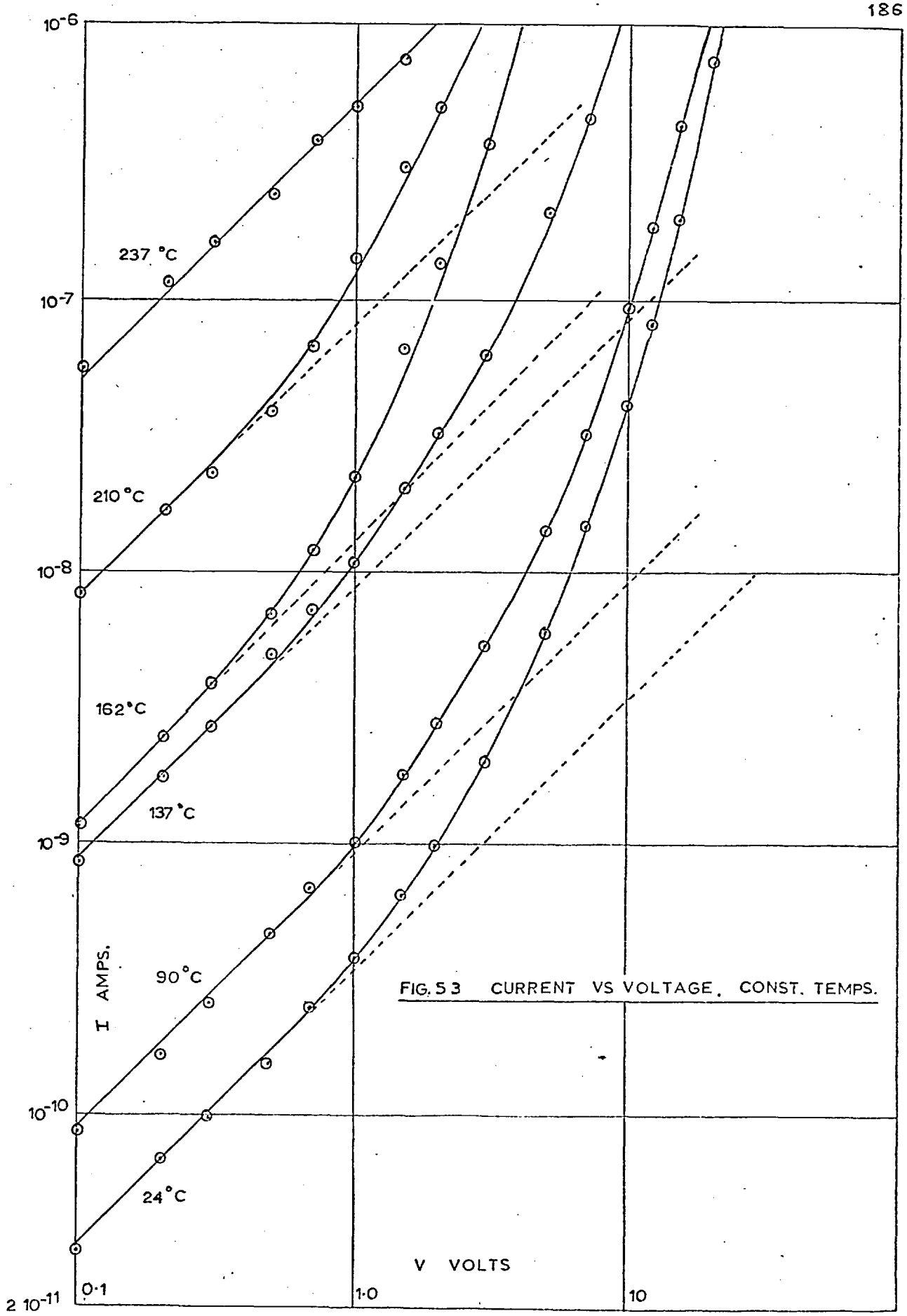

FIG. 5 3 CURRENT VS VOLTAGE, CONST. TEMPS.

FIG. 54 CONDUCTANCE OF OHMIC REGION VS. RECIPROCAL TEMPERATURE

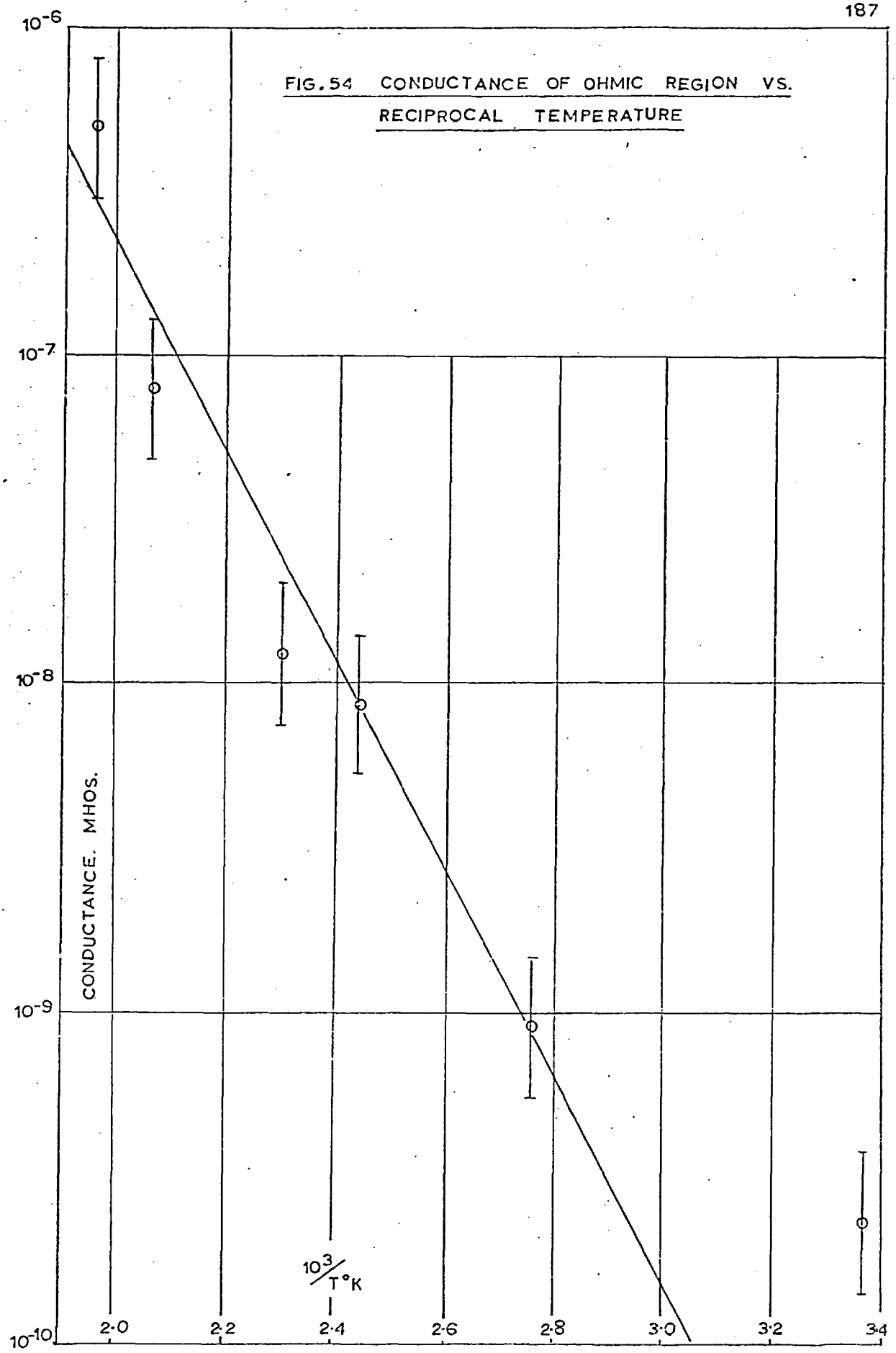

of .70 $\pm$ .15 eV.

7.1.4 High Field Conduction and Breakdown

There was a spread of results from high field measurements because breakdown sometimes occurred above 2 MV/cm. The resistance to earth was low and self-propogating breakdowns occurred. However, these usually self-healed having the effect of slightly changing the characteristics but not to the extent that further information was unobtainable. Figures (55 to 58) show the types of breakdown occurring. The method used to observe the breakdowns was optical reflection microscopy on the upper aluminium electrode. Because of the breakdown errors, readings were repeated on different specimens and the average values are quoted.

Figure (59) shows a typical set of current-voltage characteristics with log I plotted as a function of $\sqrt{V}$. The intercepts of the extrapolated straight line portion of the curves are plotted on a logarithmic scale in Figure (60) as a function of reciprocal temperature to yield an activation energy of .55 $\pm$ .05 eV. In order to investigate the possibility of Schottky Emission the intercept divided by T^2 is also plotted against reciprocal temperature in Figure (61) to yield an activation energy of .45 $\pm$ .10 eV. The slopes determined

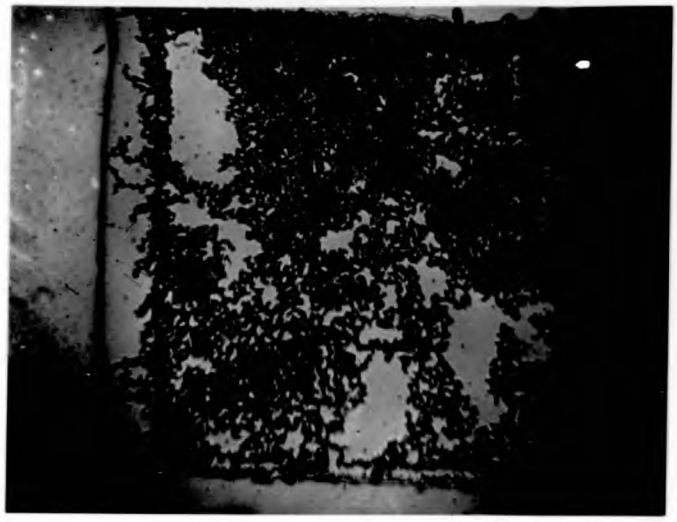

FIG.55 MULTIPLE BREAKDOWNS x 40

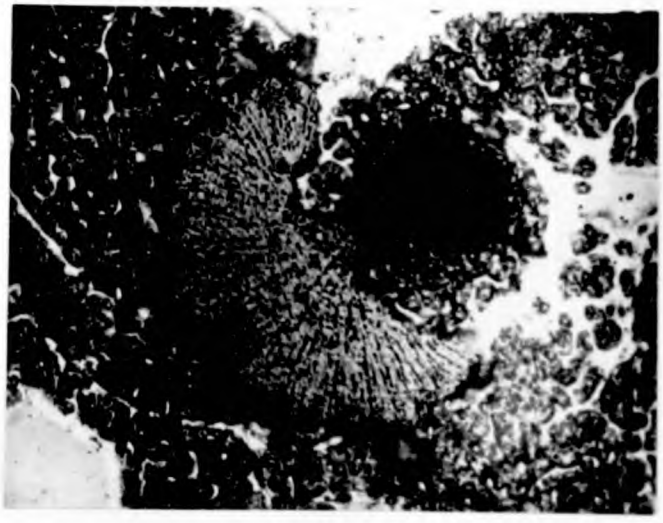

FIG.56 CLUSTER OF BREAKDOWNS x 800

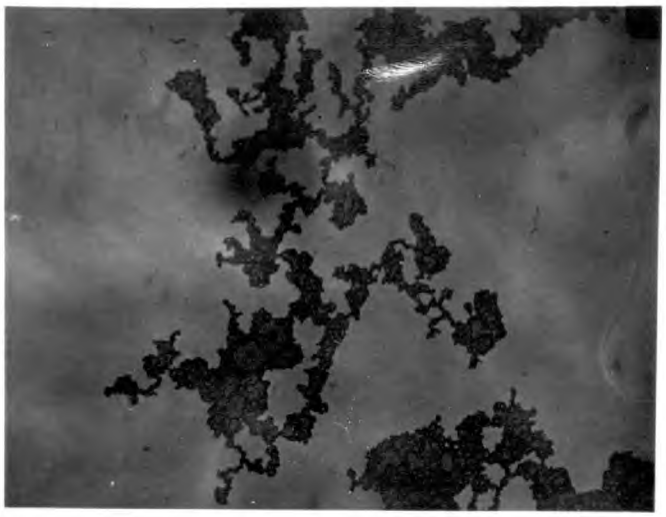

FIG. 57 PROPAGATING BREAKDOWN x 400

FIG. 58 PROPAGATING BREAKDOWN x 400

FIG. 59 CURRENT VS. (VOLTAGE)$^{1/2}$

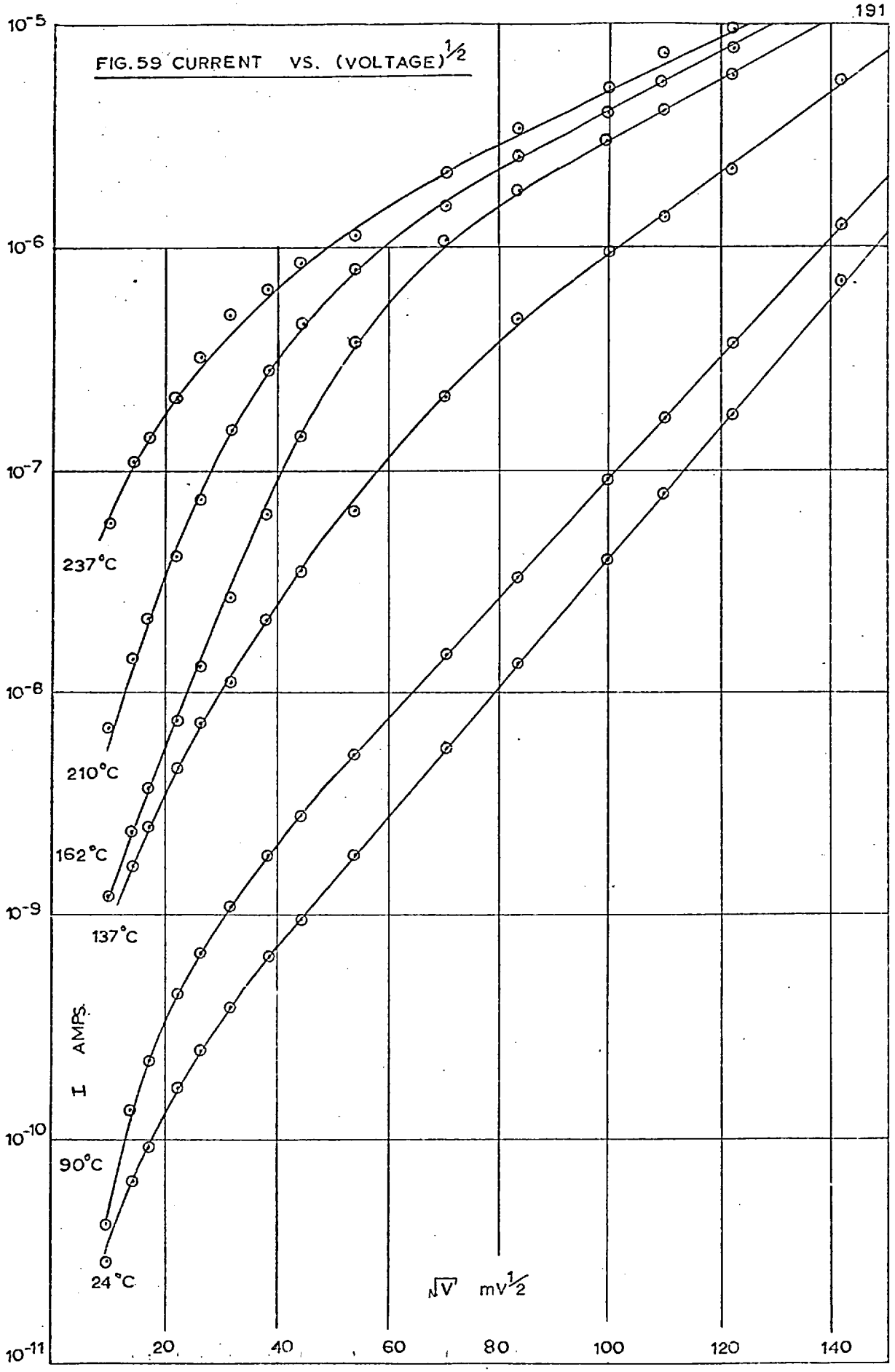

FIG. 60 LOG(I_s) VS. RECIPROCAL TEMPERATURE

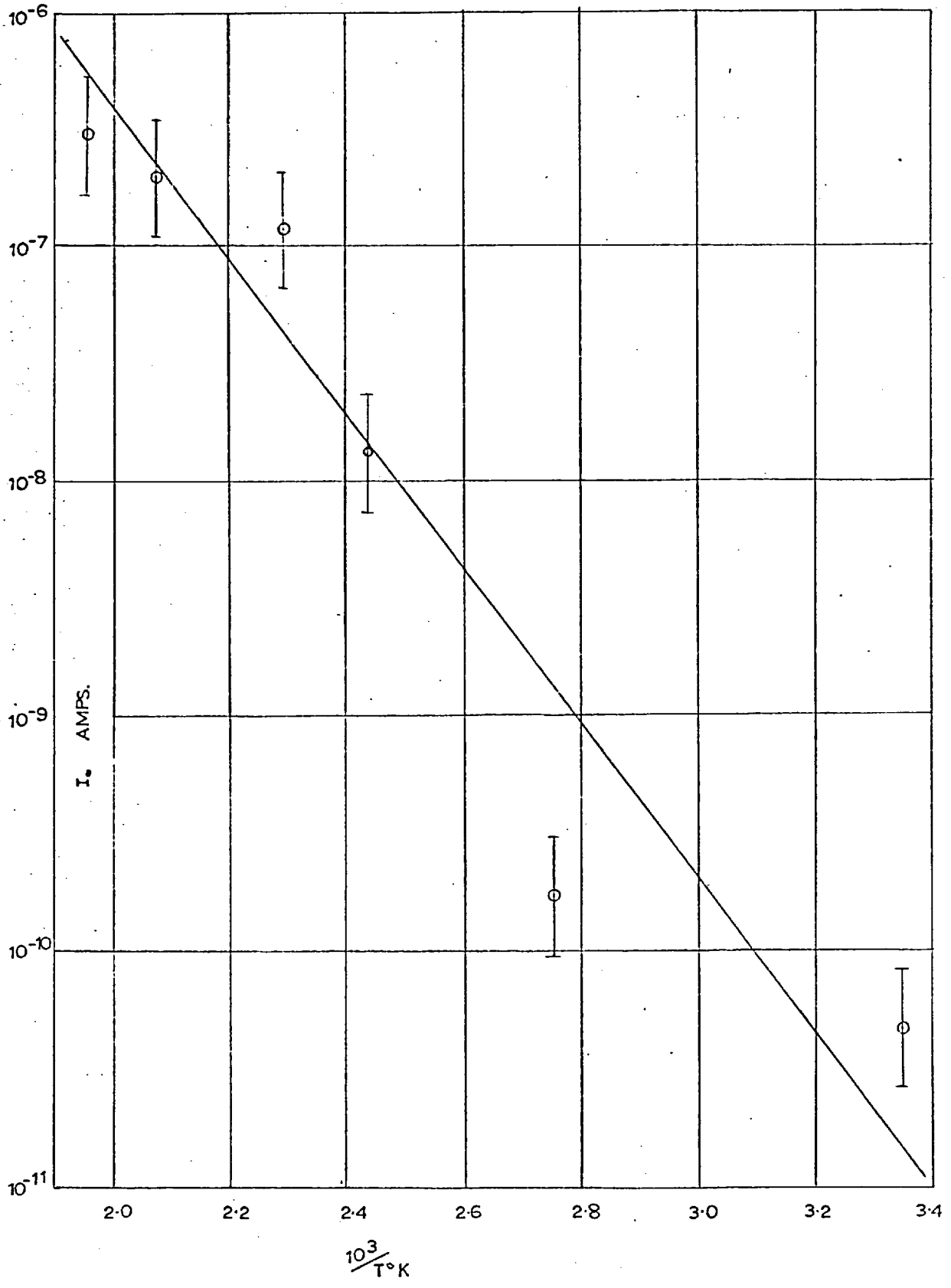

FIG. 61 LOG.(I_o/T^2) VS. RECIPROCAL TEMPERATURE

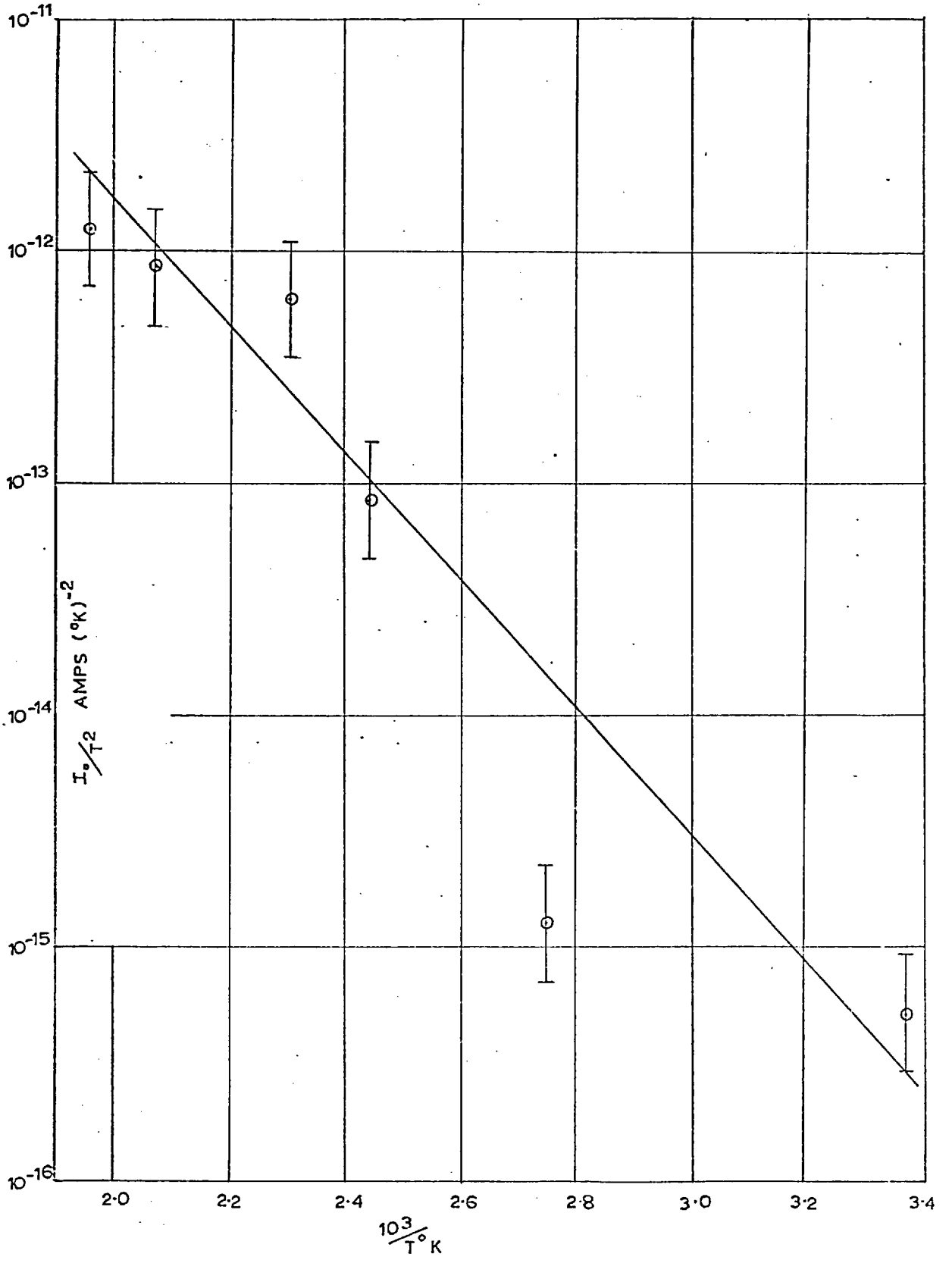

from Figure (59) are plotted as a function of reciprocal temperature in Figure (62) using the origin as a point. The resulting slope is $610 \pm 60\ ^{o}KV^{-\frac{1}{2}}$.

7.2 A.C. Results

7.2.1 Introduction

The following results refer to annealed specimens. The frequency behaviour of unannealed specimens was shown in Figure (50).

Several capacitors were prepared by different evaporations but with the same deposition conditions and subsequent heat treatment. The deposition conditions were a rate of $10\mathring{A}/sec \pm 1\mathring{A}/sec$, a pressure of 2.10^{-5} Torr during deposition and a substrate temperature of about $25^{o}C$ at the onset of deposition. The standard heat treatment was given in Section (6.8).

Despite capacitors receiving similar heat treatments and having similar deposition conditions there was a broad spread in loss tangent values at any one frequency ($0.2^{o}/o$ to $1.0^{o}/o$ at room temperature and 1 Kc/s). Their permittivities, however, were similar at 5.5 ± 0.3. The form of both capacitances and loss tangents as functions of temperature and frequency were similar and the spread in the resulting parameters was small. The curves illustrating the various behaviours

FIG. 62 SLOPES OF LOG I VS. $V^{1/2}$ GRAPH VS. RECIPROCAL TEMPERATURE

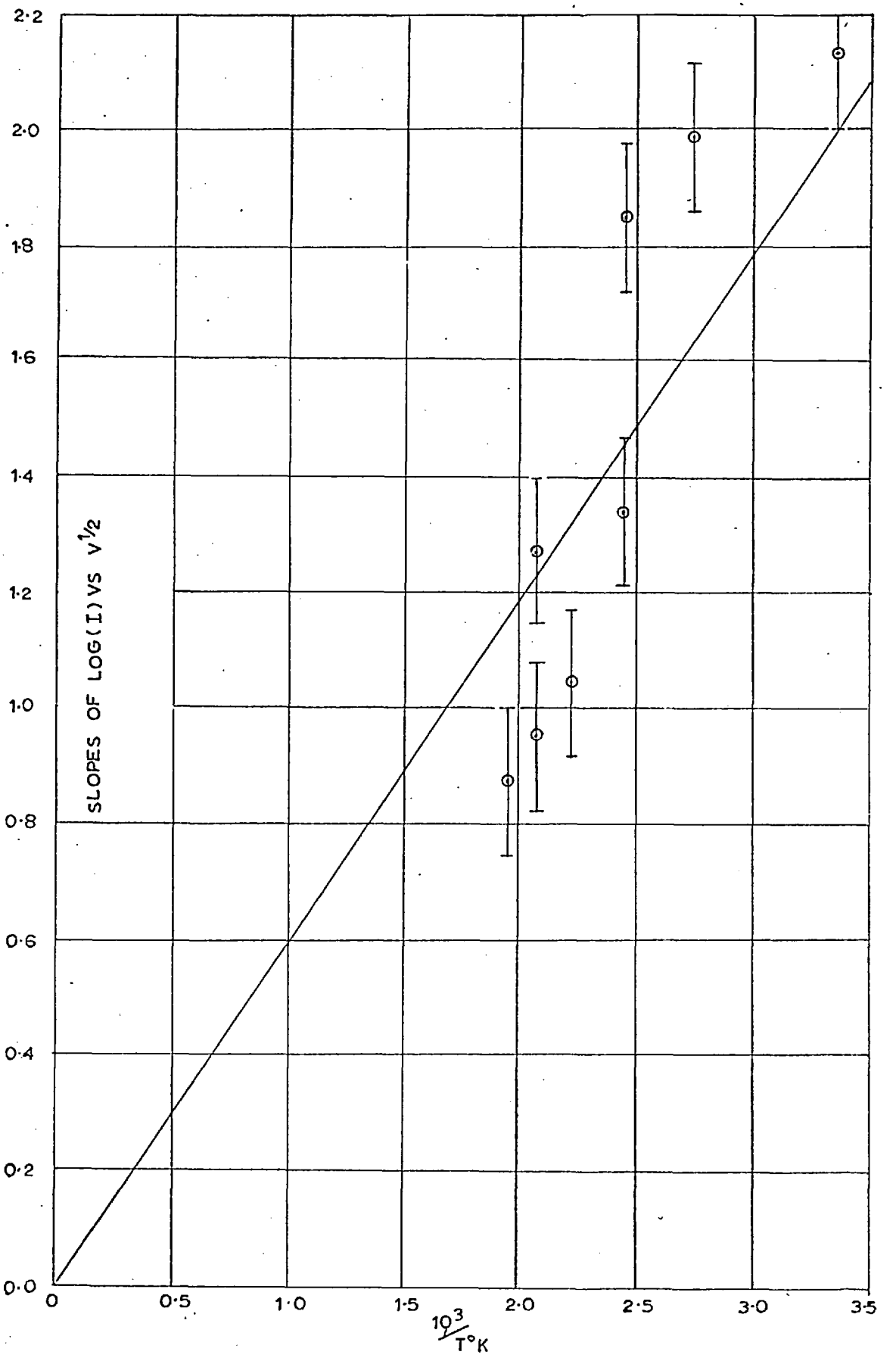

are for fairly lossy capacitors but the values quoted for the resulting parameters are averages of several experiments.

The audio frequency range measured was 300 c/s to 15 Kc/s. The frequency range 30 Kc/s to 1 Mc/s was measured using a separate bridge arrangement, which was more inaccurate than the audio frequency bridge arrangement (giving loss tangent errors of greater than 5°/o). The high frequency bridge was not calibrated sufficiently accurately to allow matching of results over the entire frequency range used. The graphs of results, therefore, only show the audio frequency range and the radio frequency results are merely quoted with the assumption that nothing unusual occurs in the frequency gap of 15 Kc/s to 30 Kc/s.

7.2.2 Audio and Radio Frequency Results

7.2.2.1 Capacitance and γ_c

Figures (63) and (64) show a sample variation of capacitance as functions of temperature and frequency. The capacitance spread at room temperature for the given frequency range is about 1°/o but this is greatly increased at temperatures above 100°C, particularly at low frequencies. For frequencies above 30 Kc/s up to 1 Mc/s the capacitance is invariant with frequency

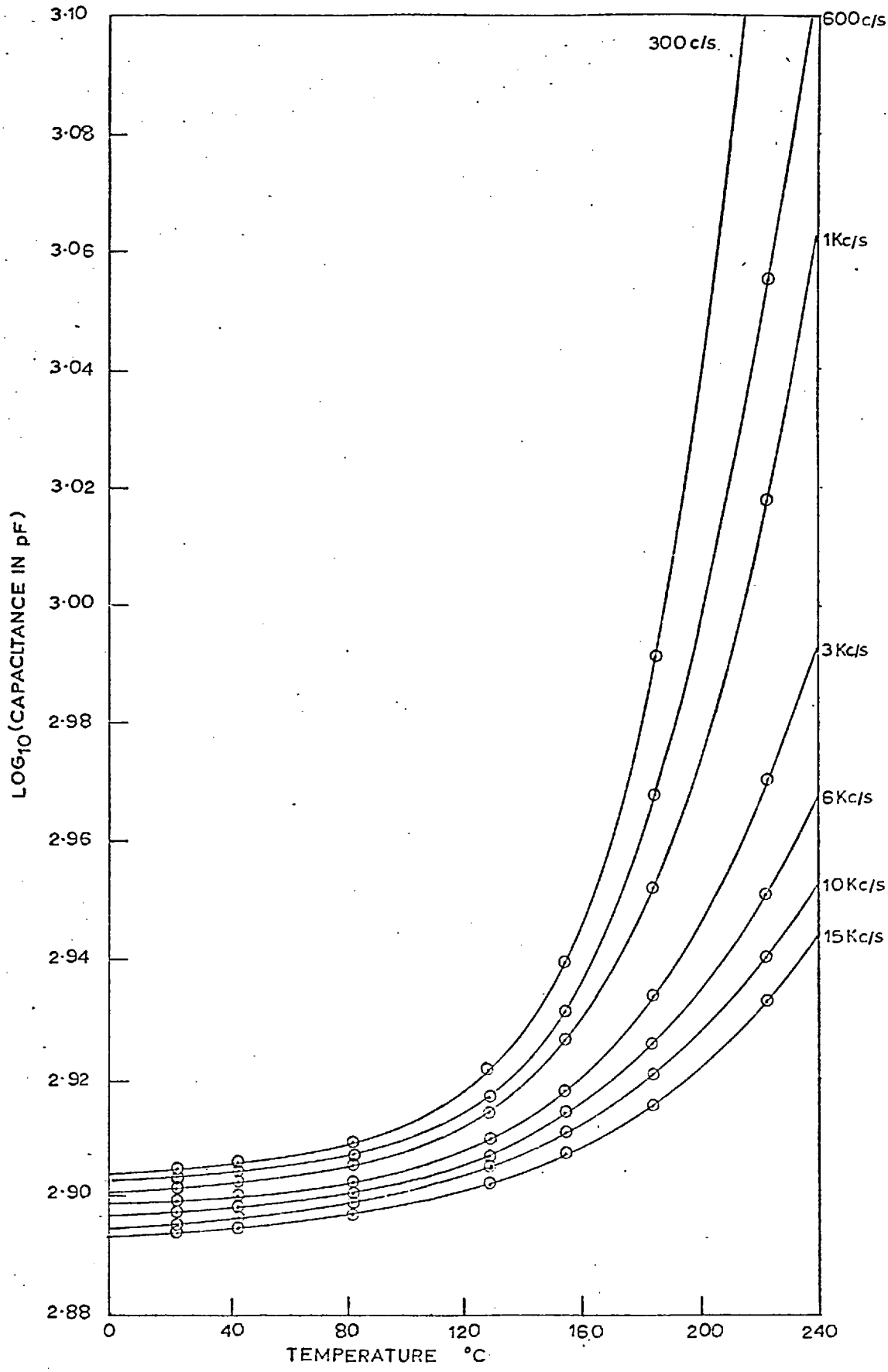

FIG. 63 VARIATION OF CAPACITANCE WITH TEMPERATURE AT FREQUENCIES IN THE AUDIO RANGE

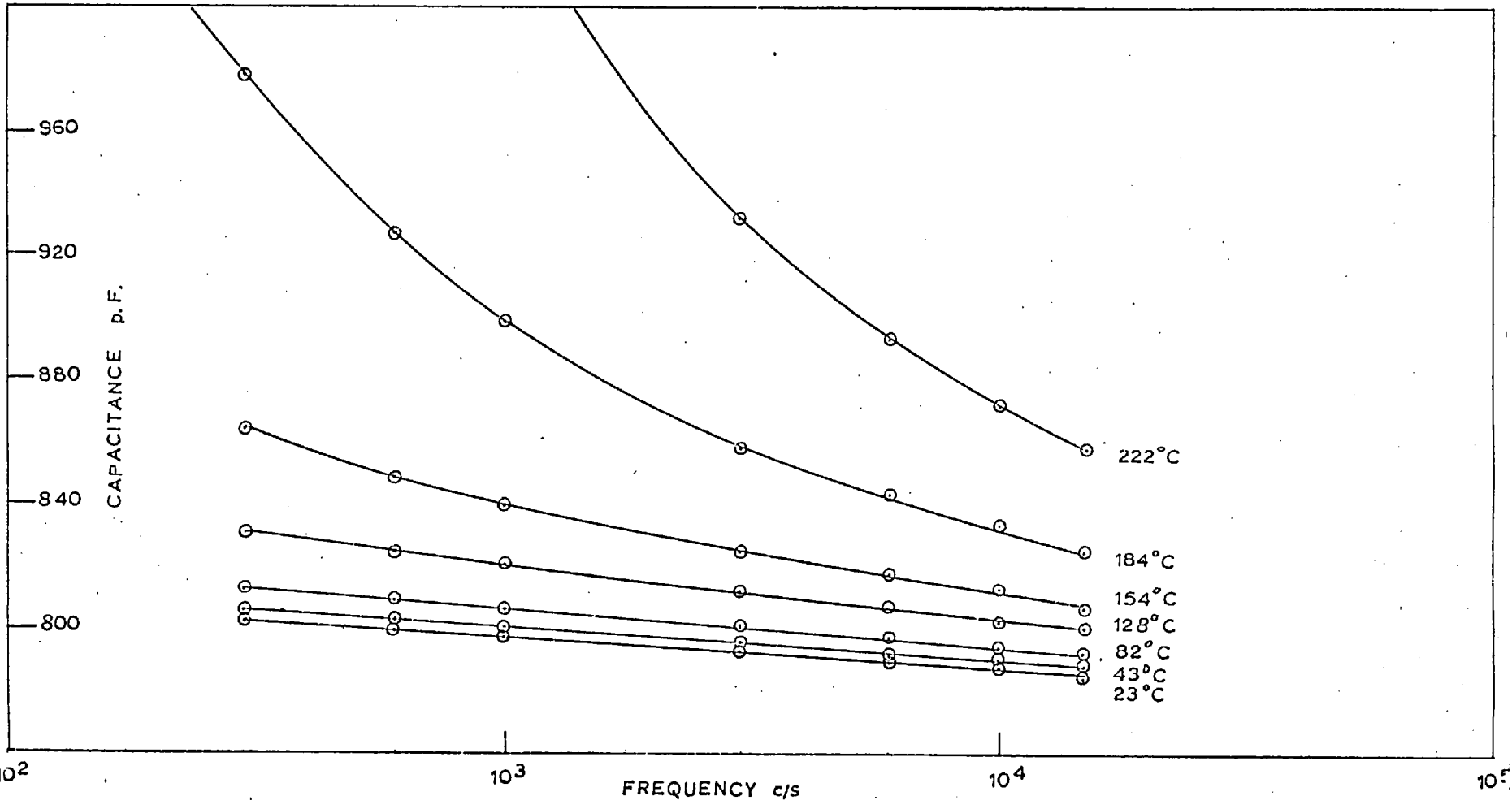

FIG. 64 CAPACITANCE VS. FREQUENCY AT CONSTANT TEMPERATURES.

and temperature to within an accuracy of $\pm$ 5°/o. The coefficient temperature/of capacitances as determined from Figure (63), are shown plotted as a function of frequency at different temperatures in Figure (65). γ_c appears to be independent of frequency above 30 Kc/s and has limiting values of 50 p.p.m./°C to 100 p.p.m./°C for capacitors with limiting losses of 0.02°/o to 0.3°/o at high frequencies, respectively. Figure (66) shows γ_c as a function of loss tangent for different capacitors. The limiting line for high loss capacitors of γ_c = .05 Tan δ is shown and the spread in values of γ_c for low loss indicated. Figure (67) shows γ_c plotted as a function of loss tangent for a number of lossy capacitors including values for unannealed capacitors. The majority of these points are for capacitors prepared for the determination of the effect of deposition conditions. The line γ_c = .05 Tan δ is plotted and also the two extremes of the constant A = 0.05 $\pm$ 0.01.

An average value of γ_c for extrapolation to zero loss tangent is 70 $\pm$ 10 p.p.m./°C.

7.2.2.2 Conductance and Tan δ Results

Figures (68) and (69) show a sample loss tangent plotted as functions of temperature and frequency. For frequencies above 30 Kc/s the loss tangent becomes

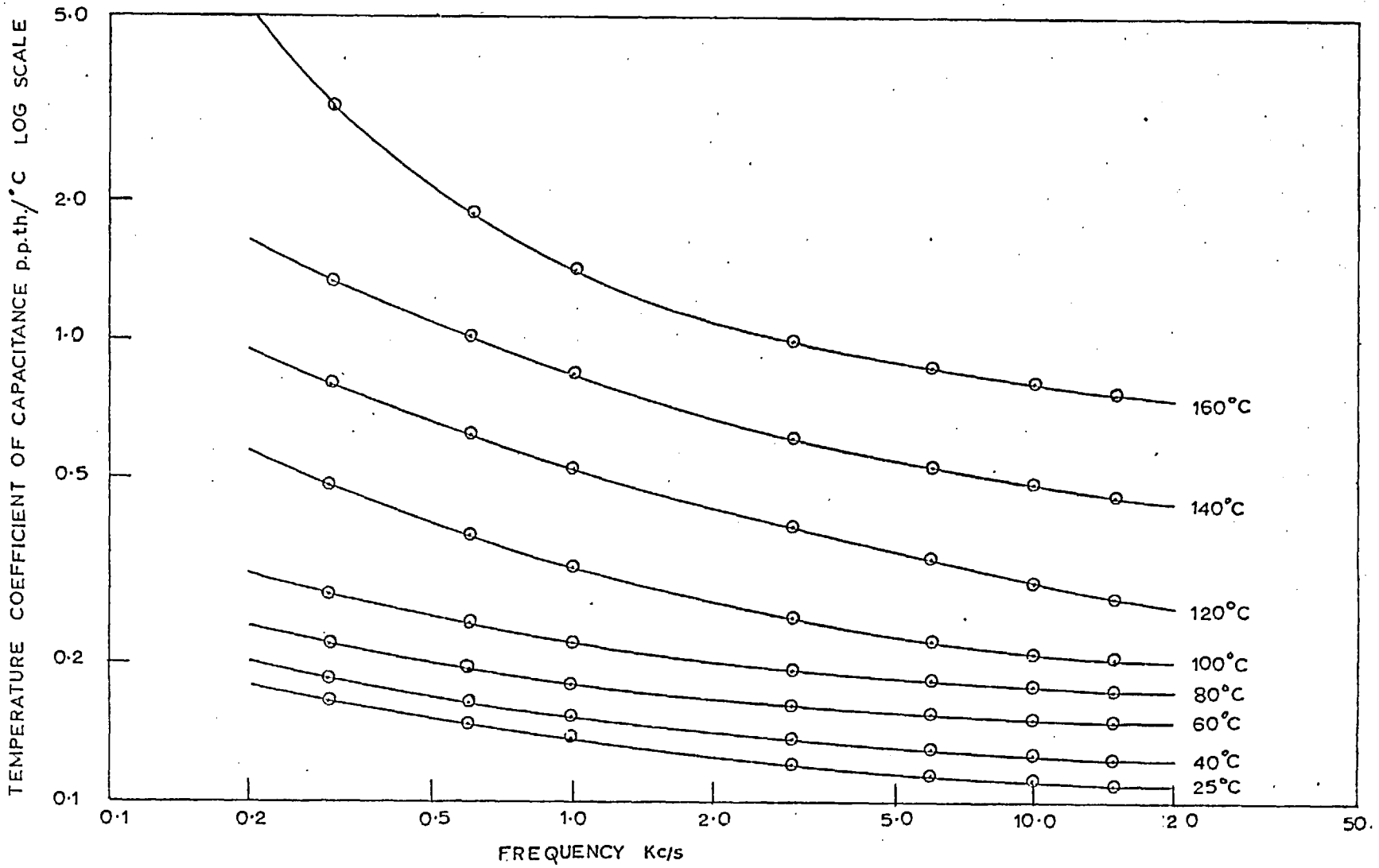

FIG. 65 TEMPERATURE COEFFICIENT OF CAPACITANCE VS. FREQUENCY AT CONSTANT TEMPERATURES

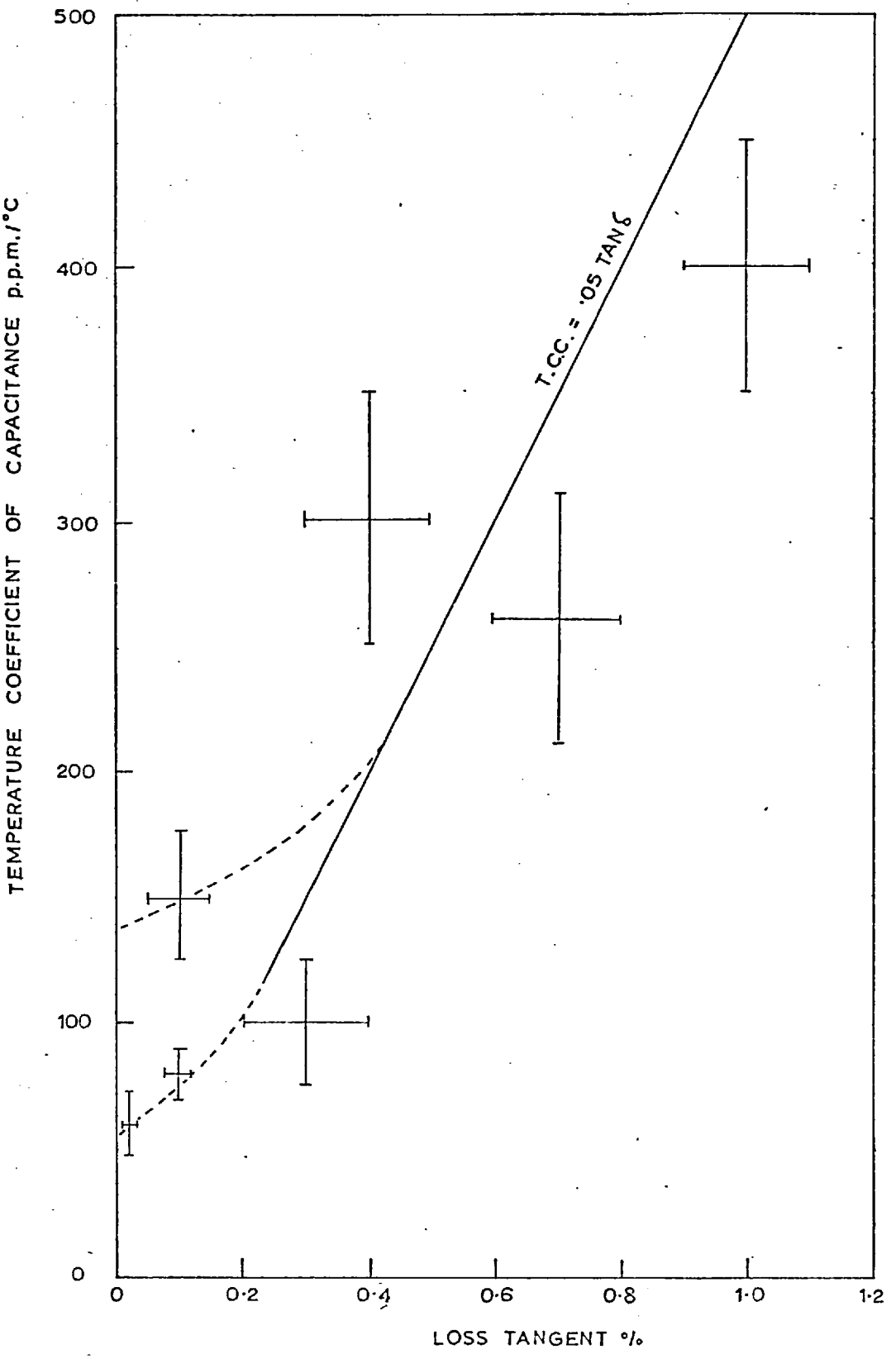

FIG. 66 TEMPERATURE COEFFICIENT OF CAPACITANCE OF LOW LOSS SILICON OXIDE CAPACITORS SHOWING SUGGESTED SPREAD AT VERY LOW LOSS.

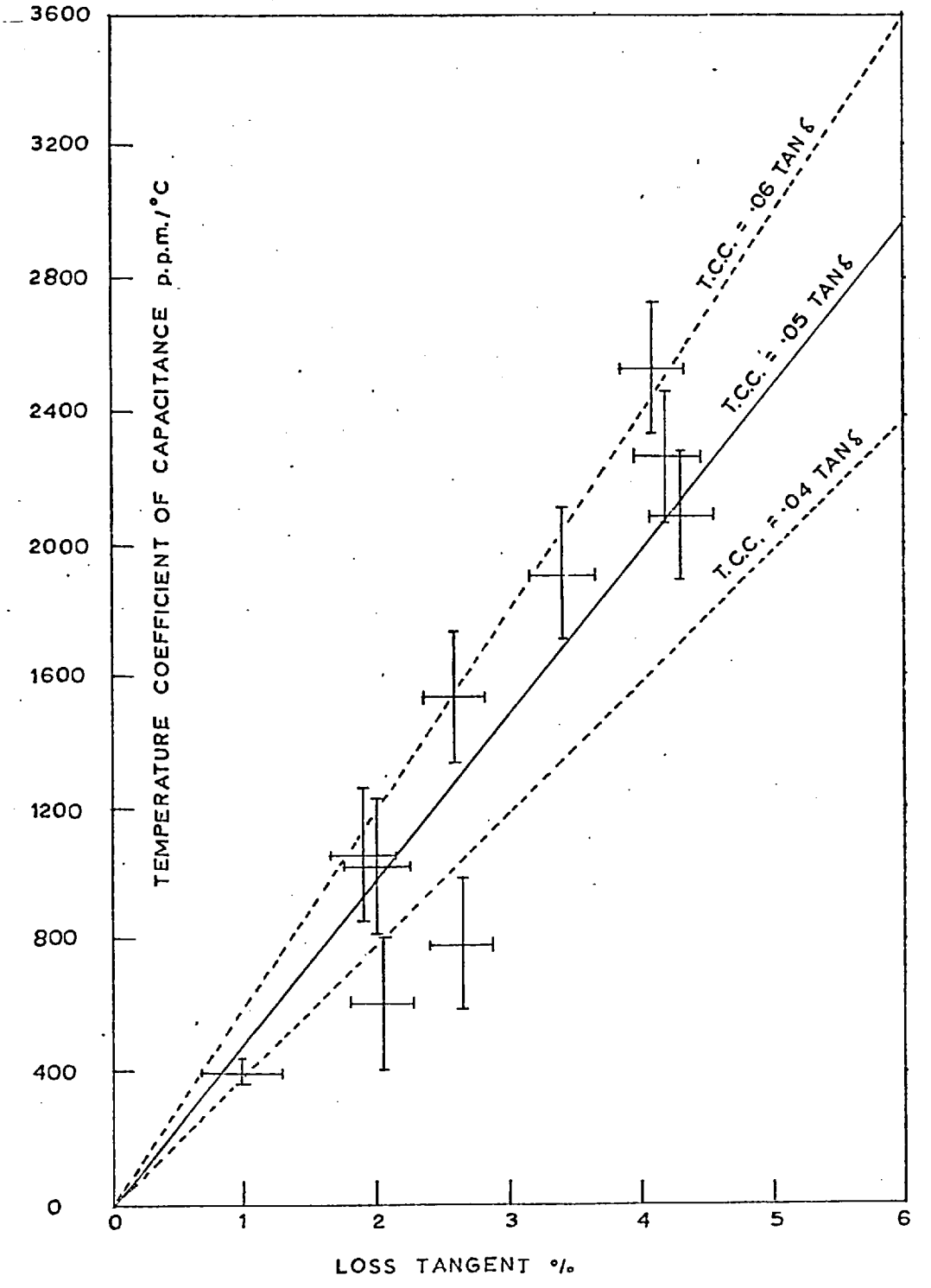

FIG.67 THE TEMPERATURE COEFFICIENT OF CAPACITANCE OF LOSSY SILICON OXIDE CAPACITORS

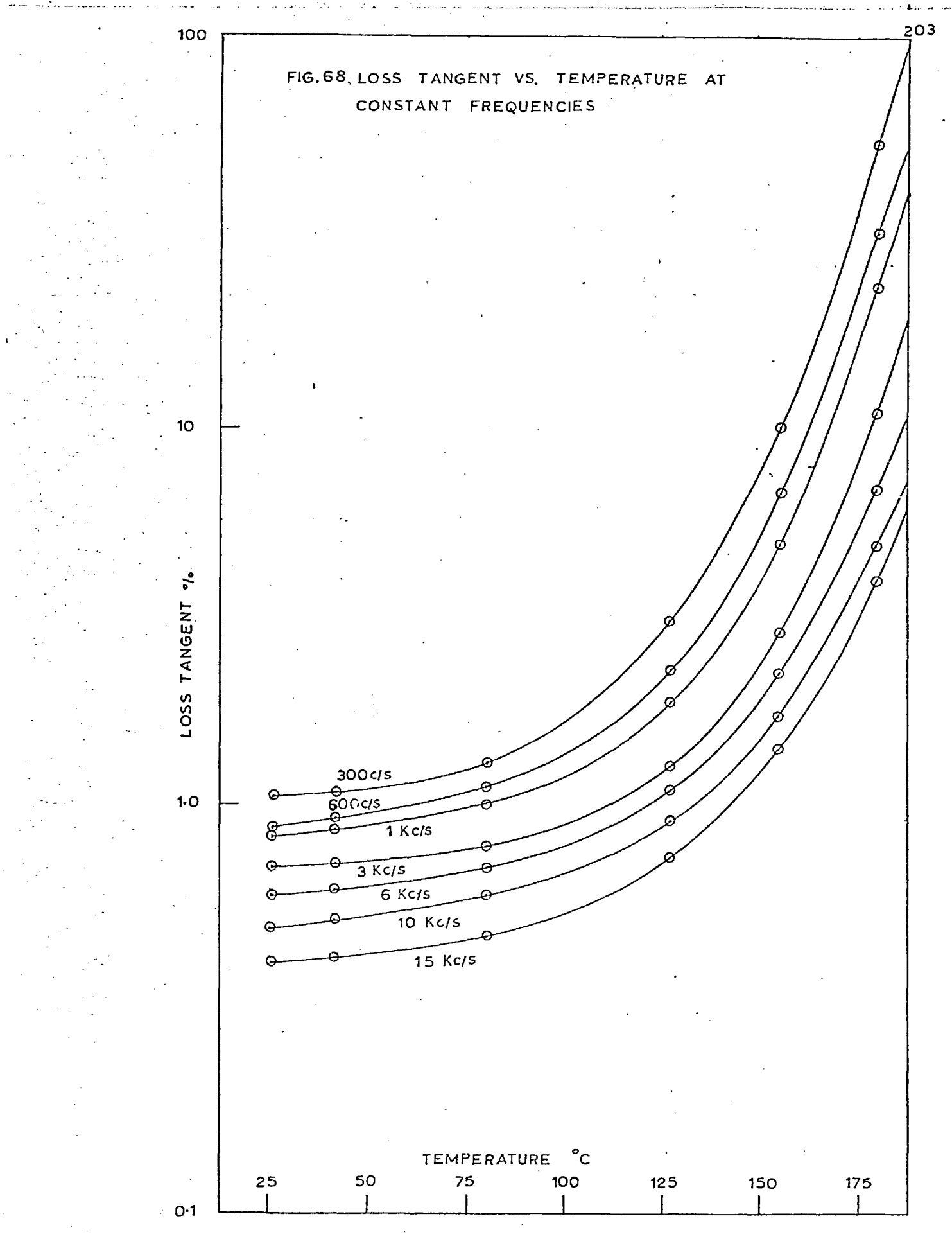
FIG. 68. LOSS TANGENT VS. TEMPERATURE AT CONSTANT FREQUENCIES
100
10
1·0
0·1
203
LOSS TANGENT %
300 c/s
600 c/s
1 Kc/s
3 Kc/s
6 Kc/s
10 Kc/s
15 Kc/s
TEMPERATURE °C
25
50
75
100
125
150
175

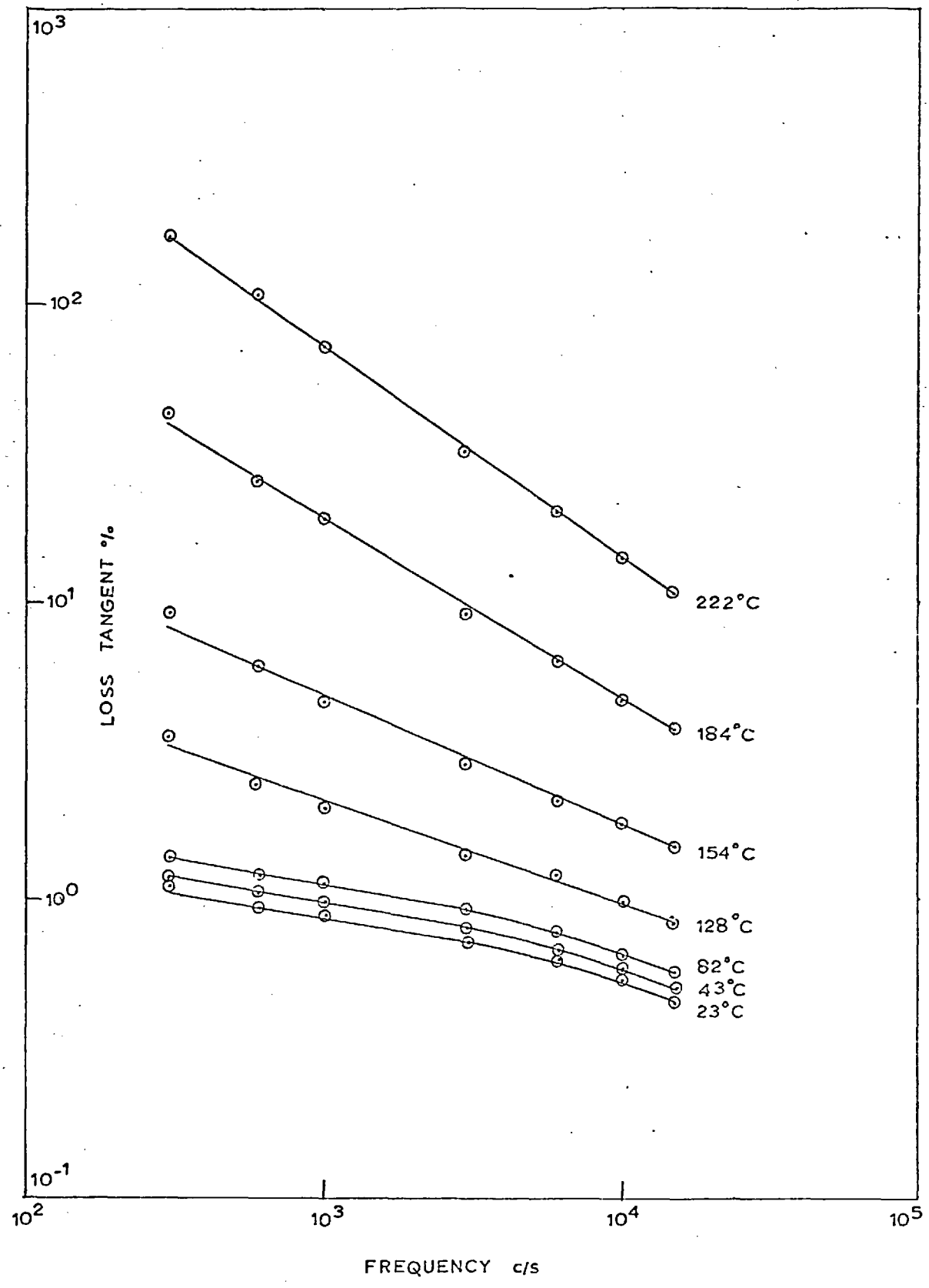

FIG. 69 LOSS TANGENT AS A FUNCTION OF FREQUENCY AT DIFFERENT TEMPERATURES

independent of frequency within the limit of experimental error of $\pm$ 5 %. The frequency spread at room temperature is about half an order of magnitude.

Figure (69) gives a series of straight lines of slope $-\gamma$ such that

$$\text{Tan } \delta \propto \omega^{-\gamma}$$

Because of the comparatively small frequency variation of capacitance the plot of conductance versus frequency (Figure (70)) produces a similar result. If the slope of the straight lines is α then the conductance 'G' is given by

$$G \propto \omega^{\alpha}$$

If we neglect the frequency variation of capacitance, then $\alpha = (1 - \gamma)$. Figure (71) shows the function α plotted as a function of temperature. Up to 80°C 'α' is constant at 0.8 but falls above 80°C to about 0.3 at 220°C.

The Arrhenius plot of Figure (72) indicates two regions with different activation energies. The low temperature activation energy does not appear to have reached a constant value but will be less than 0.1 eV. The slope of the high temperature region is about 0.8 eV. However, the analysis of Section (2.3.4) for the high

FIG. 70

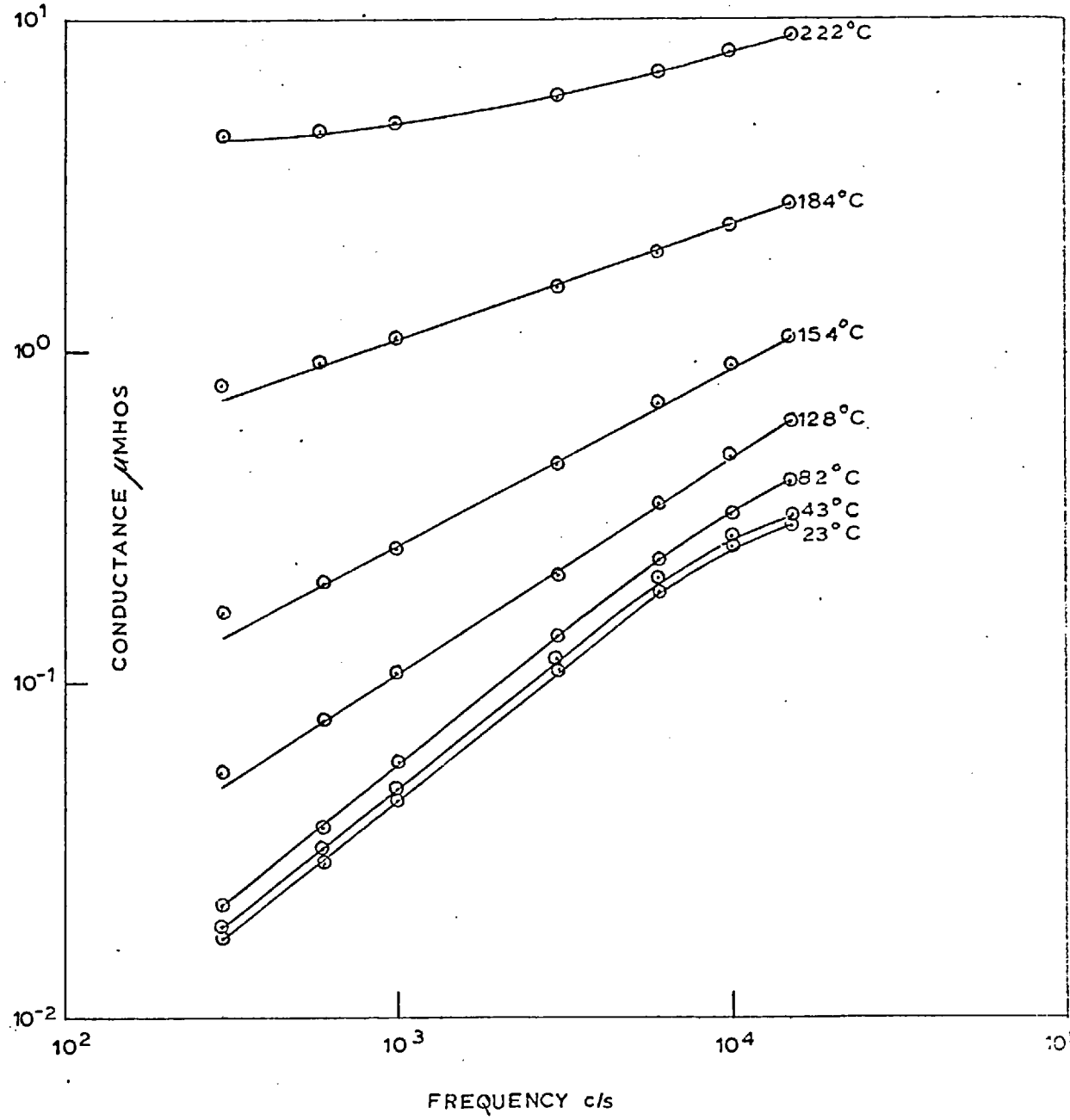

CONDUCTANCE VS. FREQUENCY AT CONSTANT TEMPERATURES.

FIG. 71 THE FUNCTION $\alpha(T) = 1 - \gamma(T)$ VS TEMPERATURE

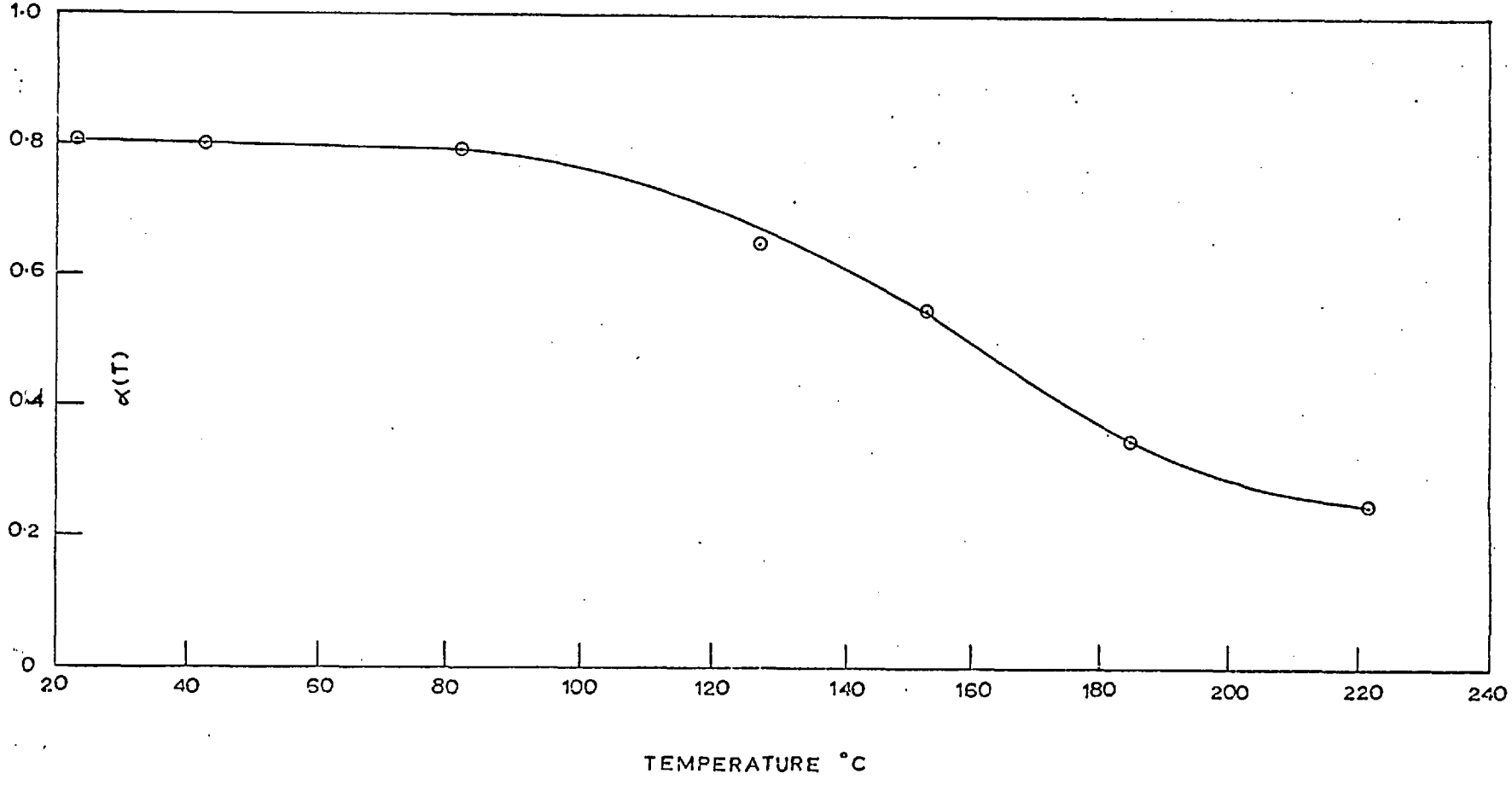

FIG. 72 CONDUCTANCE VS RECIPROCAL TEMPERATURE

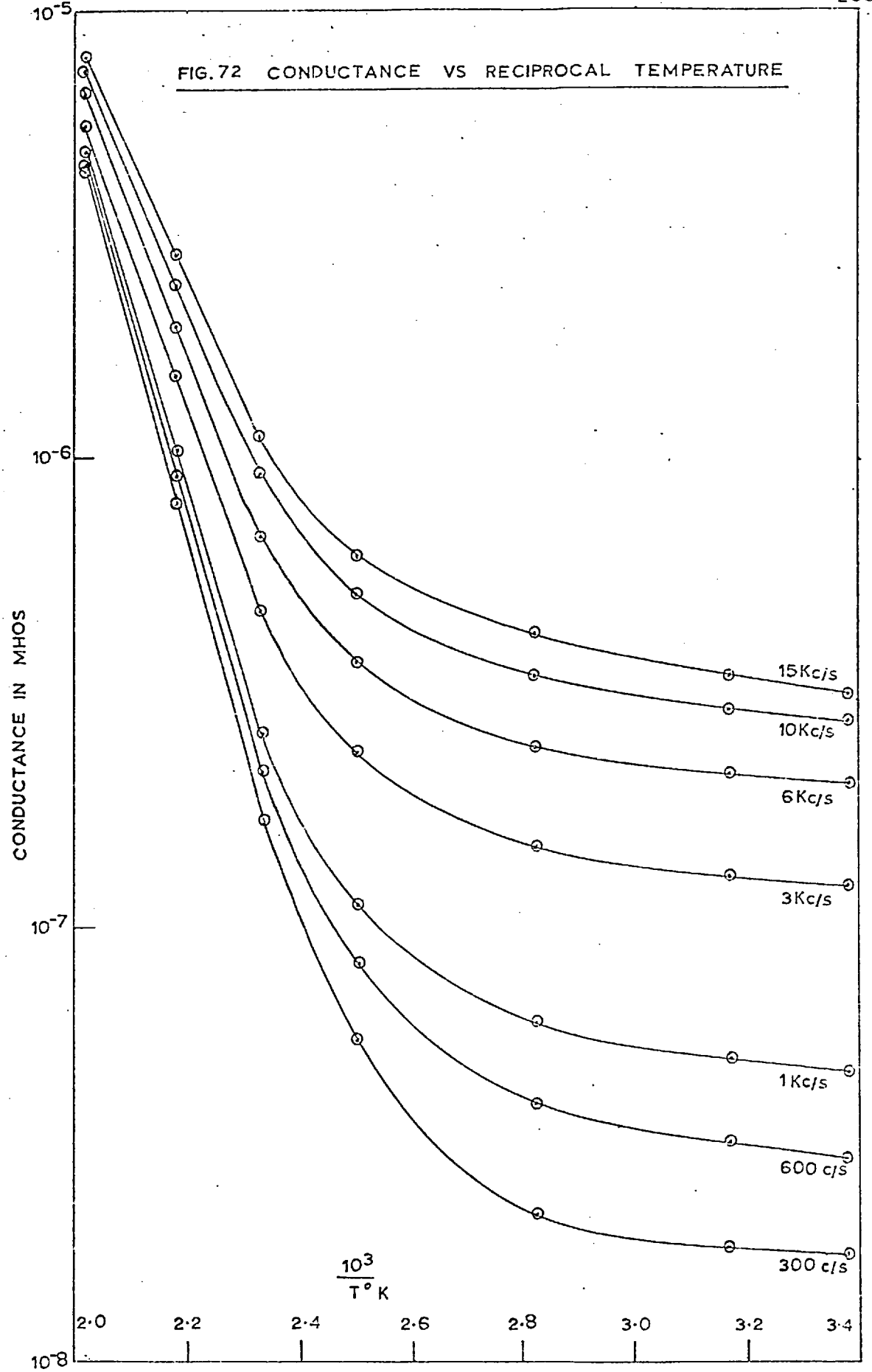

frequency approximation of the Cole-Cole[62] form of a distribution of relaxation times gives for the conductance

$$G \alpha \tau_o^{-(1-\beta)}$$

If we assume that the mean relaxation time is related to temperature by the Arrhenius relationship (see Section (2.4.1))

$$\tau_o = \tau_\infty e^{\frac{q}{kT}}$$

and $\alpha = \beta$ in the high temperature region, then for the conductivity we get

$$G \alpha \exp\left[-\frac{(1-\beta)q}{kT}\right]$$

Therefore, the mean activation energy 'q', as determined from Figure (72), is

$$q \simeq 1.0 \pm 0.1 \text{ eV}$$

CHAPTER 8

DISCUSSION OF ELECTRICAL RESULTS

8.1 Discussion of D.C. Results

8.1.1 Introduction

The D.C. results were presented in four parts and each of these will be discussed separately.

8.1.2 Absorption Current

The time varying part of the current resulting from the application of a low field across a capacitor has been related to a dispersion effect occurring at very low frequencies. Further discussion on the low frequency loss peak will be given in Section (8.2.2).

8.1.3 Low Field Region

Authors who have performed work on D.C. conduction in silicon oxide films have usually confined their attention to the high field region and very little information exists as to the cause of the ohmic conductivity. The reason is that the time taken for the current to reach a steady value is often very long and indeterminate whereas high field readings are instantaneous. However, the number of mechanisms resulting in an ohmic characteristic is limited and these will now

be discussed. The only distinguishing features available are the order of conductivity at room temperature, 10^{-13} ohms cms, and the activation energy of the process, $.70 \pm .15$ eV. Unfortunately, this is not sufficient information to distinguish between the possible conduction mechanisms.

It is first of all necessary to show that electrons cannot enter the conduction band of the insulator, or at least that any current resulting from thermionic emission is negligible. Hill[26] has discussed the various cases of injection limited conduction and for a barrier height of $\phi = 2$ eV (see Section (2.1)), the contribution from a thermionic current is 10^{-26} amps cm^{-2} at room temperature. This is shown to be constant at low fields and of course can be neglected in comparison to the observed current flow.

The two mechanisms of current flow that are possible are impurity conduction and ionic conduction. The requirements for both types of conduction have been discussed in Section (2.2).

In the case of silicon oxide, which has been shown to be amorphous, the impurity centres would be localised states. The electrons producing the current would take the easiest path through the dielectric, hopping from site to site where the overlap was sufficient. The

conduction would ultimately be limited by the most difficult hop. Mead[48] suggested that low field conduction in Ta_2O_5 dioxides was electron hopping but only at high temperatures.

Lidiard[81] suggested that the activation energy of an ionic process was in the range 0.5 eV < q < 1.5 eV. In the present experiments the value of the activation energy was 0.7 eV $\pm$ 0.15, which means that ionic conduction may have occurred.

The discussion is Section (2.3.5) suggests that the absorption current is due to ions building up at an electrode. It might be expected, therefore, that subsequent current flow is space charge limited. Hill[132] has shown that, for certain conditions, ohmic currents can still flow after a space charge region has accumulated. Unless there are two types of ion involved it is difficult to understand how the same ions can firstly, pile up at an electrode and then contribute to a conduction process. Glass technologists[59, 73] (see Section (2.5)) suggested that the initial absorption current was due to short range ion migration involving "easy jumps" along "dead-end paths". The steady state current was due to the same ions but was the net result of the flow ions over a whole range of barrier heights. If the potential was applied for sufficiently long

periods (probably of the order of several days) then the ions would either form a space charge layer at the cathode or plate out, depending whether the contact was blocking or ohmic respectively. However, since it is not certain which process is causing D.C. conduction in silicon oxide films, it is not thought necessary to discuss the above points further.

The frequency variation results (see Section (7.2.2)) showed that films were produced with a spread in loss tangent values. This was probably due to the presence of weak paths referred to as flaws or pin-holes. A spread was observed in D.C. conductivity values and therefore it was very likely that D.C. conduction was controlled by weak paths. Conduction in films involving weak paths is not understood but the resulting current-voltage characteristics may be expected to be ohmic. Since there is no evidence for the presence of weak paths, and it is probable that they will dominate the low field conduction process, when present, no firm conclusion regarding the presence or absence of the other two ohmic conduction mechanisms can be drawn.

8.1.4 High Field Region

Unlike low field conduction, the high field case is related to the intrinsic properties of the

material and not to conduction controlled by weak paths. Although several authors (see Figure (22)) have shown the $\exp(\frac{\beta V^{\frac{1}{2}}}{kT})$ relationship to exist experimentally, the actual mechanism involved is still uncertain. Despite the experimental errors involved with the measurements, the results compare favourably with those of previous workers.

The method of discounting a straightforward Poole-Frenkel mechamism is to determine the permittivity from the slope of the β vs $\frac{1}{T}$ graph, Figure (62) using the theory of Section (2.2.2). This results in a permittivity of $\varepsilon' \simeq 11$. The high frequency permittivity of the silicon oxide was $\varepsilon' \simeq 5.5$, which suggests that straightforward Poole-Frenkel conduction is not the operative mechanism.

The permittivity, assuming a Schottky Emission mechanism is $\varepsilon' \simeq 2.7$ which is nearer the high frequency value.

The only other information available for distinguishing the conduction process is the value of the activation energy. Assuming a Poole-Frenkel mechanism, the activation energy is $E \simeq .55$ eV, which appears reasonable as a trap depth below the conduction band. The Schottky Emission plot, Figure (61), results in an activation energy of $E \simeq .43$ eV. Hartman et al[105]

showed, by performing photo-response measurements, that this would not be the energy required to excite an electron over the metal-insulator interface barrier. They found that the average threshold energy was 1.77 eV and also that the experimentally determined value of the Richardson constant did not compare with the theoretical value.

The above discussion shows that the conduction mechanism is neither a straightforward Poole-Frenkel or Schottky Emission process. Johansen[44] suggested that the rate limiting process was Schottky Emission from small silicon islands with a silicon matrix. However, there is not sufficient evidence for this type of structure although it has been supported by Coleman and Thomas[19].

It was shown in Section (3.2) that the model of O'Dwyer[57] proposed by Hartman et al[105] was unlikely when considering activation energies of the order 0.5 - 0.6 eV.

The model proposed by Simmons[58] would give reasonable agreement with the experimental results if it could be assumed that the position of the fermi level was within less than 1 eV of the insulator conduction band. However, there is no experimental evidence for this and therefore such an explanation is rather uncertain.

The modifications of the Poole-Frenkel effect as suggested by Jonscher[25], would again give a model which would agree reasonably well and explains the unusually high permittivity resulting from an assumption of this model. The various plots suggested by Jonscher were not performed as the experimental errors were too large to state which would give the best fit. Also the activation energies resulting from such plots would be very little altered and would still be in the region 0.5 - 0.6 eV.

The interpretation of activation energies would be uncertain if the electron emission was into a quasi-continuum of localised levels rather than a well defined conduction band as discussed by Jonscher[25].

It is concluded, therefore, that it is not possible to give a precise interpretation of the experimental results as there is not sufficient information on the energy band structure. However, since the material probably contains localised levels distributed throughout a poorly defined "forbidden band" then it is likely that the conduction is explained by a modified form of the Poole-Frenkel effect.

8.1.5 Breakdown

Because the impedance to earth was low, all

the breakdowns were of the propogating variety. Figures (55-58) illustrated some of the aspects of breakdown. Figure (55) showed almost complete destruction of the upper Al. electrode after several breakdowns. Figures (57) and (58) showed the random propogation of the breakdown. The energy of propogation was derived from the voltage source and they were triggered by a single hole breakdown. The various modes of breakdown have been discussed by Klein and Gafni[45]. Figure (56) showed the effect of a cluster of breakdowns. This picture was very similar to that of Budenstein and Hayes[133]. At the centre of the radial streaks, the Al. electrode has been completely removed. The radial streaks consisted of coalesced Al. on the bare dielectric. According to Budenstein and Hayes, the outer edge of the streaky region was decorated with small balls of silicon.

Capacitors with large areas of breakdown were not usually short-circuited and capacitance measurements indicated a large reduction in surface area.

Breakdown analysis demonstrated that even capacitors, annealed in an ~~area~~ oven at 400°C for an hour, still contained large numbers of pin-holes. These would probably affect the conduction properties of a capacitor. The cause of the pin-holes is still not known although

several authors have studied their effects[45, 133].

8.2 Discussion on A.C. Conduction

8.2.1 Introduction

Both low and high loss films show the same characteristics and therefore will be discussed together. It is thought that the difference is caused by the effect of flaws or pin-holes in the dielectric giving rise to an additional loss.

The following discussion refers to fully annealed films. The frequency behaviour of unannealed films has been discussed in Section (6.7).

8.2.2 Absorption Current

Using Haman's equation[111], it was shown that there exists a very low frequency loss peak in the region 5.10^{-3} c/s. In order for the equation to be applicable the ionic species responsible for the current decay will also be responsible for the dispersion behaviour.

It should be pointed out, however, that Lindmayer[134] suggested that the current transients in films of silicon oxide were the result of the injected charge being trapped. These traps were distributed throughout the forbidden energy band and the relaxation time associated with the

current decay was a function of the time taken in filling the traps. He pointed out that the resulting current was not necessarily space-charge-limited. For Au-SiO-Au sandwiches the current was of the two carrier type, resulting in a cubic current voltage characteristic which was not observed in the present work.

An argument against such a model is that it is difficult to explain the A.C. low frequency loss peaks considering an electronic charge carrier. Reimerov[135] observed relaxation peaks occurring in doped TiO_2 which he attributed to electrons oscillating between localised centres surrounding defects. However, at $0^{o}C$ the frequency of the dispersion occurred at about 1 Kc/s.

If we assume that the high temperature, audio frequency behaviour is dominated by the tail of the low frequency dispersion, then the mean activation energy of the process is approximately 1.0 ± 0.1 eV. However, an inconsistency now appears in the results obtained up to this point. If a loss peak exists at 5.10^{-3} c/s at room temperature, then assuming that the loss peak is shifted by temperature according to the Arrhenius plot, at the highest temperatures used the peak should have appeared. This indicates that either the loss peak is at lower frequencies than suggested using Hamon's[76] equation, or the Arrhenius relationship

is not obeyed. Because of the errors involved in applying Hamon's equation it is thought that this is the more likely source of the inconsistency.

This was proved to be so by Argall[68]. Using Hamon's equation he predicted a loss peak at about 10^{-2} c/s but more elaborate techniques showed the room temperature type A peak to be at about 5.10^{-3} c/s.

The value of the activation energy suggests that the charge carrier involved in the low frequency dispersion is ionic. However, only certain ions will be sufficiently mobile in the silicon-oxygen network to produce the polarization. These will be H^+, He^+, Li^+, Na^+, K^+ and possible Cs. It is thought that the high temperature involved in the annealing process would be sufficient to completely remove the lighter elements H^+ and He^+ from the system. A possible source of the alkali impurity was the tungsten wire used for the aluminium electrode evaporation.

8.2.3 Discussion on Interfacial Polarization

The mechanism of interfacial polarization represents a movement of the charge carrier over distances in the region of the electrode spacing. In order to judge whether such distances of ionic migration are conceivable, let us consider the case of sodium diffusion

in vitreous silica. In this case the ions are moving under a concentration gradient rather than an electric field. The average distance an ion will move is given by: $\bar{x} = \sqrt{Dt}$ where D , the diffusion constant, is 10^{-11} cm^2/sec at room temperature. At a frequency of 10^{-2} c/s the half cycle time is 50 secs. This gives $\bar{x} \simeq 2200\text{Å}$ which is approximately the electrode spacing. This simple calculation shows that an ionic movement over distances of the electrode spacing is possible. During one half cycle of the A.C. measuring field, the charged carriers are moved to the negative electrode. If the contacts are blocking, then the carriers are not discharged at the electrode but form a space charge. If the frequency is low enough, practically all the applied A.C. voltage is dropped across the space charge region. This is equivalent to a capacitor of thickness equal to that of the space charge zone. This is observed as a dispersion in the capacitance and a maximum of the loss tangent for maximum energy absorption.

Argall suggested that his type B relaxation peak was due to interfacial polarization. There is not sufficient evidence in the present work, however, due to the limited temperature and frequency ranges, to differentiate between different mechanisms. At fre-

quencies greater than the absorption frequency the charge carrier does not have sufficient time to form a complete space charge region at the electrode. The lag in movement of the ion results in an out-of-phase component which is observed as an increased loss. There will be only a small dispersion in capacitance. At frequencies well removed from the absorption frequency the charged carrier will not have sufficient time to contribute to either the capacitance or loss tangent.

Clearly, the process will be activated, the energy representing the potential barrier at interatomic distances over which the carrier must be excited. Because of the contribution to loss and capacitance for frequencies removed from the relaxation frequency, the process will possess a broad tan δ peak, i.e. it is represented by a distribution of relaxation times as described in Section (2.3.3). Argall[68] suggested that the distribution arose because the charge carriers, which accumulated at the electrodes, originated from all over the dielectric.

The importance of the effect of the low frequency peak on the audio frequency properties results from the distribution of relaxation times involved.

8.2.4 Audio Frequency Behaviour

8.2.4.1 Capacitance and ε'_c

At room temperature the capacitance is practically independent of frequency down to the lowest frequency of measurement at 300 c/s. At high temperatures (> 80°C) and particularly at low frequencies there is a dispersion in the capacitance. This is a consequence of the low frequency peak. An increase in temperature shifts the peak to higher frequencies so that the tail comes into view at the low frequencies.

The resulting ε'_c will be much higher than expected from the theory of Section (2.4) which does not take into account particular loss mechanisms. However, Section (8.2.6) will show that even for low values of the distribution factor β, the relationship

$$\varepsilon'_c = A' \tan \delta$$

may still be used to represent the contribution to ε'_c from the relaxation mechanism. Qualitative analysis is made difficult by the fact that the loss term is that part of the loss resulting from the relaxation mechanism and the temperature and frequency variation of the separate terms is not known. Further discussion on ε'_c will follow in Section (8.2.6).

8.2.4.2 A.C. Conductivity and Loss

The conductance and loss tangent curves, as functions of frequency at different temperatures, follow the relationship

$$\sigma \propto \omega^{\alpha}$$

over all the audio frequency range.

The tail apporximation of the Cole-Cole equation for conductivity gives

$$\sigma = \frac{(\varepsilon_s - \varepsilon_\infty)}{\tau_o^{1-\beta}} \omega^{\beta} \cos\left(\frac{\beta\pi}{2}\right)$$

This would appear to indicate that the whole of the audio frequency range is being dominated by the tail of the dispersion. However, the temperature behaviour of the function α demonstrates that this is not the case. Gough[75] working on borate glasses and Owen[68] working on calcium alumino borates found 'β' to be slightly temperature dependent, but Taylor[66] and Owen and Douglas[98] working on silicates, found 'β' to be indpendent of temperature.

The situation is made clearer by observing the plot of conductance versus reciprocal temperature (Figure (72)). The audio frequency region appears to represent a transition between two conduction processes. For temperatures

below 80°C at all frequencies, a process having a very low activation energy of less than 0.1 eV appears to be the case. This region extends into the radio frequency range and is discussed later. At temperatures above 80°C the conduction becomes dominated by the low frequency dispersion. The slope of the high temperature region was about 0.8 $\pm$ 0.1 eV, but it was shown that the mean activation energy was 1 eV $\pm$ 0.1 eV.

The value of β for this process was uncertain as the graph of 'α' versus temperature did not appear to have reached a limiting value (see Figure (71). It is also not known whether β is temperature dependent. However, a rough approximation of the high temperature limit was $\beta = 0.3 \pm 0.1$.

It should be pointed out that a slope of unity of the loss tangent versus frequency would indicate D.C. conduction at low frequencies. However, the dispersion process would dominate the D.C. conduction at the frequencies considered.

Another important result indicating a relaxation phenomenon is that even at room temperature the dispersion in loss was over half an order of magnitude whereas the equivalent capacitance dispersion was about 1°/o.

8.2.5 Radio Frequency Behaviour

Above 30 Kc/s it was found that both capacitance and loss were indpendent of frequency up to the maximum temperature of measurement 200°C. The maximum frequency of measurement was 1 Mc/s. This discussion will include that part of the audio frequency region not affected by the low frequency dispersion, although there is no clear distinction between the two regions.

Above 1 Mc/s the loss was observed to increase with frequency, but the bridge circuit was being used at its upper limit and it was not possible to distinguish between an anomalous or real effect. Also the correction factor for the series lead resistance became comparable with the resistance of the film, producing an error of greater than 100°/o.

Models giving loss near invariant with frequency have already been discussed in Section (2.3.6). It is thought that because of the amorphous nature of the dielectric under consideration that the process of A.C. conduction is a form of hopping mechanism. Another important consideration in proposing such a mechanism is the low activation energies involved, probably < 0.1 eV. The experimental errors involved do not allow an estimation of whether the activation energy will be

constant with temperature. As suggested by Jonsher[25](56) this is rather an indeterminate quantity and its interpretation is very vague.

8.2.6 Discussion on χ'_c

A general equation for χ'_c, applicable to the majority of thin films was given in Section (2.4). The experimental results, however, demonstrate the necessity of defining both temperature and frequency when quoting values for χ'_c.

Silicon oxide shows an additonal contribution to χ'_c, not given in the general formula, which is due to low frequency loss mechanisms. The distribution of relaxation times involved means that an approximation, similar to that of Geres[77], can be used for the loss contribution to χ'_c.

The general equation for the dispersion contribution to χ'_p, from the Cole-Cole[62] relationship (see Section (2.4.1)), is:

$$\chi'_p = f(\beta)\,\frac{2q}{kT^2}\,\mathrm{Tan}\,\delta$$

i.e. $$A = f(\beta)\,\frac{2q}{kT^2} \quad \text{for} \quad \beta \dashrightarrow 1.$$

For frequencies well removed from the dispersion frequency $f(\beta)$ is given by:

$$f(\beta) = \frac{(1 - \beta)}{2} \text{ Tan } \frac{\beta\pi}{2}$$

which is independent of frequency.

The value of 'β' suggested by Figure (71) for the dispersion was $\beta = 0.3$. This results in a value of $A' = .03$. It is not possible to compare this with experimentally obtained values as the magnitudes of the various contributions to γ_c are not certain. At first sight it appears that the contribution to γ_c is reduced (for $\beta = 1$, $A = .05$). However, it is the large value of Tan δ which results in an increased γ_c.

Figure (67) showed that when the loss of a film was large (> 1°/o), then γ_c would be considered as resulting from the loss contribution only, other contributions being negligible ($\gamma_c = .05$ Tan δ).

For losses less than 1°/o, however, Figure (66) showed that it was necessary to take into account the other contributions. If we take an average value of $\gamma_c = 70$ p.p.m./°C extrapolated to zero loss, then it is possible to make a crude estimation of the remaining contributions. An appropriate value of the linear thermal expansion coefficient, considering the values of vitreous quartz and various glasses, is about 10 p.p.m./°C. Assuming an average permittivity of $\varepsilon' = 5.5$, this gives a negative contribution to γ_c of about

50 p.p.m./°C. This allows a determination of the intrinsic contribution to γ_c:

$$\frac{(\varepsilon' - 1)(\varepsilon' + 2)}{\varepsilon'} \frac{1}{3\alpha_m} \left(\frac{\partial \alpha_m}{\partial T}\right) \simeq 120 \text{ p.p.m./°C}$$

or

$$\frac{1}{3\alpha_m} \left(\frac{\partial \alpha_m}{\partial T}\right)_p \simeq 20 \text{ p.p.m./°C}$$

The intrinsic contributions making up the total polarizability or permittivity were discussed in Section (2.3.2.1).

The refractive index of silicon monoxide is 1.9 giving the electronic contribution to the permittivity of 3.6 which will be indpendent of temperature.

A rough approximation to the ionic contribution to the permittivity is given by the Born equation (see Section (2.3.2)):

$$\varepsilon_i = \frac{2\pi e^2}{\omega_o^2 a^3} \left(\frac{1}{m} + \frac{1}{M}\right)$$

Infrared spectroscopy (see Section (5.3)) showed the characteristic absorption to occur at a wavelength of 10μ. The mean separation 'a' is interpreted as the silicon-oxygen separation as determined by the

radial distribution analysis (see Section (5.2)). The resulting ionic contribution is $\varepsilon_i \simeq 0.6$.

The remaining contribution of 1.3 (total permittivity taken as 5.5) is probably due to the deformation effect as discussed in Section (2.3.2.3). Harrop[205] has shown this contribution to be indpendent of temperature. We conclude that the increase of the intrinsic permittivity with temperature is a result of the ionic permittivity.

An illustration of the effect of the ionic contribution to the permittivity is the case of LiF. This material has a 'γ_c' of 700 p.p.m./°C and has 90°/o ionic bonding. It is not unreasonable, therefore, to expect an intrinsic contribution of about 125 p.p.m./°C for a silicon-oxygen type material which has approximately 10°/o ionic bonding. It is not possible to make more accurate comparisons as the weighting functions of the various contributions are not known.

CHAPTER 9

SUMMARY AND CONCLUSIONS

1. The important deposition parameter is the ratio $(\frac{P}{R})$. High values promote oxidation resulting in a compressive stress and reduced loss.

2. The effect of annealing is complex but the most important effects are gas desorption (probably hydrogen vapour) and stress relief, probably associated with the reduction of pin-hole density. Empirical relationships have been derived for the long-term changes of capacitance and A.C. resistance during annealing.

3. From D.C. and A.C. measurements, four different activation energies resulted:

(i)	1.00 ± 0.1	eV
(ii)	0.70 ± 0.15	eV
(iii)	0.55 ± 0.05	eV
(iv)	<0.1	eV

(i) The activation energy of 1 eV was determined from audio frequency measurements and was the result of a low frequency dispersion process having a distribution of relaxation times ($\beta \simeq 0.3$). This was

probably due to interfacial polarization.

(ii) The value of 0.70 eV refers to the D.C. low field ohmic region. Two mechanisms resulting in an ohmic characteristic were discussed but it was thought more likely that the conduction was controlled by weak paths.

(iii) The high field region was associated with an activation energy of about 0.55 eV. The operating conduction mechanism was probably a modified form of the Poole-Frenkel effect. The activation energy would be associated with the trap depth of electrons which were excited into a poorly defined conduction band.

(iv) The activation energy for A.C. conductivity in the region where loss was near-invariant with frequency ($\beta \dashrightarrow 1$) was less than 0.1 eV. The interpretation of the activation energy was vague and probably represented a mean value. The A.C. conduction process was probably electrons hopping between localised sites. These sites were a direct result of the amorphous nature of the dielectric rather than due to a form of doping.

4. ε'_c of silicon oxide was dominated at high temperatures in the audio frequency range by the low

frequency dispersion. It was shown that for capacitors with loss $> 1^{o}/o$, δ_c was dominated by the loss contribution. At room temperature, above 10 Kc/s, γ_c had a limiting value of 70 ± 20 p.p.m./^{o}C due to intrinsic contributions. These were due to lattice expansion and the variation of ionic polarizability with temperature.

APPENDIX I

The following three pages show the computer program, written in Fortran IV, which was used to calculate the various parameters as given in Section (4.17).

```
£IBFTC DECKNM

DECKNM      -  EFN    SOURCE STATEMENT  -  IFN(S)  -

      DIMENSION G(8,5),R(8,5),C(8,5),Q(8,5),A(8,5),S(8,5),B(8,5),
     1P(8,5),D(8,5),T(8),E(5),W(1),CA(8),BA(8),SA(8),DA(8),V(8),
     2CSLOPE(7,5),BSLOPE(7,5),SSLOPE(7,5),DSLOPE(7,5),
     3CASLOP(7),BASLOP(7),SASLOP(7),DASLOP(7),
     4T1(7),T2(7),ATCC(7),ATCB(7),ATCS(7),ATCD(7),
     5ALPHAC(7,5),ALPHAB(7,5),ALPHAS(7,5),ALPHAD(7,5),
     6ALFACA(7),ALFABA(7),ALFASA(7),ALFADA(7),
     7CERROR(7),BERROR(7),SERROR(7),DERROR(7),
     8CV(7,5),BV(7,5),SV(7,5),DV(7,5),CAV(7),BAV(7),SAV(7),DAV(7)
      DO17I=1,10
      READ(5,20)(E(J),J=1,4)
   20 FORMAT(4I5)
      IF(E(1))5,17,5
    5 READ(5,18)W
   15 READ(5,1)G
      READ(5,2)C
      READ(5,4)T
   18 FORMAT(E11.5)
    1 FORMAT(8F6.4)
    2 FORMAT(8F4.1)
    4 FORMAT(8F4.1)
      WRITE(6,16)
   16 FORMAT(60H1N  TEMPERATURE CAPACITY RESISTANCE TAN DELTA SIN DELTA
     1          )
      DO10N=1,5
      WRITE(6,11)
   11 FORMAT(3HO    )
      DO10K=1,8
      V(K)=1.894*T(K)/100.+1.91*T(K)**2./100000.
      P(K,1)=138.0+9.30*V(K)
      P(K,2)=174.0+7.94*V(K)
      P(K,3)=116.0+7.34*V(K)
      P(K,4)=065.0+7.62*V(K)
      P(K,5)=214.0+8.53*V(K)
      R(K,N)=1./G(K,N)
      Q(K,N)=R(K,N)*C(K,N)*W/1000000.
      A(K,N)=P(K,N)*(1.+Q(K,N)**2.)/(R(K,N)*1000000.)
      B(K,N)=R(K,N)/(1.-A(K,N))
      S(K,N)=(1.-A(K,N))/Q(K,N)
      D(K,N)=S(K,N)/((1.+S(K,N)**2.)**.5)
   10 WRITE(6,12) N,T(K),C(K,N),B(K,N),S(K,N),D(K,N)
   12 FORMAT(I2,2X,F5.1,7X,F7.3,2X,F7.3,4X,F7.4,3X,F7.4,)
      WRITE(6,25)
   25 FORMAT(36HOAVERAGE VALUES OF THE FIVE DEVICES    )
      DO21K=1,8
      SUMC=0.
      SUMB=0.
      SUMS=0.
```

```
      SUMD=0.
      DO22N=1,5
      SUMC=SUMC+C(K,N)
      SUMB=SUMB+B(K,N)
      SUMS=SUMS+S(K,N)
      SUMD=SUMD+D(K,N)
      IF(N-5)22,23,23
   22 CONTINUE
   23 CA(K)=SUMC/5.
      BA(K)=SUMB/5.
      SA(K)=SUMS/5.
      DA(K)=SUMD/5.
   21 WRITE(6,24)T(K),CA(K),BA(K),SA(K),DA(K)
   24 FORMAT(4X,F5.1,7X,F7.3,2X,F7.3,4X,F7.4,3X,F7.4,)
      WRITE(6,19)W
   19 FORMAT(11HOFREQUENCY=E11.5)
   13 WRITE(6,14)(E(J),J=1,4)
   14 FORMAT(8HORUN NO.,I2,6H DATE ,2X,I2,1H/,I2,1H/,I2)
      WRITE(6,32)
   32 FORMAT(12X,29H TEMPERATURE COEFFICIENTS OF ,30X,37H AVERAGE TEMPER
     1ATURE COEFFICIENTS OF )
      WRITE(6,33)
   33 FORMAT(56HON  TEMPERATURE CAPACITY RESISTANCE TAN DELTA SIN DELTA
     1,7X,56H    TEMPERATURE CAPACITY RESISTANCE TAN DELTA SIN DELTA )
      WRITE(6,35)
   35 FORMAT(16X,40H P.P.TH.  PER CENT   PER CENT  PER CENT ,22X,40H P.P
     1.TH.  PER CENT   PER CENT  PER CENT )
      DO28N=1,5
      WRITE(6,31)
   31 FORMAT(3H0    )
      DO28K=1,7
      T2(K)=(T(K+1)+T(K))/2.
      CV(K,N)=(C(K+1,N)+C(K,N))/2.
      BV(K,N)=(B(K+1,N)+B(K,N))/2.
      SV(K,N)=(S(K+1,N)+S(K,N))/2.
      DV(K,N)=(D(K+1,N)+D(K,N))/2.
      CAV(K)=(CA(K+1)+CA(K))/2.
      BAV(K)=(BA(K+1)+BA(K))/2.
      SAV(K)=(SA(K+1)+SA(K))/2.
      DAV(K)=(DA(K+1)+DA(K))/2.
      T1(K)=T(K+1)-T(K)
      IF(T1(K))38,39,38
   39 T1(K)=1.
   38 CONTINUE
      CSLOPE(K,N)=(C(K+1,N)-C(K,N))/T1(K)
      BSLOPE(K,N)=(B(K+1,N)-B(K,N))/T1(K)
      SSLOPE(K,N)=(S(K+1,N)-S(K,N))/T1(K)
      DSLOPE(K,N)=(D(K+1,N)-D(K,N))/T1(K)
      CASLOP(K)=(CA(K+1)-CA(K))/T1(K)
      BASLOP(K)=(BA(K+1)-BA(K))/T1(K)
      SASLOP(K)=(SA(K+1)-SA(K))/T1(K)
      DASLOP(K)=(DA(K+1)-DA(K))/T1(K)
      ALPHAC(K,N)=CSLOPE(K,N)*1000./CV(K,N)
      ALPHAB(K,N)=BSLOPE(K,N)*100./BV(K,N)
      ALPHAS(K,N)=SSLOPE(K,N)*100./SV(K,N)
      ALPHAD(K,N)=DSLOPE(K,N)*100./DV(K,N)
```

```
      ALFACA(K)=CASLOP(K)*1000./CAV(K)
      ALFABA(K)=BASLOP(K)*100./BAV(K)
      ALFASA(K)=SASLOP(K)*100./SAV(K)
      ALFADA(K)=DASLOP(K)*100./DAV(K)
      WRITE(6,34)N,T2(K),ALPHAC(K,N),ALPHAB(K,N),ALPHAS(K,N),ALPHAD(K,N)
     1,T2(K),ALFACA(K),ALFABA(K),ALFASA(K),ALFADA(K)
   34 FORMAT(I2,2X,F5.1,7X,F7.4,2X,F7.4,4X,F7.4,3X,F7.4,14X,F5.1,7X,F7.4
     1,2X,F7.4,4X,F7.4,3X,F7.4)
   28 CONTINUE
      WRITE(6,36)
   36 FORMAT(53HOAVERAGE VALUES OF TEMP.COEFFNTS.OF THE FIVE DEVICES ,15
     1X,48H ERRORS IN TEMP.COEFFNTS.OF THE FIVE DEVICES PC )
      DO27K=1,7
      SUMAC=0
      SUMAB=0
      SUMAS=0
      SUMAD=0
      DO26N=1,5
      SUMAC=SUMAC+ALPHAC(K,N)
      SUMAB=SUMAB+ALPHAB(K,N)
      SUMAS=SUMAS+ALPHAS(K,N)
      SUMAD=SUMAD+ALPHAD(K,N)
      IF(N-5)26,29,29
   26 CONTINUE
   29 ATCC(K)=SUMAC/5.
      ATCB(K)=SUMAB/5.
      ATCS(K)=SUMAS/5.
      ATCD(K)=SUMAD/5.
      IF(ATCC(K))40,41,40
   40 IF(ATCB(K))45,42,45
   45 IF(ATCS(K))46,43,46
   46 IF(ATCD(K))47,44,47
   41 ATCC(K)=1.
      GOTO40
   42 ATCB(K)=1.
      GOTO45
   43 ATCS(K)=1.
      GOTO46
   44 ATCD(K)=1.
   47 CONTINUE
      CERROR(K)=(ATCC(K)-ALFACA(K))*100./ATCC(K)
      BERROR(K)=(ATCB(K)-ALFABA(K))*100./ATCB(K)
      SERROR(K)=(ATCS(K)-ALFASA(K))*100./ATCS(K)
      DERROR(K)=(ATCD(K)-ALFADA(K))*100./ATCD(K)
   27 WRITE(6,37)T2(K),ATCC(K),ATCB(K),ATCS(K),ATCD(K),T2(K),CERROR(K),B
     1ERROR(K),SERROR(K),DERROR(K)
   37 FORMAT(4X,F5.1,7X,F7.4,2X,F7.4,4X,F7.4,3X,F7.4,14X,F5.1,6X,F8.4,1X
     1,F8.4,3X,F8.4,2X,F8.4)
   17 CONTINUE
      STOP
      END
```

APPENDIX II

The following three pages are an example of the computed results.

N	TEMPERATURE	CAPACITY	RESISTANCE	TAN DELTA	SIN DELTA
1	28.0	192.000	31.774	0.0164	0.0164
1	40.0	192.900	28.936	0.0179	0.0179
1	76.5	196.700	20.829	0.0244	0.0244
1	120.0	205.100	6.341	0.0769	0.0767
1	156.0	226.000	0.731	0.6051	0.5177
1	183.0	257.200	0.131	2.9648	0.9476
1	26.0	192.200	31.774	0.0164	0.0164
1	28.0	192.000	31.774	0.0164	0.0164
2	28.0	203.900	25.472	0.0193	0.0193
2	40.0	205.100	23.900	0.0204	0.0204
2	76.5	209.500	17.831	0.0268	0.0268
2	120.0	220.000	4.786	0.0950	0.0946
2	156.0	246.700	0.516	0.7862	0.6181
2	183.0	286.700	0.111	3.1432	0.9529
2	26.0	204.100	23.664	0.0207	0.0207
2	28.0	203.900	25.472	0.0193	0.0193
3	28.0	213.500	20.897	0.0224	0.0224
3	40.0	214.800	19.905	0.0234	0.0234
3	76.5	219.400	15.270	0.0298	0.0298
3	120.0	230.700	4.213	0.1029	0.1024
3	156.0	259.500	0.443	0.8702	0.6564
3	183.0	304.000	0.094	3.4810	0.9611
3	26.0	214.400	20.060	0.0233	0.0232
3	28.0	213.500	20.897	0.0224	0.0224
4	28.0	211.900	26.117	0.0181	0.0181
4	40.0	213.000	23.994	0.0196	0.0196
4	76.5	219.000	16.412	0.0278	0.0278
4	120.0	233.500	3.270	0.1310	0.1299
4	156.0	267.200	0.290	1.2894	0.7902
4	183.0	313.000	0.061	5.2279	0.9822
4	26.0	212.200	24.219	0.0195	0.0195
4	28.0	211.900	26.117	0.0181	0.0181
5	28.0	205.300	25.721	0.0189	0.0189
5	40.0	206.500	24.005	0.0202	0.0202
5	76.5	211.200	17.487	0.0271	0.0271
5	120.0	222.800	4.405	0.1019	0.1014
5	156.0	249.800	0.444	0.9013	0.6695
5	183.0	290.200	0.092	3.7499	0.9662
5	26.0	205.700	24.464	0.0199	0.0199
5	28.0	211.900	25.761	0.0183	0.0183
AVERAGE VALUES OF THE FIVE DEVICES					
	28.0	205.320	25.996	0.0190	0.0190
	40.0	206.460	24.148	0.0203	0.0203
	76.5	211.160	17.566	0.0272	0.0272
	120.0	222.420	4.603	0.1015	0.1010
	156.0	249.840	0.485	0.8905	0.6504
	183.0	290.220	0.098	3.7134	0.9620
	26.0	205.720	24.836	0.0199	0.0199
	28.0	206.640	26.034	0.0189	0.0189

FREQUENCY=0.10000E 05

N	TEMPERATURE	CAPACITY P.P.TH.	RESISTANCE PER CENT	TAN DELTA PER CENT	SIN DELTA PER CENT
1	34.0	0.3906	-0.7443	0.7746	0.7743
1	58.2	0.5422	-0.6990	1.0851	1.0845
1	98.2	1.0057	-1.0483	7.3613	7.3316
1	138.0	3.0237	-0.4904	89.5162	74.7513
1	169.5	6.0185	-0.0699	33.1671	97.1316
1	104.5	2.1563	-0.6343	14.5689	36.1879
1	27.0	-0.5208	0.0004	0.0516	0.0516
2	34.0	0.4904	-0.5145	0.4963	0.4961
2	58.2	0.5912	-0.6527	0.9062	0.9056
2	98.2	1.1838	-1.1773	8.1440	8.0958
2	138.0	3.6374	-0.4657	99.7279	75.5431
2	169.5	7.2657	-0.0588	53.3885	64.4275
2	104.5	2.5803	-0.5890	03.2959	30.8455
2	27.0	-0.4904	3.5494	-3.7679	-3.7663
3	34.0	0.5074	-0.3956	0.3624	0.3622
3	58.2	0.5903	-0.6076	0.7896	0.7889
3	98.2	1.2167	-1.2164	7.4920	7.4398
3	138.0	3.7471	-0.5011	95.0931	68.6878
3	169.5	7.7197	-0.0617	31.4228	50.3597
3	104.5	2.6731	-0.6085	98.2618	26.6593
3	27.0	-2.1077	2.0027	-1.8677	-1.8667
4	34.0	0.4326	-0.6775	0.6906	0.6903
4	58.2	0.7758	-0.7953	1.2517	1.2508
4	98.2	1.5731	-1.1568	13.1236	12.9860
4	138.0	4.4177	-0.3169	78.0803	01.5277
4	169.5	8.0052	-0.0325	07.2635	39.3586
4	104.5	3.0299	-0.5892	83.5935	33.9416
4	27.0	-0.7079	3.6334	-3.8419	-3.8405
5	34.0	0.4871	-0.5562	0.5441	0.5438
5	58.2	0.6272	-0.6942	0.9987	0.9980
5	98.2	1.2989	-1.1692	9.0822	9.0213
5	138.0	3.6532	-0.4277	17.2658	83.3527
5	169.5	7.2883	-0.0507	57.1183	58.0422
5	104.5	2.6216	-0.6035	25.4579	31.8562
5	27.0	15.0999	2.5213	-4.0995	-4.0980
AVERAGE VALUES OF TEMP.COEFFNTS.OF THE FIVE DEVICES					
	34.0	0.4616	-0.5776	0.5736	0.5734
	58.2	0.6253	-0.6898	1.0062	1.0056
	98.2	1.2557	-1.1536	9.0406	8.9749
	138.0	3.6958	-0.4404	15.9366	80.7725
	169.5	7.2595	-0.0547	56.4720	61.8639
	104.5	2.6122	-0.6049	25.0356	31.8941
	27.0	2.2546	2.3415	-2.7051	-2.7040

AVERAGE TEMPERATURE COEFFICIENTS OF

TEMPERATURE	CAPACITY P.P.TH.	RESISTANCE PER CENT	TAN DELTA PER CENT	SIN DELTA PER CENT
34.0	0.4627	-0.5925	0.5592	0.5590
58.2	0.6272	-0.6937	0.9936	0.9930
98.2	1.2607	-1.1463	8.9887	8.9233
138.0	3.7097	-0.4400	15.2607	80.2852
169.5	7.2840	-0.0551	49.8912	60.7133
104.5	2.6214	-0.6061	23.7300	31.5657
27.0	2.2404	2.2466	-2.7414	-2.7403

34.0	0.4627	-0.5925	0.5592	0.5590
58.2	0.6272	-0.6937	0.9936	0.9930
98.2	1.2607	-1.1463	8.9887	8.9233
138.0	3.7097	-0.4400	15.2607	80.2852
169.5	7.2840	-0.0551	49.8912	60.7133
104.5	2.6214	-0.6061	23.7300	31.5657
27.0	2.2404	2.2466	-2.7414	-2.7403

34.0	0.4627	-0.5925	0.5592	0.5590
58.2	0.6272	-0.6937	0.9936	0.9930
98.2	1.2607	-1.1463	8.9887	8.9233
138.0	3.7097	-0.4400	15.2607	80.2852
169.5	7.2840	-0.0551	49.8912	60.7133
104.5	2.6214	-0.6061	23.7300	31.5657
27.0	2.2404	2.2466	-2.7414	-2.7403

34.0	0.4627	-0.5925	0.5592	0.5590
58.2	0.6272	-0.6937	0.9936	0.9930
98.2	1.2607	-1.1463	8.9887	8.9233
138.0	3.7097	-0.4400	15.2607	80.2852
169.5	7.2840	-0.0551	49.8912	60.7133
104.5	2.6214	-0.6061	23.7300	31.5657
27.0	2.2404	2.2466	-2.7414	-2.7403

34.0	0.4627	-0.5925	0.5592	0.5590
58.2	0.6272	-0.6937	0.9936	0.9930
98.2	1.2607	-1.1463	8.9887	8.9233
138.0	3.7097	-0.4400	15.2607	80.2852
169.5	7.2840	-0.0551	49.8912	60.7133
104.5	2.6214	-0.6061	23.7300	31.5657
27.0	2.2404	2.2466	-2.7414	-2.7403

ERRORS IN TEMP.COEFFNTS.OF THE FIVE DEVICES PC

34.0	-0.2298	-2.5865	2.5156	2.5152
58.2	-0.2895	-0.5611	1.2527	1.2530
98.2	-0.4034	0.6304	0.5742	0.5754
138.0	-0.3744	0.0793	0.5830	0.6033
169.5	-0.3380	-0.6809	1.1826	1.8599
104.5	-0.3492	-0.2011	1.0442	1.0298
27.0	0.6295	4.0496	-1.3437	-1.3432

REFERENCES

[1] 'Microminiaturization', Proc. of the A.G.A.R.D. Conf. ed. G.W.A. Dummer, p. 282, 1961

[2] HOLLAND, L.: 'Vacuum Deposition of Thin Films' Chapman and Hall

[3] HOLLAND, L.: 'Thin Film Microelectronics' Chapman and Hall, 1965

[4] HOLMES, B.E.: Microelec. 1, 46, 1967

[5] WEIMER, P.K., SADASIR, G., MERAY-HORVATH, L. and HOMA, W.S.: Proc. I.E.E.E. 54, 345, 1966

[6] MOORE, G.E., THUN, R.E., CARROLL, W.N., KRAUS, C.J., RISEMAN, J. and WAJDO, E.S.: "Microelectronics" McGraw-Hill, New York (ed. E. Keonjian) p. 220, 1963

[7] SHEPHERD, A.A.: See ref. 3, p. 89

[8] BLACKBURN, H., CAMPBELL, D.S. and MUIR, A.J.: The Radio and Electronic Engineer, 34, 2, 90, 1967

[9] SWANSON, J.G.: Ph.D. Thesis, Imperial College, London University, 1966

[10] SWANSON, J.G. and CAMPBELL, D.S.: Thin Solid Films, 1, 183, 1967

[11] ANDERSON, J.C.: "Dielectrics", Chapman and Hall, 1964

[12] JACKSON, N.F.: Private communication

[13] HOFFMAN, R.W.: "Thin Films", Amer. Soc. Metals, p. 128, 1964

[14] CAMPBELL, D.S.: Proc. Int. Symp. "Basic Problems In Thin Film Physics", Vandenhoeck and Ruprecht, Gottingen, 1966

[15] BLACKBURN, H. and CAMPBELL, D.S.: Trans. 8th Nat. Vac. Symp., New York, p. 943, 1961

[16] CHOPRA, K.L.: J.A.P. 36, 655, 1965

[17] CARPENTER, R.: "Handbook of Thin Film Technology" McGraw-Hill (ed. L. Maissel and R. Glang) to be published 1968

[18] LAMB, D.R.: "Electrical Conduction Mechanisms in Thin Films" Methuen, London, 1967

[19] COLEMAN, M.V. and THOMAS, D.J.D.: Phys. Stat. Sol. 22, 593, 1967

[20] GUBANOV, A.I.: "Quantum Electron Theory of Amorphous Conductors" Consultants Bureau, New York, 1965

[21] LOH, E.: Solid State Communications, 2, 269, 1964

[22] SIMMONS, J.G.: Trans. Metal. Soc. A.I.M.E., 233, 1965

[23] FRANK, R.I. and SIMMONS, J.G.: J.A.P., 38, 1967

[24] SIMMONS, J.G.: "Handbook of Thin Film Technology" McGraw-Hill (ed. L. Maissel and R. Glang) to be published 1968

[25] JONSCHER, A.K.: Thin Solid Films, 1, 213, 1967

[26] HILL, R.M.: Thin Solid Films, 1, 1, 1967

[27] SERVINI, A.: See ref. 25

[28] PRICE, N.F. and RADCLIFFE, J.M.: I.B.M. J. Res. Der., 3, 364

[29] FOWLER, R.H. and NORDHEIM, L.: Proc. Roy. Soc., London, A119, 173

[30] HARRISON, W.: Phys. Rev., 123, 85, 1961

[31] SCHNUPP, P.: Phys. Stat. Sol. 21, 567, 1967

[32] SCHNUPP, P.: Solid State Elec. 10, 785, 1967

[33] SIMMONS, J.G.: J.A.P. 34, 6, 1963

[34] FRANZ, W.: Z. Naturf. 11A, 522, 1956

[35] MOTT, N.F. and GURNEY, R.W.: "Electronic Processes in Ionic Crystals" 1940

[36] GEPPERT, D.V.: J.A.P. 34, 3, 1963

[37] GEPPERT, D.V.: J.A.P. 33, 10, 1962

[38] KANE, E.O.: J. Phys. Chem. Sol. 1, 245, 1957

[39] STRATTON, R.: J. Phys. Chem. Sol. 23, 1011, 1962

[40] ABRAHAMS, E. and MILLER, A.: Phys. Rev. 120, 745, 1960

[41] MOTT, N.F. and TWOSE, N.O.: Phil. Mag. Suppl. 10, 38, 1961

[42] MYCIELSKI, J.: Phys. Rev. 123, 1961

[43] DEWALD, J.F.: J. Phys. Chem. Sol. 14, 155, 1960

[44] JOHANSEN, I.T.: J.A.P. 37, 2, 1966

[45] KLEIN, N. and GAFNI, H.: I.E.E.E. Trans. Electr. Devices, ED-13, 12, 1966

[46] PRIEST, J. and CASWELL, H.L.: J.A.P. 12, 581, 1961

[47] PRIEST, J., CASWELL, H.L. and BUDO, Y.: Vacuum 12, 581, 1961

[48] MEAD, C.A.: Phys. Rev. 128, 5, 1962

[49] HICKMOTT, T.W.: J.A.P. 35, 9, 2679, 1964

[50] MOTT, N.F.: Advances in Physics 16, 61, 49, 1967

[51] BEAN, C.P. et al.: Phys. Rev. 101, 551, 1956

[52] YOUNG, L.: "Anodic Oxide Films" Academic Press (New York) 1961

[53] VERMILYEA, D.A.: "Advances In Electrochemistry and Electro-chemical Engineering" (ed. P. Delahay) Interscience, New York, p. 211, 1963

[54] YOFFE, A.F.: "The Physics of Crystals" McGraw-Hill, New York, 1928

[55] ROSE, A.: Phys. Rev. 97, 1538, 1955

[56] LAMPERT, M.A.: J.A.P. 29, 1082, 1958

[57] O'DWYER, J.J.: J.A.P. 37, 2, 599, 1966

[58] SIMMONS, J.G.: Phys. Rev. 155, 3, 657, 1967

[59] TAYLOR, H.E.: J. Soc. Glass Technol. 41, 350T-382T, 1957

[60] KITTEL, C.: "Introduction to Solid State Physics" J. Wiley, 1963

[61] HARROP, P.J.: To be published

[62] COLE, K.S. and COLE, R.H.: J. Chem. Phys. 9, 341, 1941

[63] SCAIFE, B.K.P.: Proc. Phys. Soc. London, 81, 124, 1963

[64] WAGNER, K.W.: Ann. der. Physik 40, 817

[65] FUOSS, R.M. and KIRKWOOD, J.G.: J. Amer. Ceram. Soc. 63, 38, 5, 1941

[66] TAYLOR, H.E.: Ph.D. Thesis, University of Sheffield, Dept. of Glass Tech., 1959

[67] DAVIDSON, D.W. and COLE, R.H.: J. Chem. Phys. 18, 1417, 1950

[68] ARGALL, F.: Ph.D. Thesis, Chelsea College, University of London, 1967

[69] MACFARLANE, J.C. and WEAVER, C.: Phil. Mag. 13, 671, 1966

[70] BURKHARDT, P.J.: I.E.E.E. Trans. Electronic Devices E.D.-13, 12, 268, 1965

[71] VOLGER, J., STEVELS, J.M. and van AMERONGEN, C.: Philips Research Report, 8, 452, 1953

[72] von HIPPEL, A.R.: "Dielectrics and Waves", J. Wiley, New York

[73] SUTTON, P.M.: J. Amer. Ceram. Soc. 47, 4, 188, 1964

[74] SUTTON, P.M.: J. Amer. Ceram. Soc. 47, 5, 219, 1964

[75] GOUGH, E.R.: Ph.D. Thesis, University of Sheffield, Dept. of Glass Tech., 1965

[76] HAMON, B.V.: Proc. I.E.E. 99, IV, 27, 151, 1952

[77] GEVERS, M.: Philips Research Report, 1, 129, 1946

[78] GEVERS, M. and DU PRE, F.K.: Disc. of the Fara. Soc. 42, 47, 1946

[79] GARTON, C.G.: Trans. Disc. of the Fara. Soc. 42, 56, 1946

[80] OWEN, A.E.: Prog. Ceramic Sci. 3, 110, 1963

[81] LIDIARD, A.B.: "Handbuch der Physik" (ed. S. Flügge) Springer Verlag, Berlin, 1957

[82] ARGALL, F. and JEACOCK, R.: To be published

[83] POLLACK, M. and GEBALLE, T.H.: Phys. Rev. 122, 6, 1961

[84] MOTT, N.F.: Private communication

[85] POLLACK, M.: Phys. Rev. 138, 6A, 1965

[86] POLLACK, M.: Phys. Rev. 133, 2A, 1964

[87] LUCAS, M.S.P.: Microelectronics and Reliability 6, 269, 1967

[88] HERSPRING, A.: Z. Angew. Phys. (Germany) 20, 5, 369, 1966

[89] HAVINGA, E.E.: J. Phys. Chem. Solids 18, 2/3, 253 1961

[90] BOSMAN, A.J. and HAVINGA, E.E.: Phys. Rev. 129, 4, 1963

[91] COCKBAIN, A.G. and HARROP, P.J.: To be published in Brit. J. Appl. Phys.

[92] COCKBAIN, A.G.: Proc. I.E.E. 112, 1478, 1965

[93] ZACHARIASEN, W.H.: J. Amer. Chem. Soc. 54, 3841, 1932

[94] STEVELS, J.M.: Philips Tech. Review 22, 300, 1960/61

[95] STEVELS, J.M.: Philips Tech. Review 13, 12, 360, 1952

[96] McDOWELL, L.S. and BERGEMA, H.L.: Phys. Rev. 33, 1929

[97] TAYLOR, H.E.: J. Soc. Glass Tech. 63, 124T-146T, 1959

[98] OWEN, A.E. and DOUGLAS, R.W.: J. Soc. Glass Tech. 43 159T, 1959

[99] STEVELS, J.M.: "Handbuch der Physik" 20, 350 (Springer Verlag, 1957)

[100] GEVERS, M.: Philips Res. Report 1, 187, 1945

[101] GEVERS, M.: Philips Res. Report 1, 279, 1946

[102] VOLGER, J. and STEVELS, J.M.: Philips Res. Report 11, 452, 1956

[103] TRAP, H.J.L. and STEVELS, J.M.: Physics and Chem. of Glasses 4, 5, 1963

[104] HIROSE, H. and WADA, Y.: Japan J.A.P. 3, 179, 1965

[105] HARTMAN, T.E., BLAIR, J.C. and BAUER, R.: J.A.P. 37 179, 1965

[106] STUART, M.: Brit. J.A.P. 18, 1637, 1967

[107] STUART, M.: Phys. Stat. Sol. 23, 595, 1967

[108] SIDDALL, G.: Vacuum 9, 274, 1959

[109] DRUMHELLOR, C.E.: 7th Trans. Vac. Symp., Cleveland, 1960

[110] See Ref. 6, p. 202

[111] FISHER, J.H.: Private communication

[112] MARSHALL, R., ATLAS, L. and PUTNER, T.: J. Sci. Instr. 43, 144, 1966

[113] J. Sci. Instr. 40, 1963

[114] CAMPBELL, D.S. and BLACKBURN, H.: Trans. 7th Nat. Vac. Symp. 2, p. 313, 1960

[115] BEAVITT, A.R.: J. Sci. Instr. 43, 182, 1966

[116] MASON, W.P.: "Piezoelectric Crystals and their Application to Ultrasonics". Van Nostrand, 1950

[117] SCHWARTZ, N. and BROWN, R.: Trans. 8th Nat. Vac. Symp. 2, p. 836, 1961

[118] BLACKBURN, H. and CAMPBELL, D.S.: Phil. Mag. 8, 89, 823, 1963

[119] PLISKIN, W.A. and LEHMAN, H.S.: J. Electrochem. Soc. 112, 1013, 1965

[120] ALLAM, D.S. and PITT, K.E.G.: Thin Solid Films 1, 28, 1967

[121] ANASTASIO, T.A.: J.A.P. 36, 6, 1967

[122] HILL, A.E. and HOFFMAN, G.R.: Brit. J.A.P. 18, 13, 1967

[123] WHITE, P.: Vacuum 12, 15, 1962

[124] YARWOOD, J.: "High Vacuum Technique". Chapman and Hall, 1967

[125] POAT, D.R.: Private communication

[126] COWGILL, M.G. and STRINGER, J.: J. of the Less-Common Metals 2, 233, 1960

[127] CASWELL, H.L.:"Physics of Thin Films" 1, 1, 1963

"

[128] GROBNER, O.: J. of Chem. Phys. 46, 11, 4381, 1967

[129] SIDDALL, G.: 14th Thin Film Group Meeting Abstracts

[130] STANWORTH, J.E.: "Physical Properties of Glass" Clarendon Press, 1950

[131] BARRER, R.M.: "Diffusion in and through Solids" Cambridge University Press, 1941

[132] HILL, R.M.: Private communication

[133] BUDENSTEIN, P.B. and HAYES, P.J.: J.A.P. 38, 7, 1967

[134] LINDMAYER, J.: J.A.P. 36, 1, 1965

[135] REIMEROV, L.I.: Soviet Phys. Tech. Phys. 4 [2], 229, 1959

[136] MORRISON, J.R. and WILSON, A.L.: Analyst 88, Pt. I 88, Pt. II 100, Pt. III 446, 1963

[137] PLISKIN, W.A.: 13th Nat. Vac. Symp., 1966

[138] HIROSE, H. and WADA, Y.: J.A.P, 4, 9, 639, 1965

[139] BELL, T., HETHERINGTON, G. and JACK, K.H.: Phys. Chem. Glasses 3, 141, 1962

[140] OWEN, A.E.: Ph.D. Thesis, University of Sheffield, Dept. of Glass Tech., 1959